AST NO. 300687

FINAL REPORT

LASER-ACOUSTIC ICE THICKNESS MEASUREMENTS

(Feasibility Study)

DARPA SBIR Solicitation Topic No. 9
Phase I Proposal

Contract N00014-86-C-0209
June 30, 1987

Gail A. Hickman
John A. Edmonds

APPLIED SCIENCE TECHNOLOGY, INC.
19212 Plummer Drive
Germantown, MD
20874

SECURITY CLASSIFICATION OF THIS PAGE (When Data Entered)

REPORT DOCUMENTATION PAGE

READ INSTRUCTIONS BEFORE COMPLETING FORM

1. REPORT NUMBER: AST No. 300687
2. GOVT ACCESSION NO.:
3. RECIPIENT'S CATALOG NUMBER:

4. TITLE (and Subtitle): Laser-Acoustic Ice Thickness Measurements
5. TYPE OF REPORT & PERIOD COVERED: Final Report
6. PERFORMING ORG. REPORT NUMBER:

7. AUTHOR(s): Gail A. Hickman, John A. Edmonds
8. CONTRACT OR GRANT NUMBER(s): N00014-86-C-0209

9. PERFORMING ORGANIZATION NAME AND ADDRESS:
Applied Science Technology, Inc.
19212 Plummer Dr.
Germantown, MD 20874
10. PROGRAM ELEMENT, PROJECT, TASK AREA & WORK UNIT NUMBERS:

11. CONTROLLING OFFICE NAME AND ADDRESS:
Office of Naval Research
800 N. Quincy Street ATTN: 1513A: DHP
Arlington, VA 2217
12. REPORT DATE: June 30, 1987
13. NUMBER OF PAGES: 103

14. MONITORING AGENCY NAME & ADDRESS (if different from Controlling Office):
Defense Advanced Research Projects Agency
1400 Wilson Blvd.
Arlington, VA 2209
15. SECURITY CLASS. (of this report): Unclassified
15a. DECLASSIFICATION/DOWNGRADING SCHEDULE:

16. DISTRIBUTION STATEMENT (of this Report)

Approved public release; distribution unlimited.

17. DISTRIBUTION STATEMENT (of the abstract entered in Block 20, if different from Report)

18. SUPPLEMENTARY NOTES

19. KEY WORDS (Continue on reverse side if necessary and identify by block number)

Laser-acoustics
Remote sensing
Ice thickness
Induced sound

20. ABSTRACT (Continue on reverse side if necessary and identify by block number)

The results of the SBIR Phase I contract "The Feasibility of Applying the Laser-Acoustic Technique to Remotely Sense Ice Thickness" performed by Applied Science Technology, Inc. show that it is feasible to measure ice thickness using the laser-acoustic technique. The acoustic signals generated in the ice by a CO2 laser are of sufficient strength to be reflected off the ice/water interface and be detected by a receiver in the air. The sound pressure level (SPL) of this signal was detected with a microphone in the air as 110 dB re 1 uPa for a laser

DD FORM 1 JAN 73 1473 EDITION OF 1 NOV 65 IS OBSOLETE
S/N 0102-LF-014-6601

Unclassified
SECURITY CLASSIFICATION OF THIS PAGE (When Data Entered)

energy of 6.5 J. Simultaneous detection by a hydrophone in ice and microphone in air yielded a transmission loss across the ice/air interface of 52 dB. An additional loss of 20 dB occurred when there was a 15 cm snow layer on the ice. The ice thickness derived from this technique yielded a value of 1.0 m, while the actual value was measured as 0.76 m. This discrepancy can be explained by a 4 cm height error in the microphone position. Signal/noise calculations indicate that a 50 J laser should be capable of measuring ice thickness of 10 m from an acoustic receiver in an aerodynamic bird that is towed from an altitude of 20 m. An operational system would provide the capability to remotely measure ice thickness with an accuracy of 5-10% from a helicopter.

ACKNOWLEDGEMENTS

The authors wish to thank Dr. G. Hickman, founder and former president of AST, Inc. for serving as an unpaid consultant to this contract. Dr. Hickman conceived the original concept and performed the initial measurements of using the laser-acoustic technique to measure ice thickness. The authors acknowledge Mr. Joe Gerardi of Innovative Dynamics for his engineering support during the Moosehead Lake measurements, and Dr. Joe Clark (Catholic University of America) for his valuable discussions on acoustics and his review of the final report. We also wish to thank Dr. T. Litovitz (Catholic University) for loaning to AST, Inc. the laser and recording equipment and for providing laboratory space at the University. Julius Zhu, a student at Catholic University, helped in the refurbishment of the laser system. The Fish and Wildlife Office at Greenville, Maine is also gratefully acknowledged for their discussions of the local ice conditions and site selection, and for use of their facilities. Financial support for this work was received from DARPA Contract N00014-86-C-0209.

TABLE OF CONTENTS

ABSTRACT

The results of the SBIR Phase I contract "The Feasibility of Applying the Laser-Acoustic Technique to Remotely Sense Ice Thickness" performed by Applied Science Technology, Inc. show that it is feasible to measure ice thickness using the laser-acoustic technique. The acoustic signals generated in the ice by a CO_2 laser are of sufficient strength to be reflected off the ice/water interface and be detected by a receiver in the air. The sound pressure level (SPL) of this signal was detected with a microphone in the air as 110 dB re 1 uPa for a laser energy of 6.5 J. Simultaneous detection by a hydrophone in ice and microphone in air yielded a transmission loss across the ice/air interface of 52 dB. An additional loss of 20 dB occurred when there was a 15 cm snow layer on the ice. The ice thickness derived from this technique yielded a value of 1.0 m, while the actual value was measured as 0.76 m. This discrepancy can be explained by a 4 cm height error in the microphone position. Signal/noise calculations indicate that a 50 J laser should be capable of measuring ice thickness of 10 m from an acoustic receiver in an aerodynamic bird that is towed from an altitude of 20 m. An operational system would provide the capability to remotely measure ice thickness with an accuracy of 5-10% from a helicopter.

1.0 INTRODUCTION

In studying ice cover in the Arctic, two parameters of prime interest are (1) the variations of ice thickness, and (2) roughness, or topographic relief. Ice thickness is the parameter which this study addressed. The following is a partial listing of applications that require knowledge of ice thickness:

- to model correctly the mechanics of ice interaction, to enable accurate predictions being made of the dynamics of the Arctic pack (Thorndike and Maykut, 1973),

- to enhance the accuracy of calculations of the mass budget for ice packs--used as input to climatic models (Koerner, 1973),

- input to the selection and prediction of safe loads for ice breaking operations by ships and for transporting heavy equipment over ice cover,

- airborne/submarine communications, and

- location of objects (submarines) below the ice cover.

Various techniques such as a) visible and infrared sensors, b) microwave sensors, c) impulse radar, d) airborne electromagnetic and e) laser profilometer, are or have been studied for a number of years for their use in the investigation of ice characteristics. However, presently no operational remote system is available that measures ice thickness directly. The requirement, therefore, still remains for a practical remote sensing system that can be used to measure ice thickness directly to a reasonable accuracy -- between a few cm and a couple of meters.

Applied Science Technology, Inc. (AST) is introducing a new hybrid technique, referred to as "laser-acoustics", which may have the potential for being developed into a system for measuring ice thickness. This technique consists of a pulsed CO_2 laser transmitter and a microphone receiver -- both operated in the air. The laser, when focused on ice, generates a shock wave, thereby creating a high intensity acoustic field having a relatively flat frequency spectrum out to 100 kHz. The microphone detects the sound reflected from the ice/water interface. Precise timing of these signals enables an accurate measurement to be made of ice thickness. It is possible that such a system could be

used in a stand-alone mode, or that it could be used in conjunction with other "ice sensors" to accomplish both a reasonable accuracy in ice thickness and wide area coverage -- always desired of remote sensors.

The concept of using a pulsed infrared laser for generation of acoustic signals was demonstrated in water several years ago (Brewer et al., 1964; Carome et al., 1966; Bell and Landt, 1967; Lowney and Sullivan, 1970; Bunkin et al., 1971; Cawley and Bell, 1972; Maccabee and Bell, 1977). AST developed an Experimental Laser Acoustic System (ELAS) to generate laser-acoustic signals, and to collect, analyze and plot experimental data (Hickman and Edmonds, 1981). AST has successfully demonstrated that the technique of using a CO_2 laser to generate acoustic pulses in water can be used to measure water depths (Hickman et al., 1982a). Additionally, AST has made measurements on generating signals in sand and have shown that the laser-acoustic technique may have the potential for remotely: (1) detecting objects buried in the sediment to depths as great as 0.3 to 0.6 meters, and (2) determining soil moisture (Hickman and Edmonds, 1982b). Based on the positive results of the above measurements, the question arose as to whether this same technique could be used to remotely measure the thickness of ice.

Using the ELAS, AST performed initial laser-acoustic measurements on block ice (Hickman and Edmonds, 1983a). Measurements were made on 1 cubic meter block ice. A hydrophone which was imbedded in the ice block at a distance of 0.46 m from the impact spot of the laser, measured a sound pressure level (SPL) adjusted to 1 meter, of approximately 187 dB re 1 μPa. The time from the firing of the laser to the front edge of the acoustic wavefront is used to calculate the speed of the acoustic signal, which in this case resulted in a value of 3,445 $msec^{-1}$. This value agrees with the value reported in the literature (Bogoradskii et al., 1976; Gavrilo et al., 1980).

Following these ice block experiments, the ELAS was transported to Moosehead Lake, Maine, during March 1983 for field measurements (Contract N00014-82-C-0810). Hydrophones and microphones were used to measure the acoustic signals both in and above the ice surface. The average acoustic SPL measured 30 cm above the ice surface with the microphone was 101 dB re 1 μPa. The results of the measurements successfully showed that this technique had the possibility for being used to measure ice thickness. (Hickman and Edmonds, 1983).

AST has just completed a 6-months SBIR Phase I R&D effort to study "The Feasibility of Applying the Laser-Acoustic Technique to Remotely Sense Ice Thickness". This report describes the research performed, the results obtained and the key research required to develop this technique into a viable system for remotely measuring ice thickness. The following tasks were addressed during Phase I:

1) Assemble and refurbish all the system components of the laser-acoustic system (ELAS) for this program.

2) Conduct a series of field ice measurements to assess the multipath problem and efficiency of generating the signals in ice and coupling the signals into the water.

3) Formulate a practical model of the acoustic signals in ice, which can be used to assess the utility of an operational laser-acoustic system.

4) Assess the signal to noise ratio for the receiver located either on a helicopter or tethered via cable.

5) Assess the area coverage of the sensor in a stand-alone mode, and determine benefits of using the sensor as a normalizing factor to improve wide area coverage of other ice thickness sensors.

2.0 FUNDAMENTAL CONCEPTS

Ice is a complex layered substance, a simplified three-layered model of which is shown in Fig. 2.1. The sound velocities and densities as determined by Bogorodskii (1976) are given in this figure. The longitudinal wave velocity has two minima (in the snow cover and in the "clear-ice" interlayer) and a maximum in the intermediate ice layers.

It is postulated by Bogorodskii that snow is a weakly consolidated system in which a strain wave propagates via its interconnecting air voids. The acoustic path length in the voids is greater than the rigid matrix of the system or in open space, so that the velocity of sound in snow is less than in air.

In the phase transition region between ice and water referred to as "clear-ice," the velocity is less than it is in water. This interlayer is more porous than the rest of the ice and is also a weakly consolidated system. Present are bubbles of gas precipitated out of the water and consequently this layer can be regarded as a two-component porous system containing a minute quantity of gas. Bogorodskii hypothesized that the gas bubbles formed in cystallization increase the compressibility of the system, thereby decreasing the velocity of sound to values less than the velocity of sound in the water from which the ice is formed. Similar results have been attained experimentally by measurements of sound velocity in a water-porous sand layer (Hickman, unpublished), and in water containing air bubbles (Maccabee, 1975). The sound velocity in both of these two-component systems is less than the sound velocity in each of the individual constituents which make up the system.

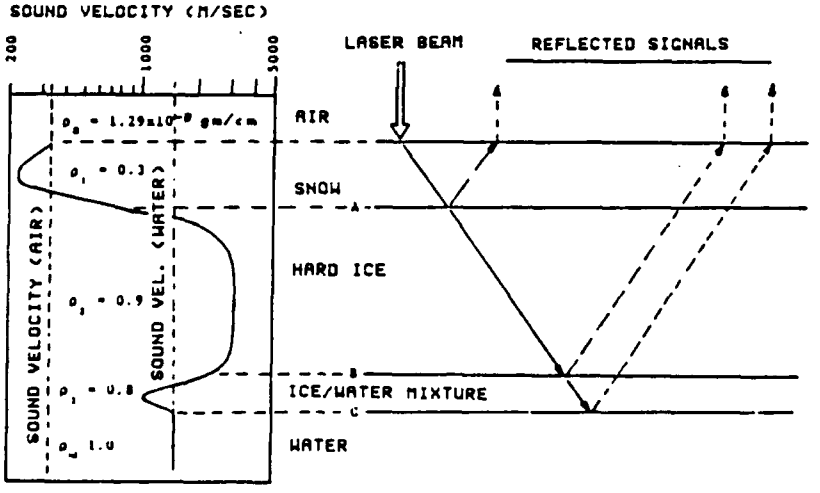

Fig. 2.1 Ice Profile. (Bogorodskii et al., 1976)

If ice were boundless, nonabsorbing and its physical properties unvarying, sound would travel at a constant speed and radiate outward in straight rays. The intensity of sound would decrease as the inverse square of distance, known as spherical spreading. Because ice is not boundless, the inverse square law alone may not always apply. It has been observed in the ocean that at extreme distances from the source, and in sound channels, sound intensity decreases as the inverse first power of distance, called cylindrical spreading. A third type of spreading also occurring in the ocean is called dipolar spreading and occurs when the intensity decreases as the inverse fourth power of distance. Some combination of these three types can also be expected whenever sound is transmitted in ice. A comparison of loss curves as a function of distance for the three types is shown in Fig. 2.2.

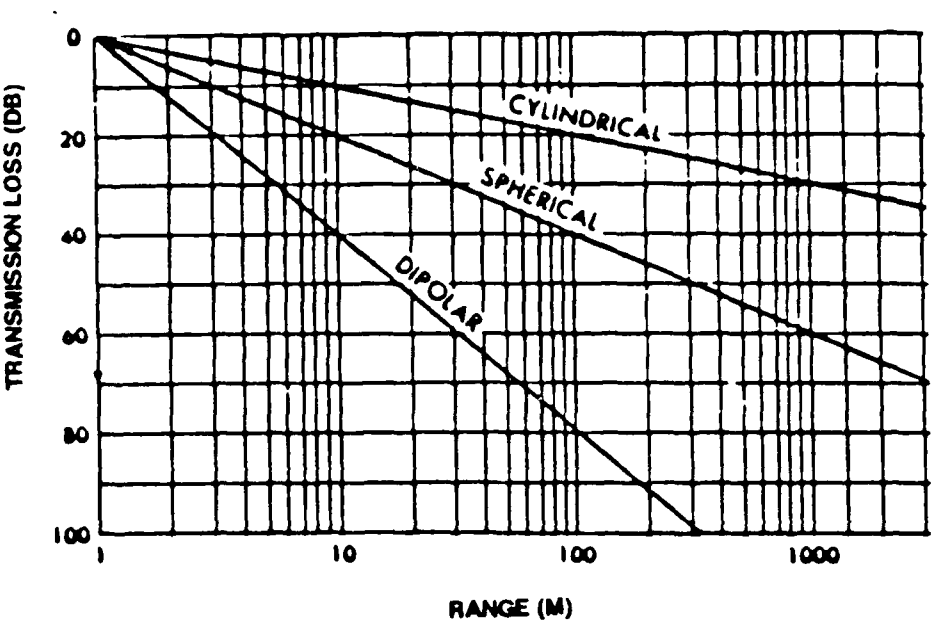

Fig. 2.2 Comparison of spreading loss.

When sound travels through ice, additional losses or gains occur from (1) attenuation (absorption and scattering), (2) refraction because of velocity gradients and (3) reflections at the boundaries. As sound propagates through a medium, some of the energy is converted into heat through the process of absorption.

Scattering loss results from reflectors in the medium such as air bubbles. Changes in the physical and chemical characteristics of the ice and the related changes in sound velocity cause the bending of sound rays (refraction) from straight line paths.

Langleben (1969) measured the acoustic attenuation in sea ice over the range 10kHz to 500 kHz. His results (see Fig. 2.3) were fit to the following empirical relation:

$$a = c_1 f + c_2 f^4 \quad (dB/m)$$

where:

f = acoustic frequency (kHz)
a = attenuation coefficient (dB/m)
c_1 = 4.45×10^{-2} (dB/m/kHz) - constant
c_2 = 2.18×10^{-10} (dB/m/kHz) - constant

Since the velocity of the compressional wave in ice varies between 3500 and 3800 m/s, the acoustic wave length at 25 kHz (region of interest to our specific problem) is approximately 14 cm. At this frequency the linear term in the above equation dominates. The Rayleigh scattering term (f^4) is only significant when the acoustic wavelength is comparable or smaller to the average ice crystal size (2-3cm), which occurs at a frequency of 130 kHz. Other scattering effects include air bubbles and brine inclusions.

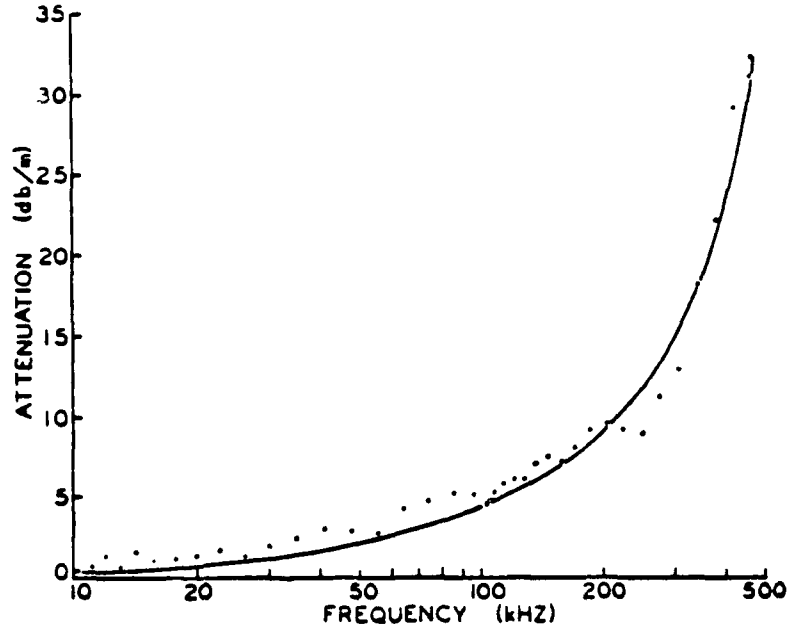

Fig. 2.3 Attenuation coefficient as a function of frequency.

The boundary between two mediums characterized by different densities (ρ) and velocities (c) is both a reflecting and refracting surface. The reflection loss of sound incident at an angle to a plane boundary is given by the Rayleigh formula. If a plane wave is incident upon the boundary between mediums of density ρ_1 and ρ_2 and of sound velocity c_1 and c_2 as indicated in Fig. 2.4, then

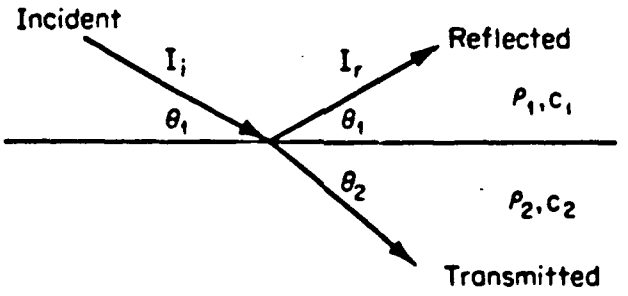

Fig. 2.4 Reflected and transmitted rays at a discontinuity between two mediums.

the intensity of the reflected wave I_r is related to the intensity of the incident wave I_i by

Rayleigh formula:

$$\frac{I_r}{I_i} = \left[\frac{m \sin\theta_1 - n \sin\theta_2}{m \sin\theta_1 + n \sin\theta_2}\right]^2 = \left[\frac{m \sin\theta_1 - (n^2 - \cos^2\theta_1)^{1/2}}{m \sin\theta_1 + (n^2 - \cos^2\theta_1)^{1/2}}\right]^2$$

where $m = \rho_2/\rho_1$ and $n = c_1/c_2$ (Brekhovskikh, 1960; Urick, 1975). The reflection loss is the logarithmic expression of the above ratio, or 10 log (I_r/I_i) dB. The reflection loss is therefore a function of the grazing angle of incidence and the ratios m and n. Fig. 2.5 shows the ratio of reflected to incident intensities with grazing angle for a plane wave traveling through ice and incident on the ice/water interface. For this case, m=1.1 and

n=2.7. Total reflection (1.0) occurs at a grazing angle of 0 deg and decreases to 0.2 at 90 deg.

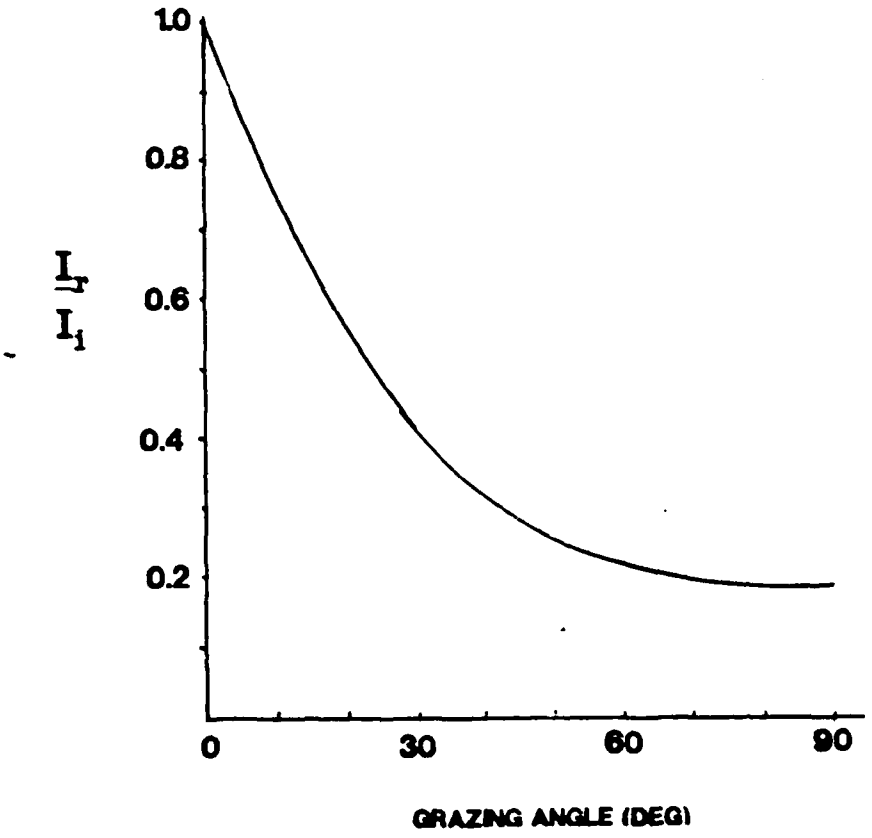

Fig. 2.5 Ratio of reflected to incident intensities with grazing angle for sound traveling through ice and incident on the ice/water plane boundary (lossless medium).

Sound reflection at the ice/water interface is, however, a complex phenomenon and the Rayleigh formula is only an approximation of the reflection loss. Most of the sea ice bottom is composed of vertically-extending dendrites which form a very irregular surface reflection. Langleben (1970) measured the amplitude of ultrasonic pulses reflected off the bottom of the Arctic ice pack. The acoustics were generated by piezoelectric transducers operating betwen 17.9 and 435 kHz. He observed lower reflectivity than had been previously assumed. No frequency dependence could be distinguished in this range although his data exhibits very wide scatter. The variation in reflectivity was

Taking into account the various transmission losses of sound propagating through the ice and into the air, one can calculate the sound pressure level of the return signal, SPL_R, from the various interfaces detected with a microphone located in the air as:

$$SPL_R = SPL_o - (R_{x,y} + T_{x,y}) - 20\log r + 20\log(\sin\theta) - \alpha r$$

where SPL_o is the SPL measured at a depth of 1 meter in the ice generated via the CO_2 laser, $R_{x,y}$ and $T_{x,y}$ are the transmission and reflection losses or gains, θ is the acoustic ray angle in the first layer, r is the acoustic path length, and α is the acoustic attenuation coefficient in ice. The term (20 logr) is the signal attenuation in ice due to spherical spreading. An additional attenuation term, (20 log ($\sin\theta$)), is added due to the fact that the acoustic signal generated in ice (similar to the effect in water as described by Hickman et al., 1982a) has an angular dependence as $\sin(\theta)^2$. The values of $R_{x,y}$ and $T_{x,y}$ are given by the following equations. Note: RL and TL are often used to denote $R_{x,y}$ and $T_{x,y}$ respectively.

$$R_{x,y} = 20 \log \left| \frac{\rho_x c_x - \rho_y c_y}{\rho_x c_x + \rho_y c_y} \right| \quad \text{(dB)}$$

$$T_{x,y} = 20 \log \left\{ \frac{2\rho_y c_y}{\rho_x c_x + \rho_y c_y} \right\} \quad \text{(dB)}$$

where x,y represent the first and second media, respectively. For simplicity, it is assumed in the calculations of these coefficients that the incident wave impinges the layer at 90 deg. Table 2.1 lists values of density, sound velocity and acoustic impedances of various media. These values are used for the calculations of the reflection and transmission losses at the medium interfaces as shown in Table 2.2. Negative values for R and T represent a loss in SPL, while positive values indicate an increase in SPL.

The following example is given for a multilayered system which is composed of air, snow, ice and water. The acoustic signal is generated at the snow surface. The appropriate values of reflection (RL) and transmission (TL) losses/gains are given in Fig. 2.7, along with the calculated total loss.

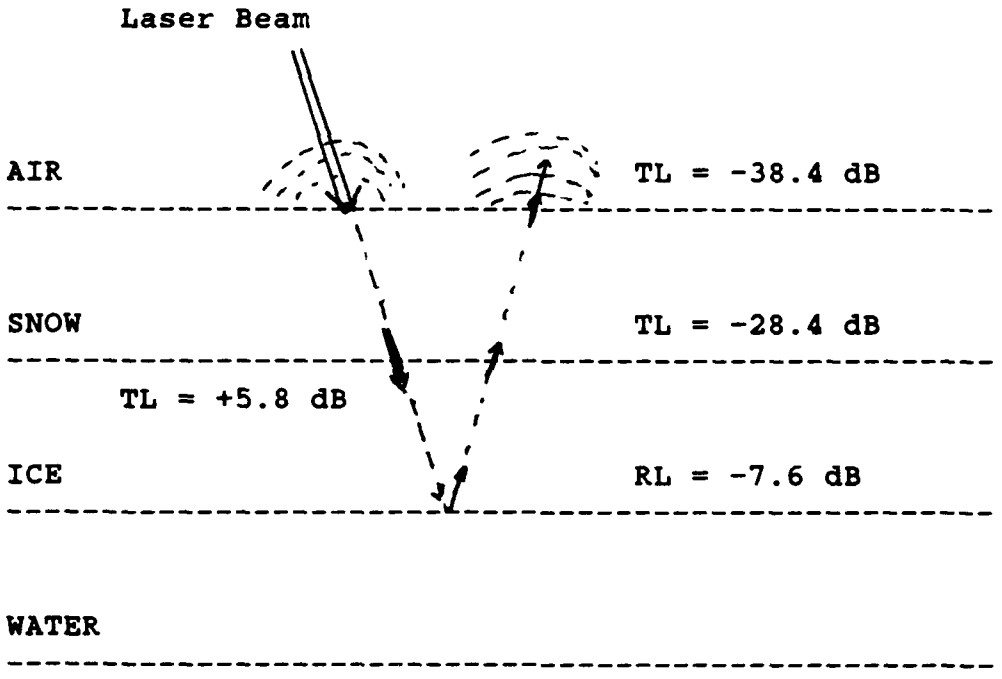

Total loss = +5.8 - 7.6 - 38.4 - 28.4
= 68.6 dB

Fig. 2.7 Transmission and reflection losses/gains for multilayered media.

Table 2.1 Nominal density, sound velocity and acoustic impedance for various media

Medium	(gm/cm^3)	c (m/s)	c ($gm/cm^2/s$)
Air	0.00129	330	0.4
Snow	0.3	220	66
Ice	0.9	3,785	3,407
Water	1.0	1,397	1,397

Table 2.2 Reflection & transmission losses/gains for various interfaces (grazing angle = 90 deg)

Sound Propagation Path	Reflection Loss/Gain (dB)	Transmission Loss/Gain (dB)
Ice to Snow	-0.3	-28.4
Snow to Ice	"	5.8
Ice to Water	-7.6	-4.7
Water to Ice	"	3.0
Snow to Air	-0.1	-38.4
Air to Snow	"	6.0
Ice to Air	-0.002	-70.5
Air to Ice	"	6.0
Water to Air	-0.005	-64.4
Air to Water	"	6.0

3.0 EXPERIMENTAL LASER/ACOUSTIC SYSTEM (ELAS)

AST's ELAS is used to generate laser acoustic signals, and to collect, analyze and plot experimental data. ELAS is comprised of a combination of standard off-the-shelf instrumentation and special control electronics designed by AST to integrate the various instruments into a complete laser/acoustic experimentation system.

The system block diagram is shown in Fig. 3.1. For purposes of our discussion, the system is divided into the following four subsystems: a) laser, b) acoustic receiving system, c) signal recording and analysis equipment, and d) computer. These subsystems are described below.

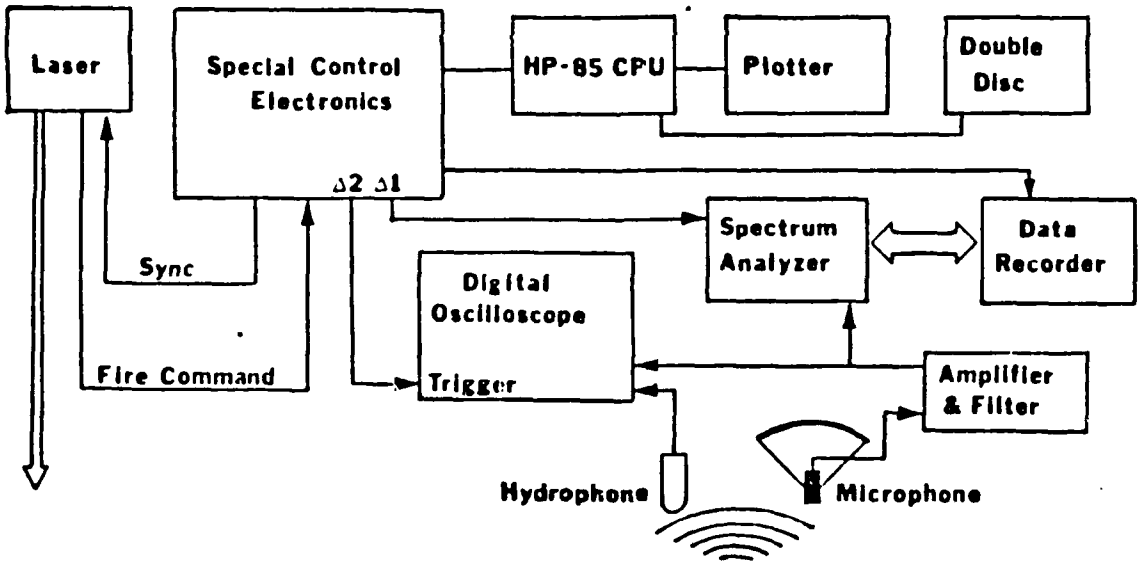

Fig. 3.1 ELAS System Block Diagram

3.1 LASER

A Lumonics model TEA-103-2 small aperture CO_2 laser capable of producing a one microsecond, 15 Joule pulse at a wavelength of 10.6 um (infrared) is used as the transmitter. The laser is shown in Fig. 3.2. The laser beam exits from the black tube at the left side of the front face of the laser. The laser specifications are:

CO_2 Laser
Type - TEA Laser
Manufacturer - Lumonics Corporation
Energy - 15 Joules
Pulse Rate - 1 pulse/2 sec
Pulse Width - 1 usec
Beam Divergence - 4 mrad
Flow Rate - N_2 - 0.5 l/min
He - 0.4 l/min
CO_2 - 0.9 l/min

A support beam is bolted to the top of the laser housing and extended 61 cm beyond the front of the laser. An adjustable infrared telescope containing germanium lenses is attached to the support beam. This telescope, which was composed of two lenses, was attached to the laser housing itself and used to focus the beam to a small spot (0.5 cm) on the ice at distances ranging from 4-30 meters. The lenses were germanium plano-convex and plano-concave, 5.08 cm diameter, (II-VI Incorporated) having focal lengths of -0.762 m and 1.0 m respectively. Air breakdown occurs, with subsequent reduction in the acoustic energy generated in the ice, when the beam is brought to a focus in air above the ice surface. Thus, focusing of the laser beam on the ice surface becomes a critical aspect of this laser/acoustic technique for generation of acoustic pulses.

The laser power supply unit contains the trigger control to fire the laser and the mixing valves for the laser gases, CO_2, N_2 and He. The laser is triggered from the front-panel push-button. There is a sync signal output which provides an electrical pulse at the instant the laser fires. Time-of-arrival measurements are referenced to this sync pulse.

In addition to the acoustic pulse generated in ice, an acoustic signal is simultaneously generated in air. This is called the "air blast" and its presence must be considered in applying the laser/acoustic technique to remote sensing problems.

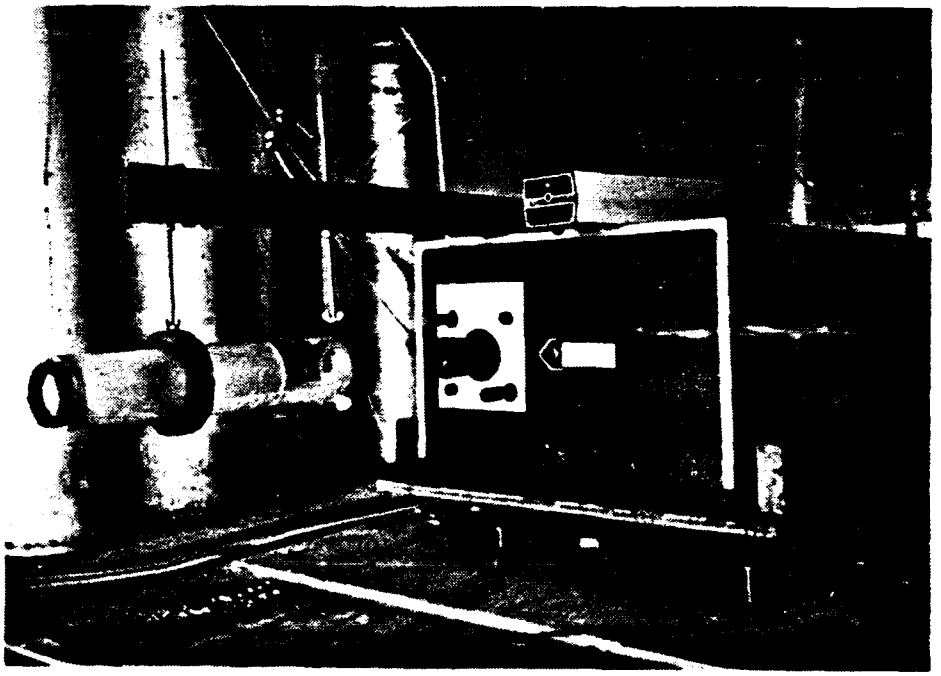

Fig. 3.2. Photograph of CO_2 laser showing focusing telescope and Helium-Neon laser

3.2. ACOUSTIC RECEIVING SYSTEM

A highly sensitive microphone is located above the ice to detect the acoustic signal after it is reflected from the ice/water interface. In air the acoustic receiver used is a Bruel and Kjaer (B&K) model 4149 (1.2 cm) microphone and model 2619 preamplifier. The power supply (B&K model 2807) for the microphone preamplifier includes a unity gain amplifier for driving low impedance coax cables.

The acoustic receiver is a hydrophone when measuring the sound pressure level of the various laser signals in ice and water. The hydrophone is a B&K model 8103 and is used in conjunction with a model 2635 conditioning amplifier.

A brief summary of the receivers used in the experiments is given below:

Microphone	
Manufacturer:	Bruel & Kjaer
Type:	Condenser Microphone 4149
Rated Sensitivity:	-38.8 dB re 1V/Pa
Frequency Range:	flat between 3.9 kHz and 40 kHz
Preamplifier:	2619
Power Supply:	2807
Size:	1.2 cm diameter
Hydrophone with Amplifier	
Manufacturer:	Bruel & Kjaer
Type:	8103
Sensitivity:	-120 to -200 dB re 1V/uPa
Size: Active Area	
Diameter:	0.3 cm
Length:	5.1 cm
Overall	
Diameter:	2.5 cm
Length:	15 cm
Frequency Response:	flat between 1 Hz and 150 kHz
Beam:	omni in XY plane
Conditioning Amplifier:	B&K 2635

When necessary, a Hewlett-Packard 450 AR amplifier (20/40 dB gain) and a tunable bandpass filter are used in conjunction with both the microphone and hydrophone. The tunable filter is a Krohn-Hite model 3202 active filter. It contains two independent, four-pole filters, each of which can be used as either a high or low pass filter. Bandpass and bandreject characteristics can be obtained by cascading the two filters. The filter is used to reduce out-of-band signals and noise. The filter has a gain of 0 dB in the passband.

3.3. SIGNAL RECORDING AND ANALYSIS EQUIPMENT

The signal recording and analysis equipment includes:

a) Nicolet Scientific model 446B real-time spectrum analyzer
b) Nicolet Scientific model 144 data recorder
c) Tektronix 100 MHz digital oscilloscope model 2230
d) special control electronics designed by AST to provide pulse time synchronization

The Nicolet 446B is a real time spectrum analyzer which performs a digital Fast Fourier Transform (FFT) of digitized time domain signal data to obtain the frequency spectrum of the incoming signal. The frequency spectrum covered by the Nicolet 446B extends from DC to 100 kHz. The maximum input sensitivity of the analyzer is obtained using the 100 mV RMS setting. This results in a display range of $\pm$140 mV in the time mode.

The analyzer is triggered externally by the Special Control Electronics (SCE). When using the 50 kHz range, one millisecond of pretrigger time data plus seven milliseconds of post-trigger time data is stored and displayed by the analyzer as a sequence of 1024 equally spaced (in time representation) digitized signal levels values, with an amplitude resolution of 12 bits.

The analyzer is connected to the Model 144 data recorder via a high-speed parallel data bus. The displayed time data can be recorded by actuating a front panel push button. The data recording is accomplished in slightly under one half second. Approximately 1000 such data images may be stored on one 3M model 300A magnetic tape cartridge. Each image is identified with a unique tape file number. All of the spectrum analyzer front panel settings are also recorded on the tape.

The data may be retrieved from the tape by dialing in the appropriate tape file number and transferring the data back into the analyzer. The analyzer can compute the spectrum of any signal retrieved from the data tape.

The spectrum analyzer may be controlled by the HP-85 computer via the standard HP Interface Bus (HP-IB, IEEE 488). Time and spectrum data may be transferred, in either direction, between the computer and analyzer via the HP-IB. Only the external trigger is supplied by another source -- the SCE.

The SCE accepts the laser sync pulse as a start pulse for the trigger delay timer and provides trigger delays for the spectrum analyzer and the digital scope. Since the laser operation requires the switching of high energy, short duration pulses (40 kV, 1 usec) care must be taken to avoid either radiated or conducted electromagnetic interference. For this reason, both the laser trigger input and the sync output are electrically isolated from the SCE logic circuitry by means of an optically coupled isolator (optocoupler).

The SCE used a 1 MHz crystal controlled oscillator and a six decade counter as an elapsed time counter. The counter is started upon receipt of the laser sync pulse and is stopped on completion of exactly one second elapsed time. The desired spectrum analyzer or digital oscilloscope trigger delay time is preset in a two digit storage register (milliseconds) by manually pushing button switches on the front panel. A digital comparator generates the trigger pulse when the value of the elapsed time counter equals the preset register value. Fig. 3.3 shows the spectrum analyzer, data recorder and the SCE.

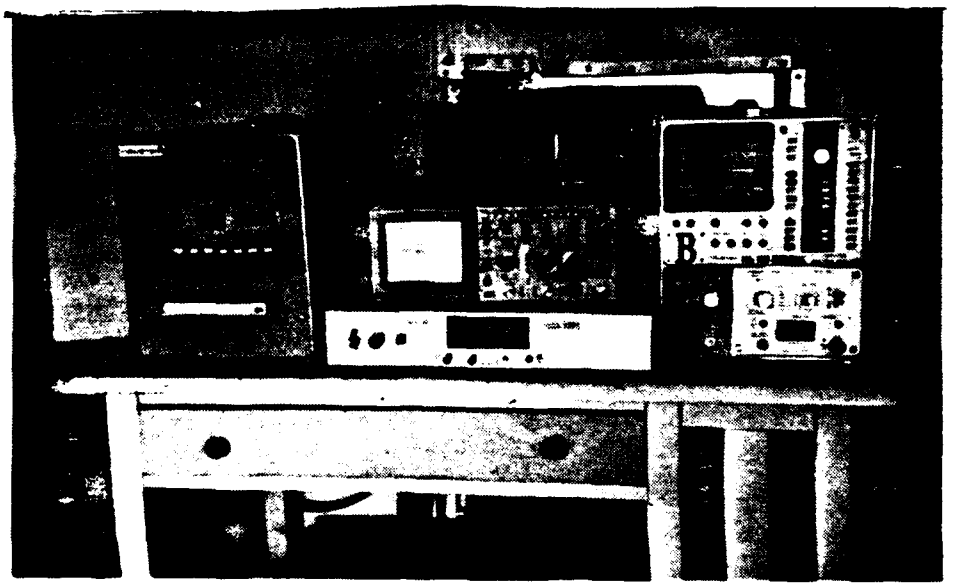

Fig. 3.3. Photograph of Spectrum Analyzer, Data Recorder and Special Control Electronics

3.4. COMPUTER

The Hewlett-Packard model 85 computer is a personal size computer which is ideally suited for scientific applications. The HP-85 benefits from its ease of interfacing with other instrumentation, available peripheral devices, and support software. The computer is comprised of:

a) HP-85 computer with built in CRT, magnetic tape drive and thermal alphanumeric printer,
b) 32K Random Access Memory (RAM),
c) Model 82901M Dual Disc Drive,
d) Model 7225B Graphic Plotter,
e) Basic programming language,
f) HP-IB (IEEE-488) and General Purpose Input/Output (GPIO) interfaces.

The HP-85 computer is used to perform post-experiment analysis of the data.

4.0 LASER/ACOUSTIC EXPERIMENTS

The ELAS was assembled into a 4 meter truck as shown in Fig. 4.1. The truck was equipped with a motor generator which enabled the equipment to be transported to any remote site and operate independently.

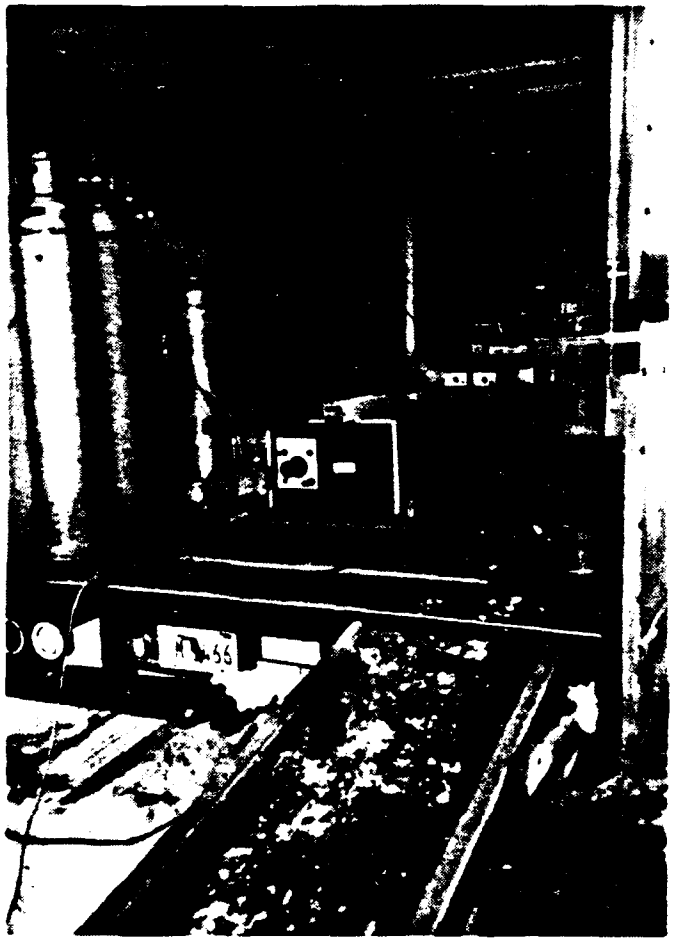

Fig. 4.1. Photograph of ELAS equipment installed in truck for field measurements

Moosehead Lake, Maine was chosen as the test site to conduct the ice measurements under the present SBIR contract. These measurements were made during February, 1987. The main reasons that this site was chosen are as follows: (1) generally the ice thickness at Moosehead Lake is approximately 1 meter during February/March, and ranks among the thickest ice in eastern U.S., and (2) the initial field ice measurements performed using this technique were conducted here in March, 1983 (see Appendix B for experimental data).

The general test set-up is shown in Fig. 4.2. The laser beam, after it passes through the infrared telescope, is directed downwards toward the ice surface by a 45-degree mirror where it is focused to a small spot on the ice surface. The acoustic signal generated by the interaction of the laser with the ice is detected by microphones in the air and hydrophones in the ice and water. The total laser energy was measured periodically by means of a thermopile calorimeter (Scientech 38-0401). The average measured energy of the laser beam after it had passed through the telescope was 6.5 J.

Fig. 4.2 Photograph of laser/acoustic experiments at Moosehead Lake

Measurements were taken at two different test sites on Moosehead Lake. At the first site, the truck was operated on the shore and the laser impact spot was approximately 30.5m from the laser. Sixty-three test shots were recorded on the Nicolet data recorder. The following week the truck was moved to a different location directly on the ice and 117 additional shots were recorded. The laser impact spot at this second location was located much closer to the laser, at a distance of approximately 4.6m. At both locations, the actual ice thickness was measured by drilling a hole through the ice with an ice auger shown in Fig. 4.3. The ice was approximately 0.76m (30in) thick and was composed of two visible layers. The top layer, called the "snow" ice, was 0.33m thick while the bottom layer, called "black" ice, comprised the rest of the ice. These two layers are clearly visible in Fig. 4.4. The "snow" ice is composed of snow which has been continuously melted and refrozen and has a white appearance, while the "black" ice derives its color from the reflection of the water on the ice. This ice is frozen directly from the lake itself. The water depth under the ice was approximately 0.61m at the first site, and 5.6m at the second.

A summary of the basic experiments that were performed at Moosehead Lake are given below:

1) Hydrophone measurements in ice
2) Hydrophone measurements in water
3) Microphone measurements in air (without snow cover)
4) Microphone measurements in air (with snow cover)

The measurement data are presented in Appendices C and D. Typical curves for each experiment will be discussed in the following sections.

Fig. 4.3 Ice auger used to drill holes

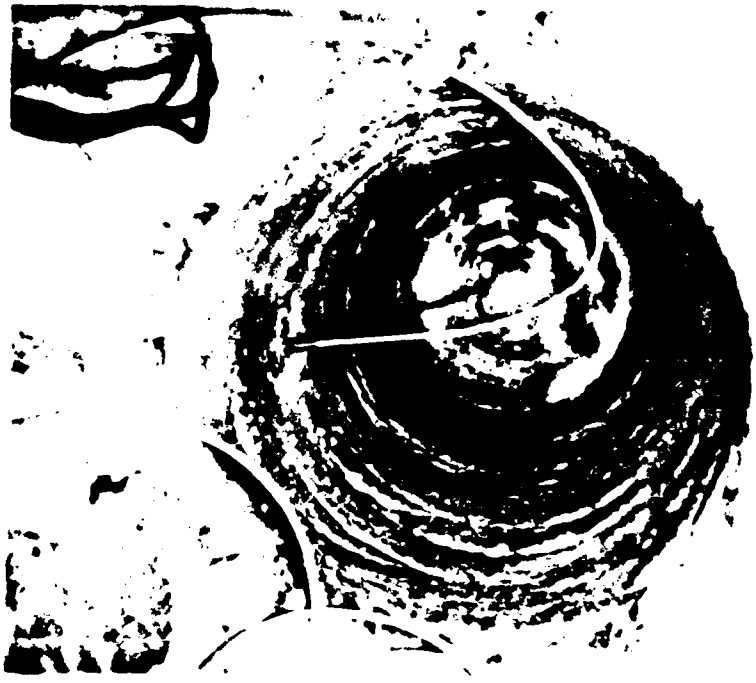

Fig. 4.4 Ice hole showing the snow and black ice

4.1 HYDROPHONE MEASUREMENTS IN ICE

Objective - to use the hydrophone to measure the acoustic velocity of laser-generated acoustic waves (0-40kHz) in ice. The velocity results will be used in the analysis of the hydrophone and microphone experiments.

The hydrophone was imbedded in the top of the ice, perpendicular to the surface, at distances from the laser impact spot of 0.91m and 3.05m. In addition, at 6.10m from the laser impact, a 0.6m hole was drilled into the ice and the hydrophone was inserted into the side of the hole, parallel to the ice surface and 0.38m from the top ice surface. Figure 4.5 depicts the hydrophone test configurations.

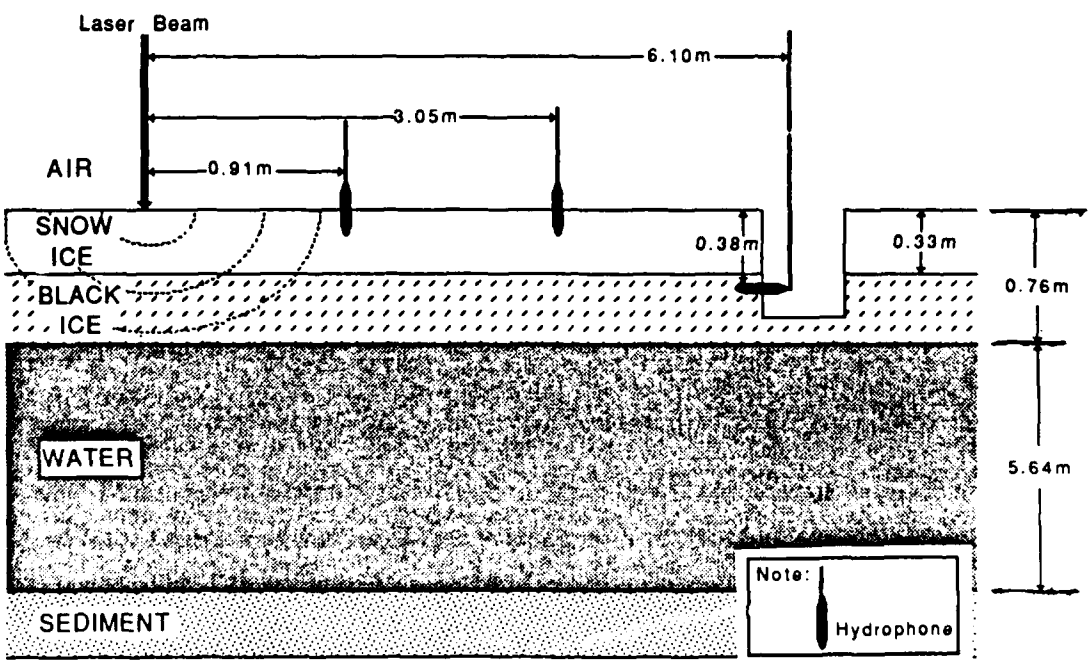

Fig. 4.5 Test configuration for measurements of sound velocity in ice

Typical acoustic hydrophone response curves have been selected from Appendix C and are shown in Figs. 4.6a - 4.6c. These curves are for the three laser impact-to-receiver distances, D, of 0.91m, 3.05m and 6.10m, respectively. The initial spike at time $t_0=0$ is the laser pulse itself, which is also used to trigger the spectrum analyzer. The next pulse train that occurs is that due to the initial acoustic pulse that reaches the hydrophone receiver at time t_1. Following this initial acoustic pulse is a complicated acoustic pulse train due to reverberation within the ice layer. This set of curves depicts these pulses occuring at later times as the horizontal distance, D, increases.

Knowing the distance between the laser impact point and the hydrophone receiver, and the measured time delay of the initial acoustic signal pulse, t_1, allows one to calculate the acoustic velocity in ice. The velocity calculations were made using the data shown in Appendix C. These results yield an average acoustic velocity of sound in ice of 3785 $\pm$100 m/s. This value compares with the compressional wave speed in hard ice reported in the literature of 3500 to 3800 m/s (Bogorodskii et al., 1976; Gavrilo et al., 1980). Velocity calculations for Figs. 4.6a - 4.6c are given in Table 4.1.

Table 4.1. Calculated ice sound velocity derived from hydrophone data

Distance between hydrophone & laser impact, D (m)	Time t_1 (ms)	Calculated sound velocity in ice (m/s)
0.91	0.24	3810
3.05	0.84	3630
6.10	1.60	3810

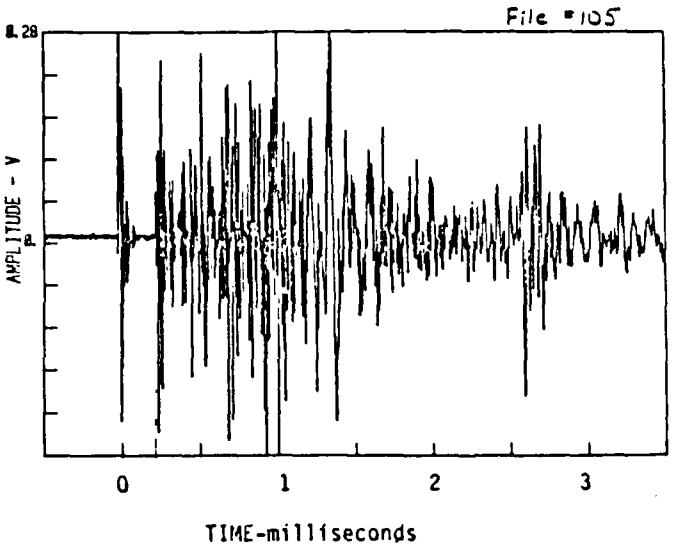

Fig. 4.6a Hydrophone receiver on ice surface
D = 0.91m

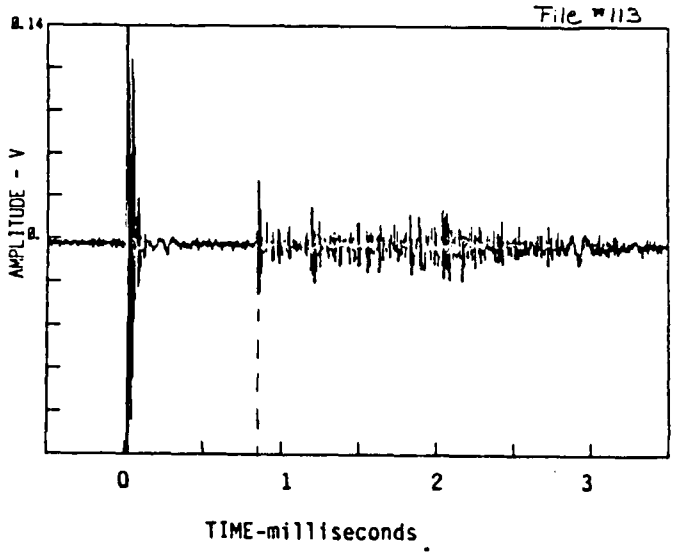

Fig. 4.6b Hydrophone receiver on ice surface
D = 3.05m

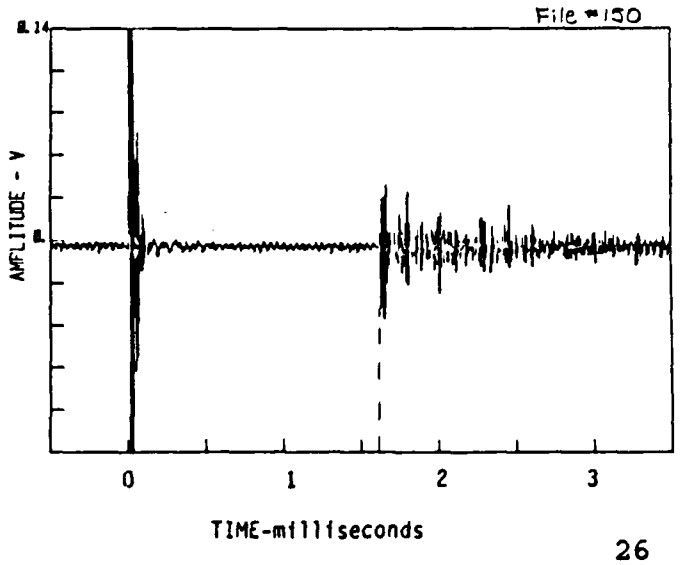

Fig. 4.6c Hydrophone receiver 0.38m into ice
D = 6.10m

4.2 HYDROPHONE MEASUREMENTS IN WATER

Objective - to investigate the transmission of sound through the ice layer and coupling into the underlying water.

Holes were drilled through the ice at distances, D, ranging from 3.05m to 9.14m and a hydrophone attached to the end of a wood pole was lowered to water depths, d, of approximately 1.0, 1.8, and 2.3m. Figure 4.7 is a diagram of the test configuration used in this set of measurements.

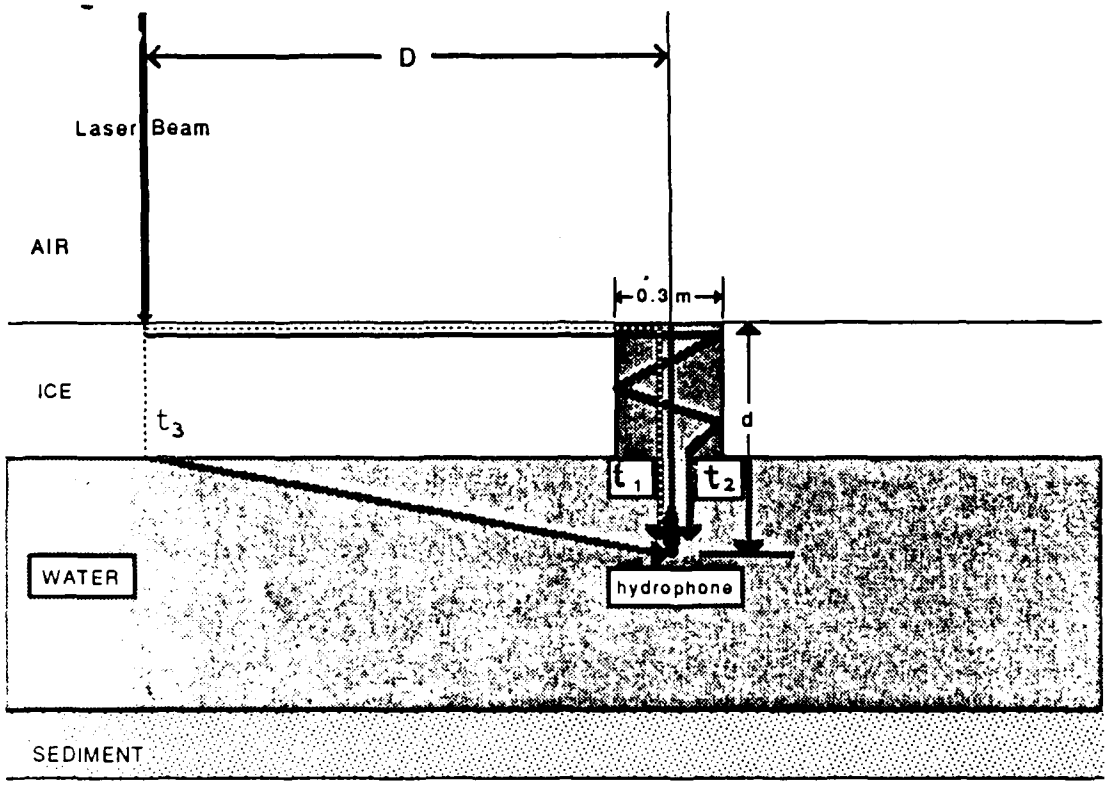

Fig. 4.7 Test configuration of hydrophone - ice/water measurements

Figures 4.8a - 4.8d are typical acoustic response curves obtained with a hydrophone as it was lowered into the water through drill holes at distances of 3m and 6m from the laser impact spot on the ice. The times when the various acoustic

signals are detected by the hydrophone are marked on these curves at t_1, t_2, and t_3. The analysis of these signals is as follows.

One postulates that acoustic signals t_1, t_2, and t_3 travel the paths as shown in Fig. 4.7. The first acoustic signal detected at t_1 could travel through the top surface of the ice into the water hole and down through the water to the receiver. The second signal, t_2, also travels through the top ice surface and then down into the water where the sound is propagated by repeated reflections within the ice hole. This effect is similar to "sound channels" in the Arctic regions (Urick, 1975). The third signal, t_3, appears to travel straight down through the ice (0.76m) and through the water to the receiver. Table 4.2 is a comparison of the measured and calculated times of these three acoustic signals. These calculations assume the velocity of sound in ice is 3785 m/s as determined in section 4.1, and the velocity of sound in water is 1400 m/s (Urick, 1975). Due to the complexity in calculating the acoustic reverbation in the sound channel (ice hole), the time, t_2, that the second signal reaches the hydrophone at a depth of 0.9m is only measured. This value is used to calculate the expected return time of the signal for different hydrophone depths. The measured values compare with the calculated values to within 5% for signals t_1 and t_2 and 10% for signal t_3.

To determine the transmission loss of sound traveling through the ice/water interface into the water, the maximum SPL of the acoustic signal in the ice and in the water for a given distance, D, was determined from the data. The difference between the SPLs detected in the ice and water is approximately 7 dB. This compares with the theoretical value of 5 dB predicted using the Rayleigh formula.

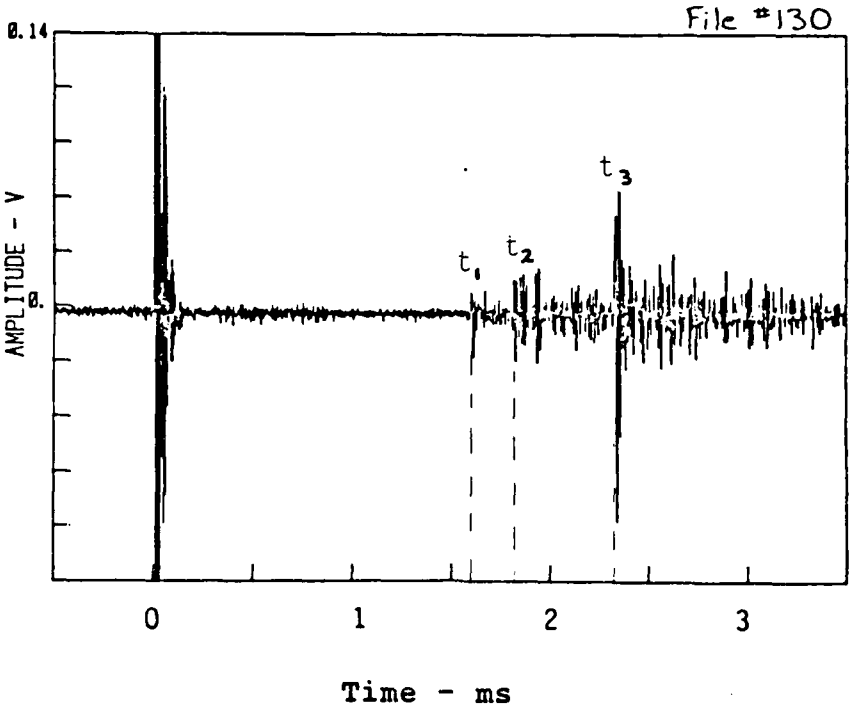

Fig. 4.8a. Hydrophone receiver in water
D = 3.05m, d = 0.91m

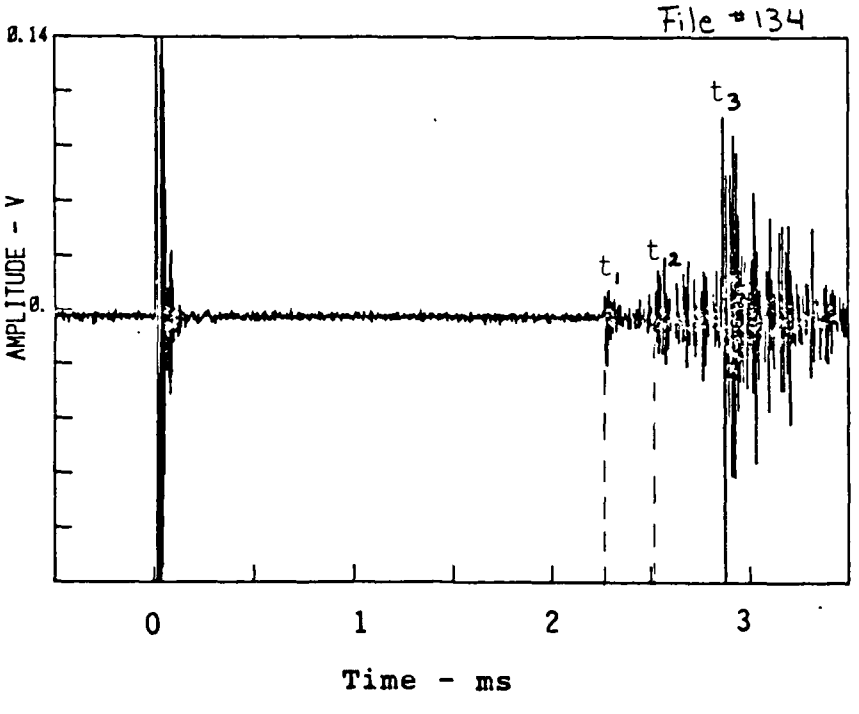

Fig. 4.8b. Hydrophone receiver in water
D = 3.05m, d = 1.83m

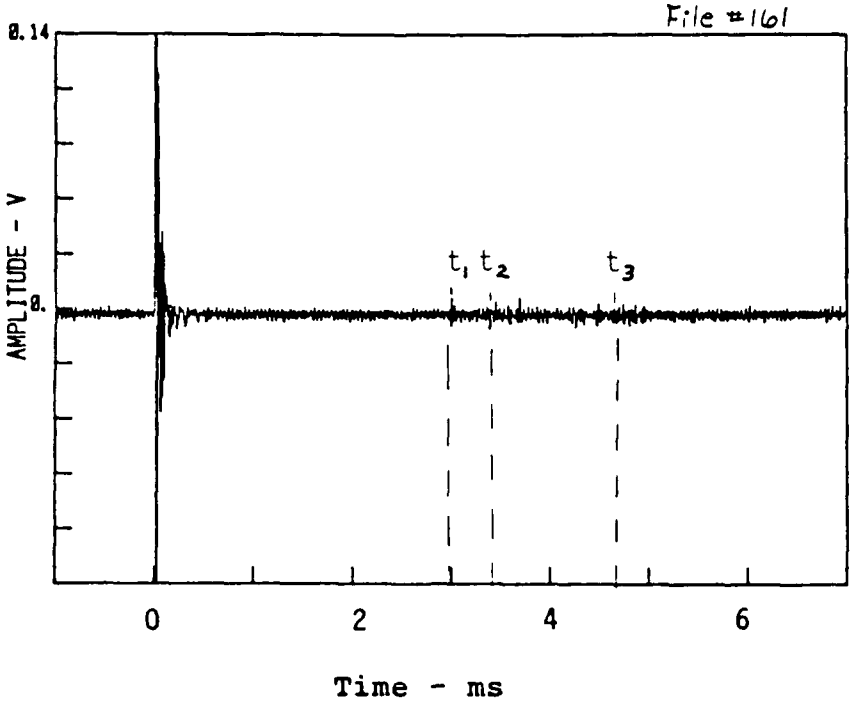

Fig. 4.8c Hydrophone receiver in water
D = 6.01m, d = 1.83m

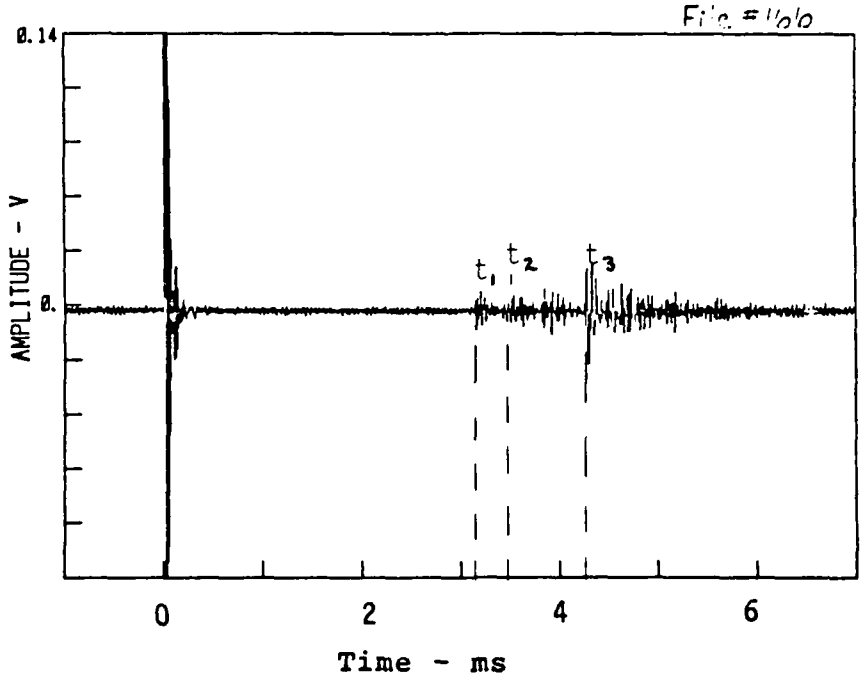

Fig. 4.8d Hydrophone receiver in water
D = 6.10m, d = 2.29m

Table 4.2 Comparison of Measured vs Calculated Acoustic Signal Time - Hydrophone in Water

D (m)	d (m)	Time - ms									File No.
		t_1			t_2			t_3			
		Exp	Calc	Δ	Exp	Calc	Δ	Exp	Calc	Δ	
3.05	0.91	1.59	1.46	0.13	1.81	--	--	2.33	2.38	0.05	130
3.05	1.83	2.30	2.12	0.18	2.50	2.46	0.04	2.90	2.51	0.39	134
6.10	1.83	3.00	2.92	0.08	3.30	3.26	0.04	4.30	4.65	0.35	161
6.10	2.29	3.20	3.25	0.05	3.50	3.59	0.09	4.30	4.69	0.39	166
			AVG:	0.11		AVG:	0.06		AVG:	0.30	

Note: Exp = Experimental
Calc = Calculated
Δ = Difference between experimental and calculated values

4.3 MICROPHONE MEASUREMENTS IN AIR

Objective - to measure the time and amplitude of the acoustic signal reflected from the ice/water interface deploying a microphone in air -- the signal strength is used to determine the transmission loss through the ice/air interface, while the return times are used to determine ice thickness (see Section 5.0).

Figure 4.9 shows the test set-up for the microphone measurements. The microphone was suspended above the ice surface from a wooden rod which was supported on each side by a sawhorse. Measurements of the acoustic response were made with the microphone placed at a distance, D, from the laser impact spot ranging from 0.91m to 1.83m at heights above the ice surface of 0.46m and 0.51m.

Figure 4.10 is a typical microphone measurement of the laser generated signals. This figure shows the spike associated with the firing of the laser occurring at $t_0=0$, followed by the acoustic signal reflected from the ice/water interface, t_1, and the airblast. The acoustic paths of these signals are shown in Fig. 4.9. Note: the large signal occurring at t_0 is caused by RF interference.

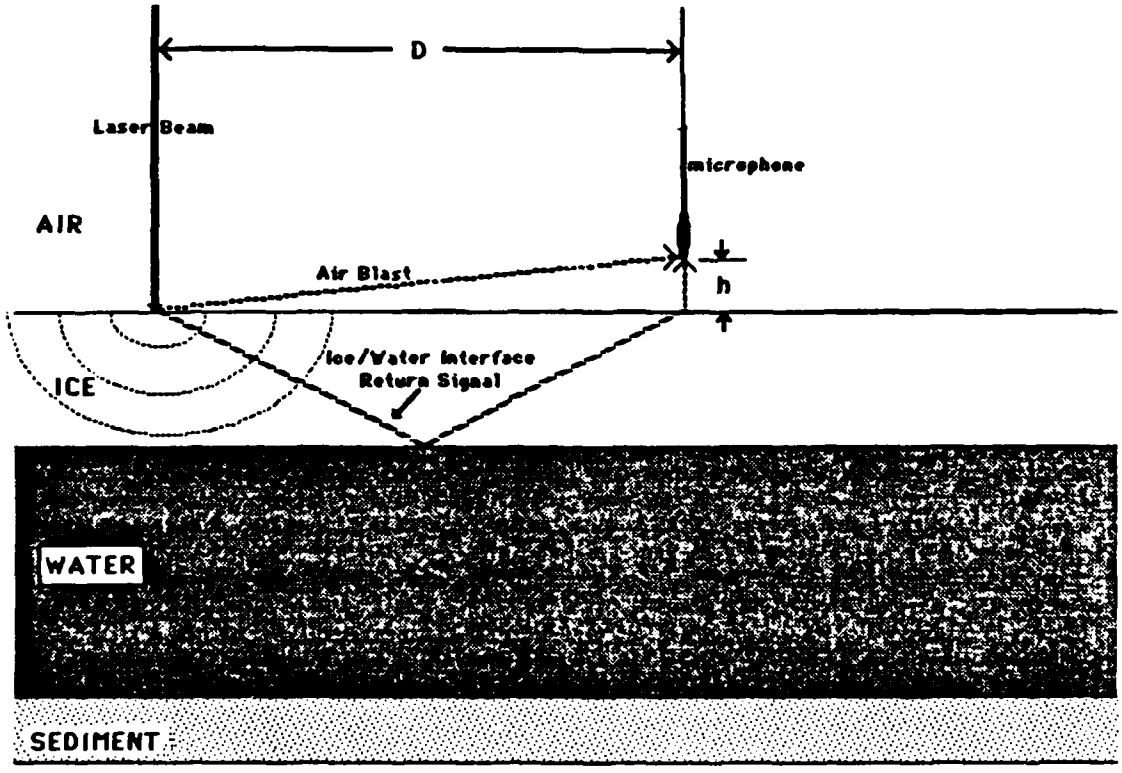

Fig. 4.9 Schematic diagram of microphone measurements

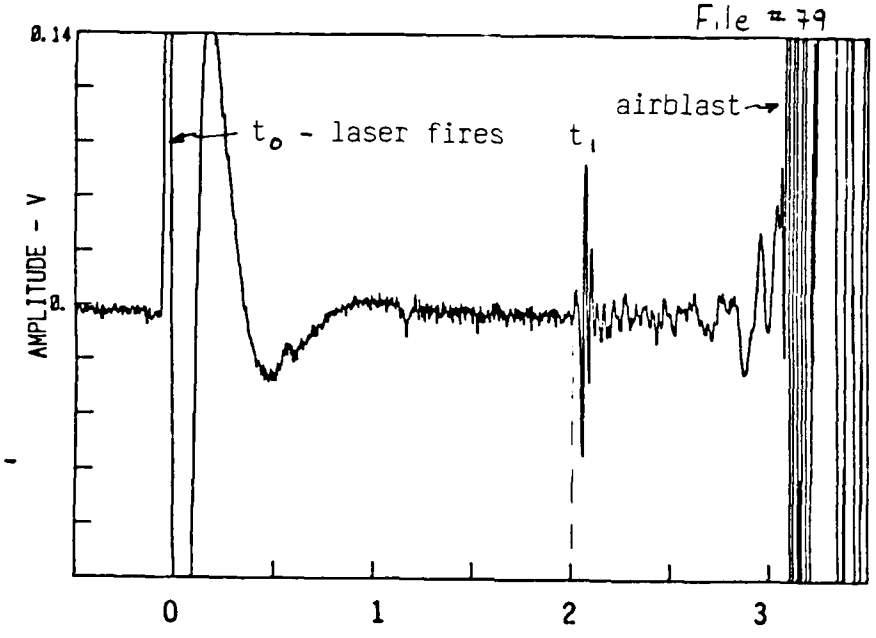

D = 0.91m
h = 0.46m

Fig. 4.10 Microphone receiver response

The loss in signal intensity through the ice/air interface, was measured by positioning the hydrophone (Fig. 4.11) in ice directly under the microphone position (Fig. 4.10).

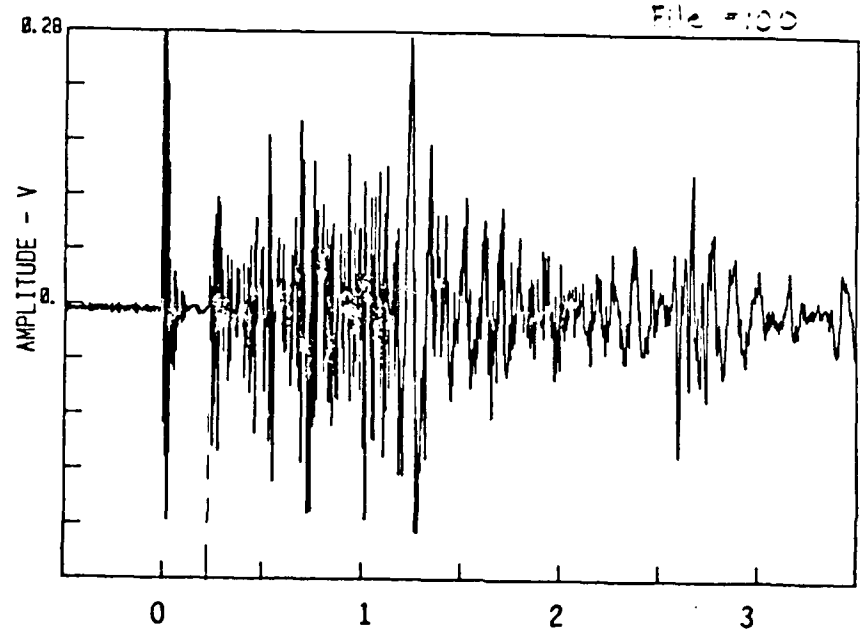

D = 0.91m
d = 0

Fig. 4.11 Hydrophone receiver response

Acoustic Transmission Loss Through Ice/Air Interface:

The following calculation is used to convert the voltage reading of the acoustic signals to a SPL:

Volt reading (V) = SPL (re 1 uPa) * Sensitivity(V/uPa)

SPL (dB re 1 uPa) = Volt reading (dBV) - Sensitivity (dBV/uPa).

The sensitivity of the microphone and hydrophone system at the input to the spectrum analyzer (or oscilloscope) is given below:

Microphone System Sensitivity(S_M):

$$\begin{array}{rl} -38.8 & \text{dB re 1V/Pa (microphone)} \\ +40 & \text{dB (amplifier gain)} \\ \hline S_M = & 1.2 \text{ dB re 1V/Pa} = -118.8 \text{ dB re 1V/uPa} \end{array}$$

Hydrophone System Sensitivity(S_H): hydrophone amp setting (10 mV/Pa)

$$S_H = -160 \text{ dB re 1V/uPa}$$

The peak-to-peak voltage of the ice/water interface pulse, t_1, detected with the microphone from Fig. 4.10 is 0.074 V (-22.6dBV) which corresponds to the following SPL:

$$\begin{aligned} \text{SPL} &= -22.6\text{dBV} + 118.8 \text{ dB re 1V/uPa} \\ &= 96.2 \text{ dB re 1V/uPa.} \end{aligned}$$

The peak-to-peak voltage of the direct pulse (first pulse) detected with the hydrophone from Fig. 4.11 is 0.15 V (-16.6dBV) which corresponds to the following SPL:

$$\begin{aligned} \text{SPL} &= -16.6\text{dBV} + 160 \text{ dB re 1V/uPa} \\ &= 143.4 \text{ dB re 1V/uPa.} \end{aligned}$$

The transmission loss which occurs when the signal travels from the ice into the air across the ice/air interface is then

$$\begin{aligned} \text{TL} &= 143.4 - 96.2 \\ &= 47.2 \text{ dB.} \end{aligned}$$

Simultaneous measurements were also made with the hydrophone in the ice and the microphone in the air at the same distance, D. These measurements were recorded on a dual channel digital oscilloscope and then photographed. A typical acoustic response using both receivers simultaneously is shown in Fig. 4.12. The SPL of the signal detected in air and ice is 101.7 and 157.5 dB re 1V/uPa, respectively, which translates to a transmission loss of 55.8 dB. The 9 dB difference between this simultaneous recording and the above individual recordings is probably due to changes in incident (laser spot) energy density caused by fluctuations in the laser itself and also by focusing differences caused by slight differences in the test set-ups (ie. adjustment of the 45 deg mirror and telescope setting). An average of 10 measurements yielded a value of the transmission loss through the ice/air interface of 52 dB. This value is between the value predicted by the Rayleigh formula for the signal passing from snow to air (38 dB) and for the signal passing from ice to air (70 dB).

Oscilloscope Settings:
Horizontal=0.5ms/div

a) Microphone
Vertical=0.2V/div
h = 0.46m

Note:
1 div = 6.5mm

b) Hydrophone
Vertical=0.5V/div
d = 0m

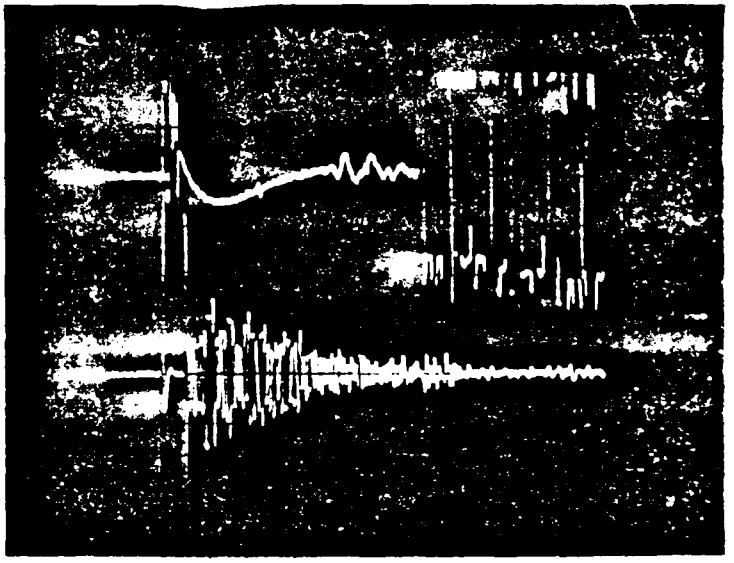

Fig. 4.12. Simultaneously recorded a) microphone and b) hydrophone measurements (D = 0.91m).

4.4 MICROPHONE MEASUREMENTS IN AIR WITH SNOW COVER

Objective - to investigate the effect of snow overlying the ice surface on the acoustic signal strength detected with a microphone.

The microphone was mounted above the ice, as described in the previous section, at a distance D ranging from 1.07 to 1.22m and height of 0.46m. The acoustic signal going through a 0.10m snow layer at the laser impact spot and/or a 0.10m snow layer between the microphone and the ice surface was of sufficient strength to be detected. (see Appendix C). A similar test was performed during the March 1983 tests at a microphone distance D of 0.76m and height of 0.30m. The signal was detected after it passed through a 0.15m layer of snow between the ice surface and microphone. Fig. 4.13a and 4.13b is a comparison of the microphone response without and with snow, respectively. As expected, the snow decreases the intensity of the return signal from the ice/water interface. The transmission loss is measured to be approximately 20 dB. Note: the first signal detected by the microphone at t_1 (the ice/water return pulse) arrives later if the signal passes through an additional snow layer. This increased delay time results from the slower sound velocity in snow (220 m/s) than in air (330 m/s).

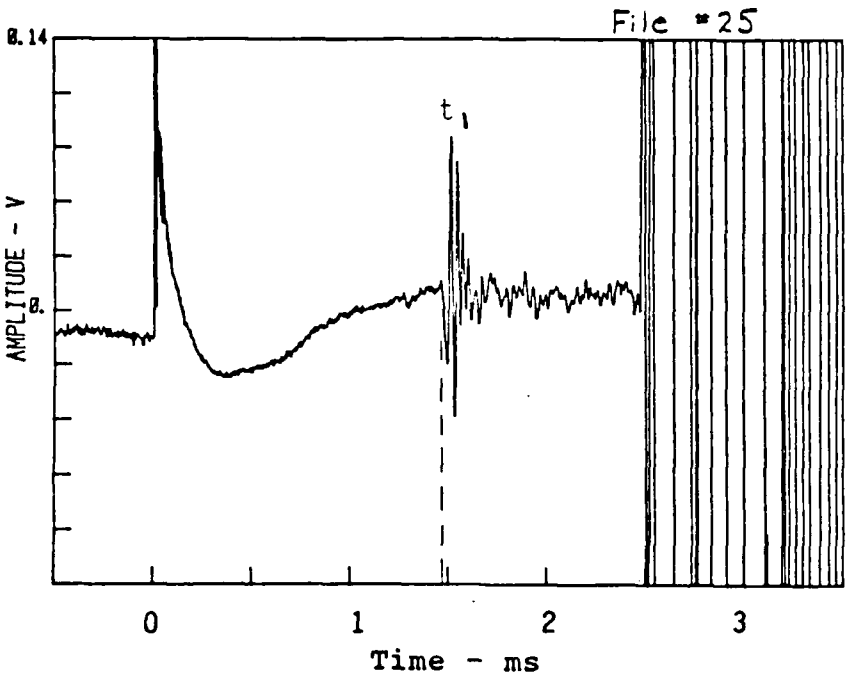

Fig. 4.13a. Microphone receiver - no snow
D = 0.76m, h = 0.30m

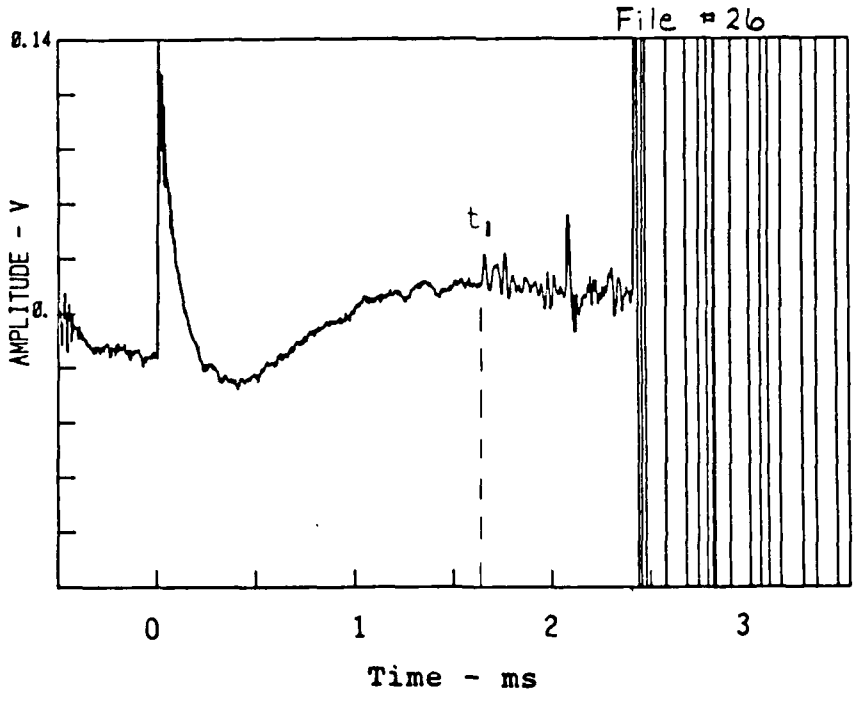

Fig. 4.13b. Microphone receiver - 15 cm snow between receiver and ice
D = 0.76m, h = 0.30m

5.0 ICE THICKNESS CALCULATIONS

The following sketch is used to derive ice thickness from a typical acoustic signal return time:

File No. 79

D = 0.91 m
h = 0.46 m

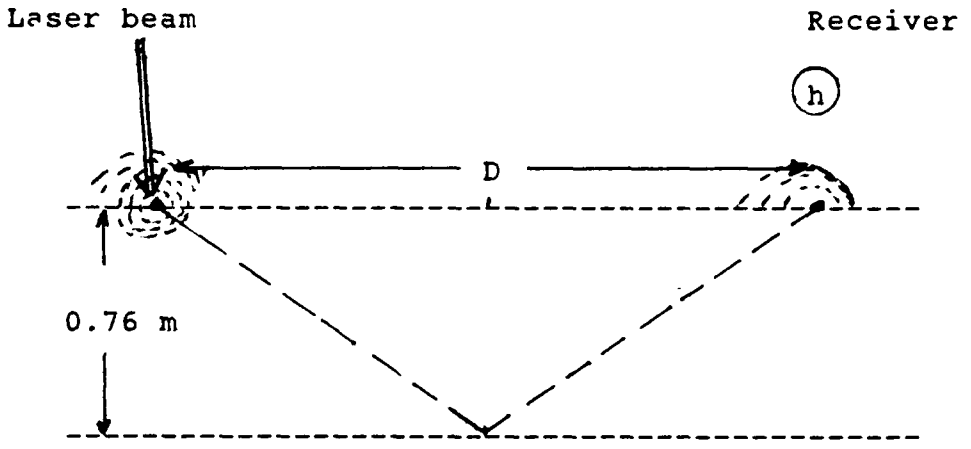

Distance in ice: 1.77 m c (ice) = 3785 m/s
Distance in air: 0.46 m c (air) = 330 m/s

Time (ice) = 0.47 ms
Time (air) = 1.39 ms
Total = 1.86 ms

This calculated time of 1.86 ms is to be compared with the measured time of 2.00 ms, i.e., a difference of 0.14 ms.

The measured time (2.00 ms) of the received acoustic pulse is now used to calculate a value of 1.00 m for the ice thickness. Since the ice thickness was measured as 0.76 m at Moosehead Lake, there is a discrepancy of 26 cm.

These calculations are repeated for two other cases of slightly different values of D and h, with/without snow on top of the ice. These results are given in Table 5.1. The three files shown in this table are representative of the large number of laser/acoustic results given in Appendices C and D.

Table 5.1 Ice Thickness Calculations for Typical Microphone Data

D (m)	h (m)	Snow layer (m)	Return signal Time-ms Exp	Calc	Δ	Ice Depth (m)	File No.
0.91	0.46	-	2.00	1.86	0.14	1.05	79
0.76	0.30	-	1.49	1.36	0.13	1.03	25*
0.76	0.30	0.15	1.65	1.59	0.06	0.89	26*

Exp - Experimental
Calc - Calculated
Δ - Difference between experimental and calculated values
* - March 1983 results

The above calculations used the sound velocity of 3785 m/s that was measured in section 4.0 and the velocity of sound in air (at -7° C) of 330 m/s.

The main parameters that affect the accuracy of the measurement of ice thickness are: (1) the determination of the height of the microphone receiver, (2) the velocity of sound in snow/ice, and (3) the velocity of sound in air.

Microphone Height

Table 5.2 gives the error in the calculation of ice thickness as a function of ice thickness and microphone height for height uncertainties of 5 and 10 cm. This table shows a nearly constant absolute error of 60 cm for a 10 cm microphone height uncertainty, and a 30 cm error for a 5 cm height uncertainty. This has the effect of having a large percentage error in the measurement of thin ice (1 m). However, for thick ice ($\geq$ 5 m) the uncertainty of the microphone's height above the ice surface has substanially less effect ($\leq$ 10%) on the determination of ice thickness.

In the example shown in this section, a change of only 4 cm in the microphone's height (10%) results in agreement between the measured and calculated values for ice thickness.

Table 5.2 Errors in Ice Thickness Determination For Microphone Height Uncertainties of (a) 10 cm, (b) 5 cm.

Ice Thickness (m)	Height Uncertainties 10 cm	5 cm
1	61 cm (60%)	31 cm (30%)
5	58 cm (10%)	29 cm (5%)
10	57 cm (5%)	28 cm (2.5%)

Velocity of Sound in Ice

The sound velocity in ice is another parameter which must be considered. The percentage error in the measurement of ice depth is directly proportional to the error in the velocity of sound in the ice; therefore, a 10% error in the ice velocity will result in a 10% error in ice depth. If a nominal value is chosen for sound velocity in ice that is characteristic of the region in which one is operating the laser-acoustic system, any uncertainty in the velocity of sound in ice should constitute only a small amount to the total error budget in the calculation of ice thickness.

Velocity of Sound in Air

The third parameter which affects the measurement accuracy of ice thickness is a knowledge of the velocity of sound in air. A typical air temperature during our measurements was -7° C. A sound velocity in air corresponding to this temperature of 330 m/s was used in the calculations. A 5° error in the air temperature is calculated to produce a 3 m/s error in the sound velocity. This results in a 2 cm error in the determination of the ice thickness for the case where the microphone is at a height of 0.5 m. This error is directly proportional to the height of the microphone, i.e., at 10 m the ice thickness error has increased to 40 cm. Reducing the error in temperature to 1° reduces the error in ice thickness measurement to 8 cm.

6.0 SUMMARY

6.1 EXPERIMENTAL RESULTS

The results of the Phase I effort show that it is feasible to measure ice thickness using the laser-acoustic technique. The acoustic signals generated in the ice by the CO_2 laser are of sufficient strength to be reflected off the ice/water interface and be detected by a receiver in the air. Approximately 180 laser shots were recorded for the purpose of measuring water/ice/air parameters required for determing ice thickness. The nominal distances of the hydrophone and microphone were as follows: (1) maximum horizontal distance of the hydrophone in ice from the laser impact was 9 m, (2) the maximum horizontal distance of the microphone in air from the laser impact was 2 m, and (3) the height of the microphone above the ice surface was 0.5 m. The following conclusions are made:

- The velocity of sound in ice was measured as 3785 m/s, which is in agreement with values occurring in the literature which range between 3500 - 3800 m/s.

- The SPL of the acoustic signal reflected from the ice/water interface as detected with a microphone near the ice surface was measured as 110 dB re 1 uPa. This value agreed to within 10 dB of the calculated value.

- Simultaneous measurements of the hydrophone and microphone signals (in ice and air) resulted in a direct measurement of the transmission loss at the ice/air interface of 52 dB. This value compares with the theoretical value ranging between 38-70 dB, depending on the ice/snow conditions.

- An additional 20 dB transmission loss was observed when there was a 15 cm snow layer on the ice.

- A transmission loss of 7 dB was observed at the ice/water interface -- compares with the theoretical value of 5 dB.

- The ice thickness derived from the laser-acoustic measurements yielded a value of 1.0 m, while the actual value was measured as 0.76 m. This result is highly dependent on the accuracy of the measurement of the height of the microphone. For example, a 4 cm error in the microphone's height could account for the apparent error in the ice thickness determination.

6.2 AIRBORNE SYSTEM OPERATION

The feasibility of extending and refining this technique into an airborne operational system to remotely measure ice thickness appears to be quite promising. One of the critical factors to be considered is environmental and system noise.

Signal to Noise Calculation

The signal to noise ratio (S/N) for a microphone receiver located in the air above the ice surface is given below.

The SPL of the desired ice/water return pulse, SPL_S, measured at the ice surface by a microphone in the air for an ice thickness of approximately 1m is calculated using the following sonar equation:

$$SPL_S = SPL_o - RL - TL - 20\log r - \alpha r$$

where SPL_o = SPL at 1m depth in ice
= 187 dB re 1 uPa (measurement)
RL = reflection loss at ice/water interface
= 7.6 dB (theory)
TL = 52 dB (measurement)
r = acoustic path length
= 2m (vertical depth of 1m)
α = acoustic attenuation coefficient in ice
= 0.45 dB/m (10 kHz)

or,

$$SPL_S = 120.5 \text{ dB re 1 uPa.}$$

This value compares with the measured SPL of 110 dB re 1 uPa. The latter value is used in the following signal to noise calculations.

To calculate the SPL_S measured by a microphone at different altitudes, h, additional losses due to spreading loss in air and absorption must be included. It is assumed that the absorption coefficient for air is 0.1 dB/m at 10 kHz (see Fig. 2.6) and that the spreading loss is (10 log h). Since the total loss occurring in air for a microphone receiver at an altitude of 20m is

calculated to be 15 dB, the SPL measured by the microphone (SPL_R) at 20m is

$$SPL_S = 110 - 15 = 95 \text{ dB re 1 uPa.}$$

The signal strength can be increased if the laser energy is increased. For instance, the laser energy measured in the in-situ experiments was 6.5 J. Increasing the laser energy to 15 J (the rated energy of the CO_2 TEA Lumonics laser) increases the acoustic signal strength by 4 dB, while increasing it to 50 J increases the signal strength by 9 dB.

The SPL of the helicopter noise used in the S/N calculations is 70 dB re 1 uPa/1 Hz (BW). This SPL is an average value determined from the literature (Brown, 1972) and from actual helicopter noise measurements made by AST shown in Fig. 6.1.

$$\begin{aligned} SPL_N &= 70 \text{ dB re 1 uPa/1 Hz (BW)} \\ &= 70 \text{ dB re 1 uPa} + 10\log BW \\ &= 110 \text{ dB re 1 uPa (10 kHz)} \end{aligned}$$

where BW is the bandwidth in Hz.

Through noise reduction techniques, the noise level can be reduced. Fig. 6.1 shows that even by crude shielding of the microphone, using acoustic foam can reduce the noise level by 20 dB. It is estimated that the noise can further be reduced by at least 10 dB by additional shielding and signal processing techniques -- resulting in a helicopter noise of 80 dB re 1 uPa for a 10 kHz BW.

The signal to noise ratio for an ice depth of 1 m measured by a microphone (10 kHz BW) at an altitude of 20 m is then:

$$\begin{aligned} S/N &= SPL_S - SPL_N \\ &= 95 \text{ dB} - 80 \text{ dB (re 1 uPa)} \\ &= 15 \text{ dB} \end{aligned}$$

Fig. 6.2 shows the S/N ratio for ice depths ranging from 1 to 10 m for a microphone receiver at an altitude of 20 m and laser energies of 6.5 J, 15 J* and 50 J* (Note: 15 J* and 50 J* curves include a 20 dB gain from receiver improvement as discussed below). For example, assuming a S/N of 10 dB is required to detect the signal, approximately 2 m of ice can be detected using a 6.5 J laser. Increasing the laser energy to 50 J enables measurement of 10 m of ice.

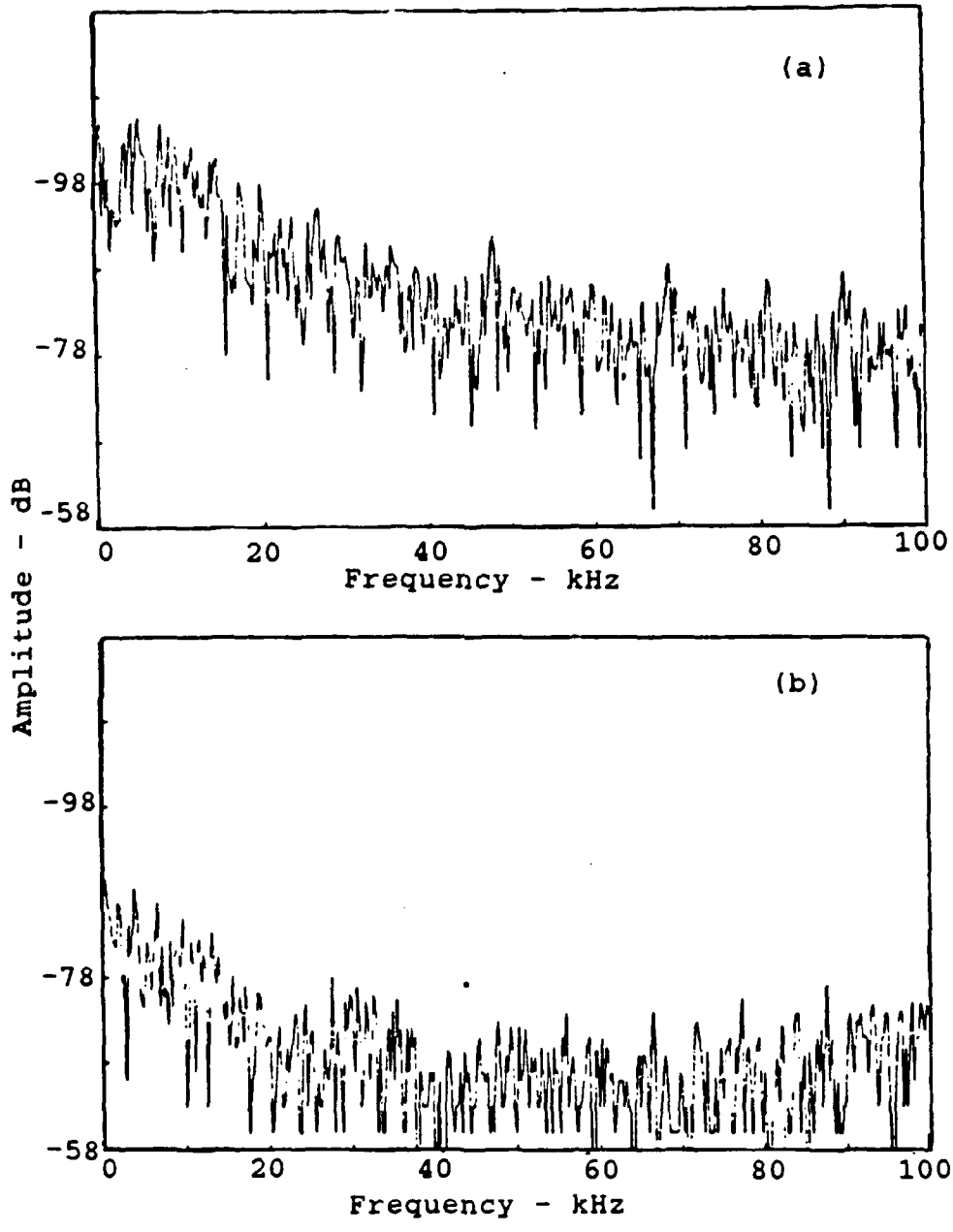

Fig. 6.1 Bell 47D1 helicopter spectra - microphone at 3 m a)Unshielded, b) Shielded with foam.

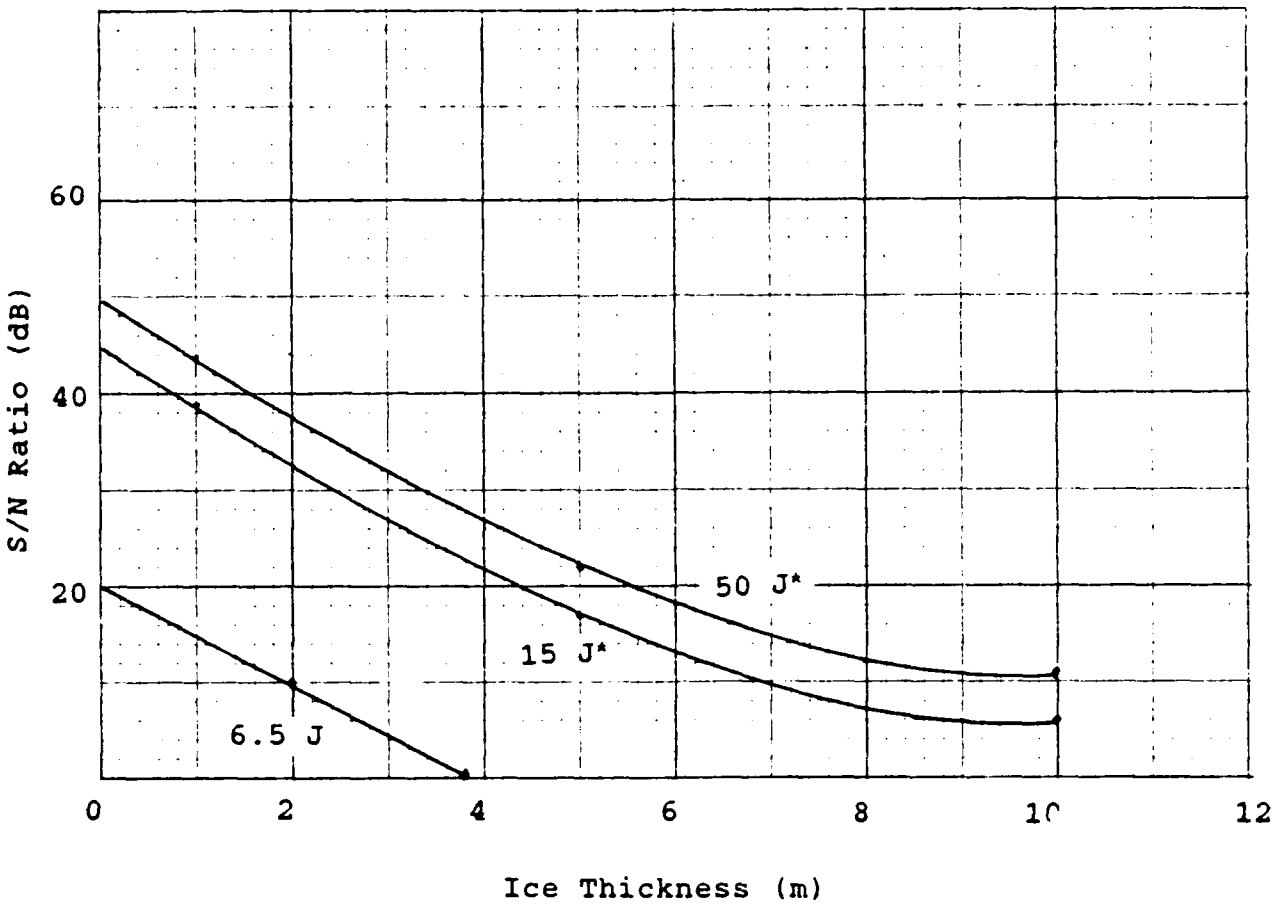

Fig.6.2 Airborne detection S/N at altitude of 20 m

Receiver Improvements

A previous report (Hickman and Edmonds, 1981) showed that it was fairly straight forward to obtain gains of 20 dB-30 dB with paraboloid reflectors in the order of 0.5 m in diameter. Other possible receiver improvements are: (1) a single large aperture reflector with a multiplicity of feeds on the focal surface, (2) a single large aperture acoustic Luneberg lens with a multiplicity of feeds, or (3) a multielement array disposed over a single large aperture from which the required beam set could be synthesized.

Operational Scenario

A potential operational scenario for the laser-acoustic system is depicted in Figs. 6.3a and 6.3b. The laser is shown operating from the helicopter and hitting the ice surface. The receiver is located on a tethered bird that is flying close to the ice. In the calculation of the S/N ratio, it was determined that a reasonable receiver altitude would be 20 m. Acoustic shielding on the bird will be used to reduce the helicopter noise at the receiver.

An adjustable infrared telescope on the helicopter will focus the laser to the required energy density to cause acoustic breakdown of the laser beam on the ice surface. A laser altimeter will be used on a pulse-to-pulse basis to feedback accurate altimeter data to adjust the focusing telescope. The digitization of the acoustic signal will be performed in the bird, while the main signal processing will be performed in the helicopter.

The area coverage of the laser-acoustic sensor in a stand-alone mode is depicted in Fig. 6.3b. For a flight time of 4 hours, a laser repetition rate of 1 pps and platform velocity of 45 m/s (100 mph), a matrix of data points will be generated covering an area of 5 km on a side having a grid spacing of 50 m. In certain applications the laser-acoustic system is valuable as a stand-alone sensor, i.e., for relatively small areas to be surveyed such as aircraft landing strips or ground truthing for other localized area experiments.

An important application of the laser-acoustic system is as the yardstick to calibrate other ice sensors, such as active microwave which is used to identify first and second year ice to infer ice thicknes. The footprint of the laser-acoustic system is much smaller than the current remote sensors used in ice research. This footprint is a function of the receiver directivity and aircraft altitude. For example if the receiver has a directivity of between 1° and 10° and operates from an altitude of 20 m, the horizontal footprint would be in the order of 0.3 to 3 m. This is to be compared with an aircraft SAR footprint of 30 m and a satellite footprint of 30 km.

It appears like there is a definite place for the helicopter laser-acoustic system as a remote sensor for directly measuring ice thickness. Currently, there is no remote sensor available for directly measuring ice thickness.

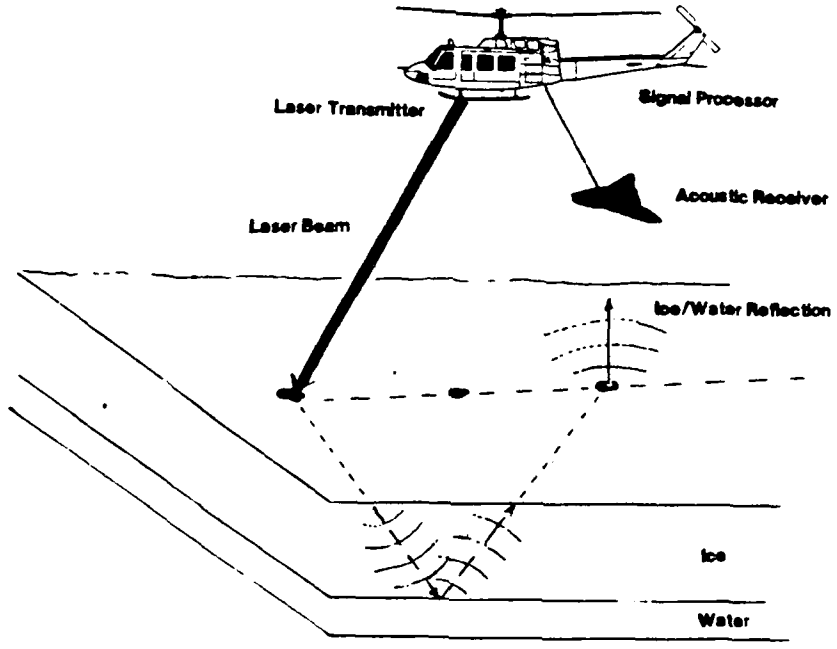

(a) Helicopter operation of system

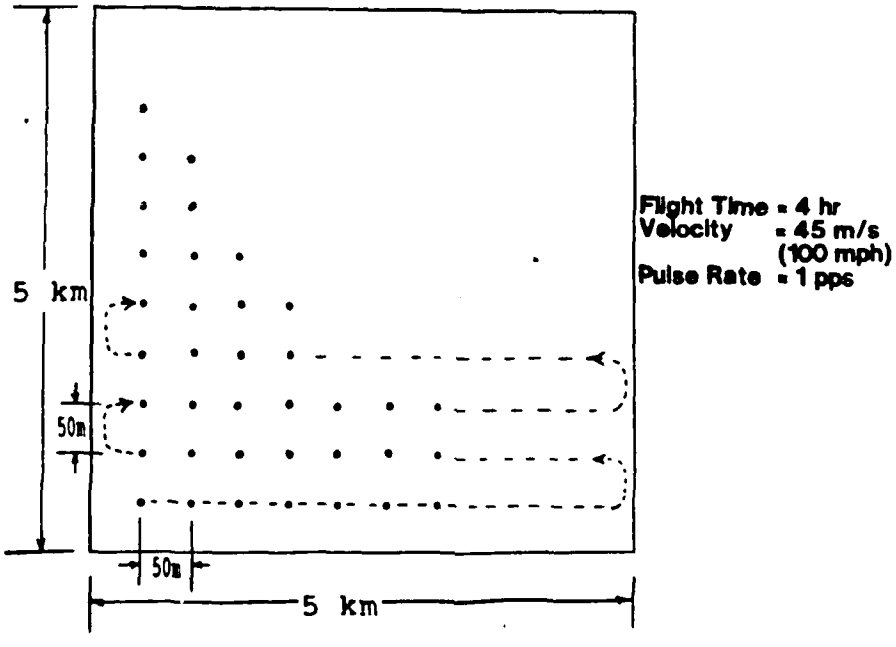

(b) Area coverage

Fig. 6.3 Potential operational scenario

Appendix A. Summary of Current Ice Thickness Measurement Techniques

This is a brief description of the various sensors that have been investigated for their use in directly measuring or inferring ice thickness. The following sensors and or techniques discussed here are visible, infrared, microwave, impulse radar, airborne electromagnetic and laser profilometer. In conclusion, a comparative list of the salient characteristics of each is given.

A.1 Visible and Infrared Sensors

Visible, near infrared and thermal infrared sensors onboard Landsat and the NOAA weather satellites can provide information relative to lake depth and ice thickness. Considerable analysis has been performed to classify ice types by noting tonal differencs in the satellite imagery and thereby infer relative ice thickness (Foster et al., 1978; Sellman et al., 1975; Leshkevich, 1981; Wartha, 1977; Assel et al., 1979; Wiesnet, 1979). In some cases ice age (first-year or multiyear) can be qualitatively determined using visible and infrared imagery. Multiyear ice floes have greater surface roughness due to greater deformation than first-year floes. The edges of multiyear floes are not as angular as are the edges of first-year floes.

Landsat imagery, available since 1972, has a spatial resolution of 30 m for visible, near-infrared and middle infrared data and a resolution of 120 m for thermal infrared data. It has a swath width of 185 km, and data are not collected continuously along each orbit. Each frame is imaged once every 18 days for Landsats 1,2 and 3 and once every 16 days for Landsats 4 and 5. The Landsat satellites operate in near-polar sun-synchronous orbits (USGS, 1979). The NOAA satellites operate in orbits similar to the Landsat orbits except at a higher altitude, allowing greater coverage per scene and more frequent coverage (twice daily) but poorer resolution. Visible and infrared images from the NOAA satellites have a resolution of approximately 1 to 4 km and a swath width of 3,000 km (Lillesand and Kiefer, 1979).

A major disadvatage of the sensors operating in the visible and near infrared wavelengths is that they cannot produce an image through clouds and require sunlight. Thermal infrared data can be obtained at night but not through cloud cover. Additionally, thermal infrared data is of marginal utility during the summer as the surface temperature of the ice approaches the sea

surface temperature. Another drawback to using visible and infrared imagery for sea ice analysis is their inability to differentiate new sea ice from sea water. Ice is generally not detectable with 1 km resolution imagery until it reaches the thickness of young ice (10-30 cm) (Rosner, 1985).

A.2 Microwave Sensors

Microwave sensors are either passive or active. They are passive when they measure electromagnetic energy of thermal origin emitted from materials (emissivity). They are active when they send coherent energy from their own source and measure the reflected energy from the target. Microwave sensors rely mostly on the detection of dielectric properties of the material. The microwave response is also affected by volume scattering caused by inhomogeneity in the material and its surface roughness, and of course by instrument parameters such as wavelength, polarization and incidence angle.

Microwave data is advantageous for remotely monitoring ice conditions because it can be obtained day or night and through most cloud cover. It offers the capability for wide area coverage from satellite altitudes. Presently, however, the data is more difficult to interpret than visible, near-infrared and thermal infrared data because so many factors influence the microwave response.

A.2.1 Passive Microwave

Passive microwave sensors measure the brightness temperature (TB) of the Earth's surface with a radiometer. TB is given by the product of the emissivity of the material times its physical surface temperature. The dielectric constant, which strongly influences the emissivity, changes in the presence of water. Water is a highly polarizing material and has a large dielectric constant, 80, in the microwave range. It is therefore highly reflective and has a low emissivity of 0.3 to 0.5. Ice has a much lower dielectric constant, 3.2, and higher emissivity of 0.8 to 0.92, depending on ice type. Because of this variation, there is a striking TB difference between the "warmer" ice and "colder" water (Swift et al., 1980)

Microwave data is useful in inferring ice thickness of lake ice. A uniform slab of freshwater ice will emit microwave radiation in a quantity proportional to its thickness. In clear

smooth lake ice where there are few scatterers, the emissivity is predominantly affected by the ice/air interface, the ice/water interface, the attenuation coefficient and the ice thickness. Bubbles present in the ice, and the ice/water interface at the bottom of the ice sheet scatter the microwave radiation and lower the emissivity, causing a decrease in the effective TB. (Swift et al, 1980).

The depth of penetration of upwelling microwave radiation through ice and snow is wavelength dependent. Longer wavelength microwave radiation can be sensed from deeper within the ice than can shorter wavelength radiation. For freshwater lake ice studies, short wavelengths, e.g. 0.81cm (37 GHz) to 1.4cm (22.22 GHz) sense the snow overlying the ice while longer wavelengths, e.g. 6.0cm (5.0 GHz), 21.0cm (1.4 GHz) and longer sense the entire thickness of the ice and the ice/water interface. At the short wavelengths the overlying snow is contributing more to the observed TB than is the ice because snow grains are large with respect to the radiation to cause scattering. However, snow grains are generally not large, compared to 6.0 or 21.0 cm radiation to cause significant scattering. Therefore, brightness temperature decreases with increasing wavelength (or increasing penetration through the ice) because the longer wavelength radiation is emanating from the underlying water at the ice/water interface, and water has a very low emissivity and TB (Hall et al., 1981).

Microwave data is also useful in discriminating between first-year and multiyear sea ice from which relative ice thickness is inferred . As the ice ages, brine drains out. If sea ice could be frozen very slowly, pure ice would result because of rejection of all salts during the freezing process. However, the freezing rate is normally too rapid to allow pure ice to form, thus brine is trapped in the structure of the ice. During the brine drainage process, numerous gas bubbles result. These bubbles scatter the microwave emission and contribute to a lower microwave TB in multiyear as compared to first-year sea ice.

There are ambiguities, however, in the interpretation of the brightness temperature of sea ice in the Arctic and Antarctic. In the Arctic during the summer months microwave data is not reliable. The presence of surficial meltwater obliterates the radiance from the ice below. In the Weddell Sea region of the southern ocean, low surface melt in the summers impedes the brine drainage process. Therefore, multiyear sea ice is radiometrically similar to first-year ice (Zwally et al., 1983). Also, the ice

appears newer on the microwave data than it really is due to the high percentage of frazil ice which entraps brine.

The resolution of passive microwave imagers varies as a function of altitude. Thus, low-level flights offer increased spatial resolution but a narrower swath width on the resulting imagery as compared to higher altitude flights for which the resolution is poorer but the swath is wider. High resolution from spacecraft altitudes would require the use of extremely large antennas. Surface resolution of spacecraft passive microwave sensors ranges from 30 km for the Nimbus 7 Scanning Multifrequency Microwave Radiometer (SMMR) (Swift et al., 1985) to 16 x 14 km for the Defense Meteorological Satellite's Special Sensor Microwave/Imager (SMM/I) (Lo et al., 1984).

A.2.2 Active Microwave - SAR,SLAR

Synthetic Aperature Radar and Side-Looking Airborne Radar are terrain-mapping imaging radars. While both can and are flown in airplanes, only SAR can provide high resolution images from spacecraft altitudes. SAR systems designed for satellites take advantage of the orbital motion to store and combine information from a number of pulses along the track to synthesize high resolution observations as if they were obtained via the use of a very large antenna. The Seasat SAR launched in June 1978 (no longer operable) had a resolution of 25m and a swath width of 100km (Thomas et al., 1985).

Radar imagery is useful for classifying ice types. The major factor contributing to the strength of the return is surface roughness. The freshwater ice types which have been identified using SAR range from smooth black ice which gives low radar returns to very rough ice with correspondingly higher (brighter) radar returns. (Bryan and Larson, 1975). First-year and multiyear sea ice have also been distinguished because the roughness of sea ice often increases as the ice ages. The relative thickness of the ice can then be inferred since multiyear sea ice is usually thicker. (Zwally and Gloersen, 1977). Although no quantitative assessment can be made of the ice thickness, knowledge of the location of such areas is useful to the shipping industry because rough ice is usually very difficult to negotiate.

Ambiguities in the interpretation of surface roughness can result, however, especially if snow is present on the ice. This is particularly true if the snow is wet. Thus smooth, first-year ice can give high returns similar to those found for multiyear

ice. These ambiguities can usually be resolved if simultaneous X-band (8-12.5 GHz) and L-band (1.2 GHz) imagery is available. The L-band will generally penetrate thin snow overlying sea ice, whereas the X-band will not. High L-band returns are associated with a rough surface. Additional ambiguities in interpretation of radar imagery of snow-covered sea ice occur in the marginal ice zone where there is a considerable likelihood of thin ice and large temperature fluctuations. These factors may contribute to higher X-band returns even from smooth first-year ice because of recrystallization of ice and snow in the surface layers of the snow-covered sea ice. Again, L-band radar should be used to improve the interpretation.

SLAR imagery has been used to determine relative ice thicknesses of lakes using X- and L-band radars: (1) lakes that were frozen to the bottom gave low (dark) returns, and (2) lakes that were not frozen to the bottom gave high (bright) returns. This difference in returns is caused by the higher constrast in dielectric constant between freshwater ice and water (e=3.2 and 80 respectively) than ice and frozen sediment (e=3.2 and 8) (Elachi et al., 1976). Also, numerous columnar bubbles present in the ice contribute to the high returns from the lakes that are not frozen to the bottom by causing additional scattering (Weeks et al., 1978 and 1981; Mellor, 1982).

However, ambiquities in the interpretation of the radar data can result for deep lakes (>4m) that are not frozen to the bottom. Few bubbles will form when there is a substantial amount of water beneath the ice cover to accept the gases being emitted so the lake will have low radar returns, similar to completely frozen lakes (Mellor,1982).

While radar imagery is useful for limited ice classification, and SAR has high resolution (<=10 m) from spacecraft altitudes, the use of radar to unambiguously distinguish ice type is not recommended at this time (Hall et al., 1985).

A.3 Impulse Radar

Impulse and FM/CW radars have been shown to be useful for quantitative measurement of ice thickness. An electromagnetic pulse is generated and penetrates into the ice medium to an extent that is dependent upon the wavelength and the properties of the material. The wave is partially reflected upon incidence at the interface of the air and ice or snow and ice. Part of the wave continues on through the ice at a slower velocity because of

the increased relative dielectric constant. At the ice-water interface total reflection takes place. In order to convert the two-way travel time of the signal from the ice-water interface to an ice thickness measurement, the velocity of propagation of the EM pulse within the medium must be known. From the effective propagation velocity, the ice thickness can be determined from:

$$X = V_e * t_d/2$$

where X = ice thickness
V_e = effective velocity of EM signal
t_d = travel time from transceiver antenna to and from subsurface interface.

For certain homogeneous materials, such as fresh-water ice, the velocity of propagation can be calculated from:

$$V_e = c / (e_r)^{0.5}$$

where c = velocity of EM pulse in air = $3 * 10^8$ m/s
e_r = dielectric constant
= 81 for freshwater, 3.2 for fresh-water ice.

Unfortunately, the effective dielectric constant of ice varies for different ice types. Therefore, the radar system must be calibrated using drill hole information.

An S-band impulse radar mounted on an all-terraind vehicle was used by Cooper et al. (1976) to measure freshwater ice thickness. The ice varied from 20 to 60 cm in thickness and measurements with the radar agreed to within 3.5 cm. Using aircraft data, they found that the aircraft system could not measure ice thickness less than 10 cm in thickness because the two return signals could not be separated for such thin ice. Snow cover did not interfere with the ice thickness measurements; however, water on top of the ice and rain prevented radar penetration.

The Cold Regions Research and Engineering Laboratory in April 1976 tested a modified system which has two antennas; one operates in the standard transmit-receive mode and the second in the receive-only mode (Kovacs, 1977). With this system it is possible to determine the velocity of propagation of the EM impulse and the effective dielectric constant at any time. The effective propagation velocity of the EM pulse is

$$V_e = X / (t^2 - t_d^2)^{0.5}$$

where X = distance between centers of two antennae
t_d = vertical travel time from transceiver antenna to and from subsurface interface
t = travel time from transceiver antenna to subsurface interface to receive-only antenna plus air-wave travel time between antennas.

With the velocity of the EM impulse thus determined, it is then possible to determine the thickness of ice and its effective dielectric constant using the previous equations discussed above.

In March 1979, measurements were made using this dual antenna with a center frequency of 280 MHz, with the -3 dB points of the spectrum at 220 and 350 MHz. The radiated time domain wavelet was about 6 ns in duration. Both antennae were enclosed in one housing; the distance between the centers of the dipole antennae was about 30 cm. Results show that implementation of the dual antenna mode for propagation velocity measurement may be limited due to inherent limitations in accurately measuring signal flight times of less than 0.5 ns. The flight altitude should be less than twice the antenna separation (X). This method assumes that most of the electromagnetic anisotropic effects occur in the lower 10% of the ice sheet (Kovacs and Morey, 1980).

Sea ice exhibits anisotropic behavior with respect to electromagnetic reflectivity (but not propagation velocity) when the crystal structure at the bottom of sea ice has a horizontal c axis with a preferred azmuthal orientation. Radar reflectivity is at maximum when the antenna E field is aligned parallel to the c axes and at minimum when aligned perpendicular to the c axes. This polarization has been related to the ordered arrangement of brine inclusions and their increasing conductivity with depth in the ice. Thus for best results, the optimum antenna orientation must be determined (Kovacs and Morey, 1978).

The absorption loss within sea ice increases with ice thickness and brine volume. Brine volume is a function of temperature and the attenuation can vary from 1 dB/m for "warm" ice at 100 MHz, to 100 dB/m at 1 GHz. Kovacs (1978) measured a multi-year pressure ridge having a maximum thickness of 14m. This ridge consisted of solid ice which the radar could penetrate. First-year pressure ridges are comprised of ice blocks having large voids. Voids below sea level are filled with highly conductive sea water which the radar will not penetrate.

The absorption loss, spreading loss and ice surface characteristics determine the maximum altitude at which the radar

may be flown. For this radar (75 dB radiated to received power ratio, 1.5 antenna gain) and 2.5 m thick ice having a 2 dB/m attenuation, Kovacs (1978) calculated a maximum altitude of 30 m. For warm ice having an attenuation coefficient of 5 dB/m, this altitude reduces to 4.5 m. Snow cover, particularly wet snow substantially increases the losses. He postulates that a 30 dB gain in radar performance is achievable and will allow sea ice profiling from an altitude of 100m under cold winter conditions.

As the antenna elevation increases, the target area also increases. For the case described above, a target area of radius 4m is obtained at an antenna altitude of 10m. For an altitude of 5m, the radius reduces to 2.8m. These altitudes are extremely low for a helicopter carrying the radar over ice structures containing pressure ridges.

A.4. Airborne Electromagnetic Method

A possible application of the airborne electromagnetic (AEM) method being investigated by the Naval Ocean Research and Development Activity (NORDA) is to determine the sea-ice thickness (Won and Smits, 1985). Since ice is transparent to EM waves up to several tens of kilohertz, determining sea-ice thickness is reduced to an EM altimetry problem involving the distance up to the ice/water boundary. If the distance to the air/ice boundary can be measured by a radar (or laser) altimeter, the difference between the EM and the radar altitudes represents the ice thickness.

The AEM method has been applied to the bathymetric charting in the shallow ocean (Won and Smits, 1985). The AEM system was a commercially available Dighem III. The system was equipped with two horizontal coplanar coil pairs operating at 385 Hz and 7200 Hz, both having an 8 m coil separation. A Sikorsky S58T twin-engine helicopter towed the sensor platform which maintained an altitude ranging from 40 m to 50 m above the sea level. Bathymetric results derived from this experimental survey data showed excellent agreement with ground truth data. The response, however, decreases rapidly with an increasing sensor altitude and therefore limits the usable range of the AEM method.

A.5. Laser Profilometer

The laser profilometer measures the vertical distance from an overflying aircraft to the ice surface. A helium-neon CW laser

beam, modulated at a high frequency serves as the transmitter. The receiver compares the phase of the reflected signal with that of the laser modulation. The desired resolution dictates a modulation frequency -- for example, at 49 MHz it provides a 0 to 360 deg phase change for a 0 to 3.0 m change in height. When this range interval is exceded, the phase, and therefore the indicated height, jumps back to zero and starts again. The real height of the ice is determined by counting the phase jumps. Alternatively, the modulation frequency may be lowered to increase the range interval, but this is obtained at the expense of vertical resolution.

The measured phase angle is converted to a proportional analog voltage which may be smoothed by integrating over a 1 - 100 ms period. Aircraft speed and expected surface roughness impact the integration time. Longer integration times reduce horizontal resolution.

The output signal contains components due to both surface roughness and aircraft altitude variations. A three step filtering process has been successfully used in eliminating the aircraft variations. The aircraft component is assumed to have a lower frequency spectrum than the surface roughness. This is generally true, however, some overlap exists and can lead to an under-estimation of ridge heights. Accuracies on the order of a few cm (height) and spatial resolutions of 2 - 4 m (horizontal) are possible (Hengeveld, 1974; Hibler, 1975).

The frequency characteristics of each particular ice type are identifiable in the laser profile. New ice will have a relatively smooth profile while second year ice is characterized by large rough ridges and generally rough topography. Grey white ice will have a relatively smooth profile with an occassional spike indicating a small ridge (Hengeveld, 1974).

Ice may be distinguished from open water by observing the reflected signal strength. The reflection from open water is much lower than the reflection from ice (Hibler, 1975). Snow cover is indistinguishable from ice and must be estimated by other means (Ackley et al., 1976; Hengeveld, 1974; Hibler, 1975).

Comparison of Ice Sensor Capabilities:

1) Visible and Infrared

Resolution: (horizontal) - 30-20m (Landsat)

Advantages:
- Classify ice types
- Classify ice age
- Infer ice thickness

Disadvantages:
- Visible and near infrared cannot penetrate clouds and require sunlight
- Thermal infrared cannot penetrate clouds

2) Passive microwave

Resolution: (horizontal) - 30 km (Nimbus 7 SMMR)

Advantages:
- all weather capability
- sea ice edge location
- ice concentration by type (first-year vs multiyear): ice thickness is inferred
- wide-swath (1394 km for SSM/I)

Disadvantages:
- low resolution from satellites (30km for Nimbus 7 SMMR)
- ice classification ambiguities result when ice is wet or snow-covered

3) SAR,SLAR

Resolution: (horizontal)
- 30m (AN/APS-94 SLAR)
- 15m (AN/APD-102 SAR at 11,300m altitude)

Advantages:
- feature identification (ridges, leads, floes, berg populations)
- high resolution (SAR)
- limited classification (open water, first-year,old)
- (dry) snow penetration

Disadvantages:
- classification ambiguities: distinguishing open water from new smooth ice; first-year

from multiyear during melt and freeze-up: wet snow cover
- very high data rates
- complex processing (SAR)

4) **Impulse Radar**

Resolution: (thickness) - 4 cm (Cooper et al., 1976)

Advantages:
- capability for quantitative measurement of ice thickness for limited ice conditions

Disadvantages:
- must be conducted near the surface ($\leq$ 30m)
- not capable of measuring thickness for all ice types and under all conditions ie. wet snow on top, first-year pressure ridges

5) **Airborne Electromagnetic Method**

Resolution: (thickness) - 0.3-1.0m

Advantages:
- possible quantitative ice thickness measurement

Disadvantages:
- decreasing resolution with increasing altitude

6) **Laser Profilometry**

Resolution: (height) - few cm

Advantages:
- Identify ice types
- Infer ice depth from sail heights
- Identify ice from open water

Disadvantages:
- Snow cover indistinguishable from ice

Appendix B. Results from Moosehead Lake, Maine Ice Tests in March 1983

List of Figures - Hydrophone Receiver Response

Fig No.	L (m)	D (cm)	d (cm)	Equipment Settings: Spectrum Analyzer Sens(mV)	Freq(kHz)	Filter (kHz)	Hydrophone Amp. (mV/div)	File No.	
1	30	91	0	200	100	-	31.6	29	
2	"	"	15	"	"	2	"	94	
3	"	"	"	"	"	"	"	95	1
4	"	"	"	100	"	"	"	96	
5	"	"	"	1000	"	"	316	103	
6	"	305	91	100	50	"	31.6	97	
7	"	"	122	"	"	"	"	98	2
8	"	"	"	"	"	"	"	99	
9	"	"	"	500	"	"	1000	102	
10	"	366	5	200	100	"	316	107	
11	"	"	"	"	"	"	"	108	
12	"	"	"	100	"	"	"	109	1
13	"	"	"	200	"	"	1000	111	
14	"	"	10	"	"	"	"	119	

List of Figures - Microphone Receiver Response

Fig No.	L (m)	D (cm)	h (cm)	Equipment Settings: Spectrum Analyzer Sens(mV)	Freq(kHz)	Gain (dB)	File No.	
15	30	76	30	100	100	40	25	
16	"	"	"	"	"	"	26	3
17	"	"	"	"	"	"	28	

Note:

1) Hydrophone in ice
2) Hydrophone in water
3) 15 cm snow layer between microphone and ice surface

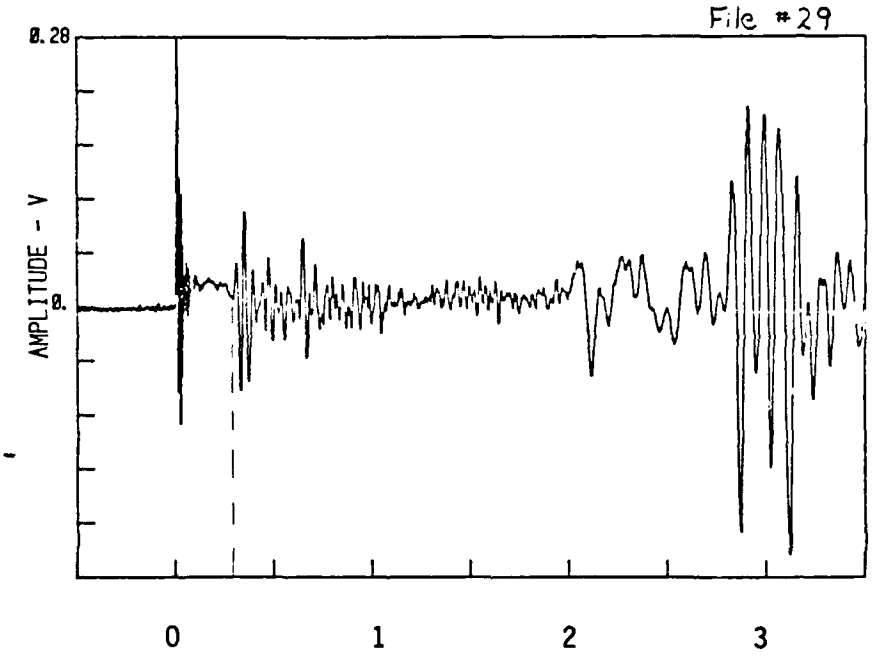

Figure B.1

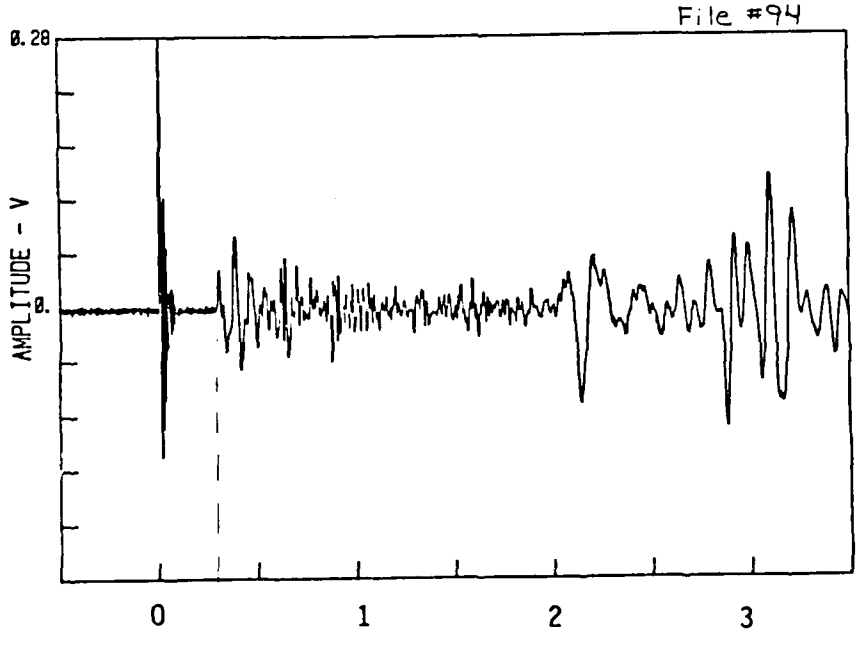

Figure B.2

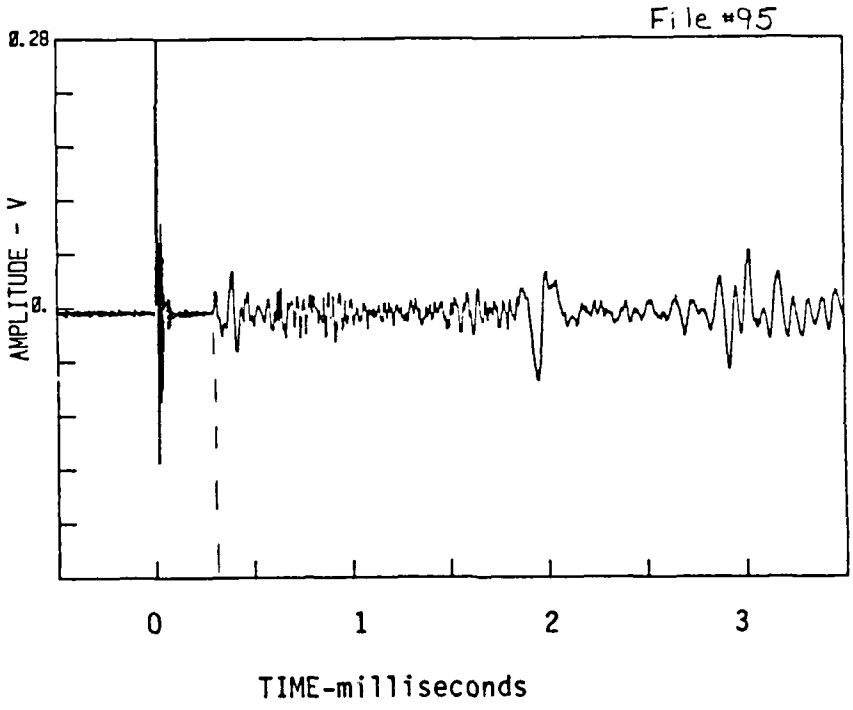
File #95
0.28
AMPLITUDE - V
0.
0
1
2
3
TIME-milliseconds

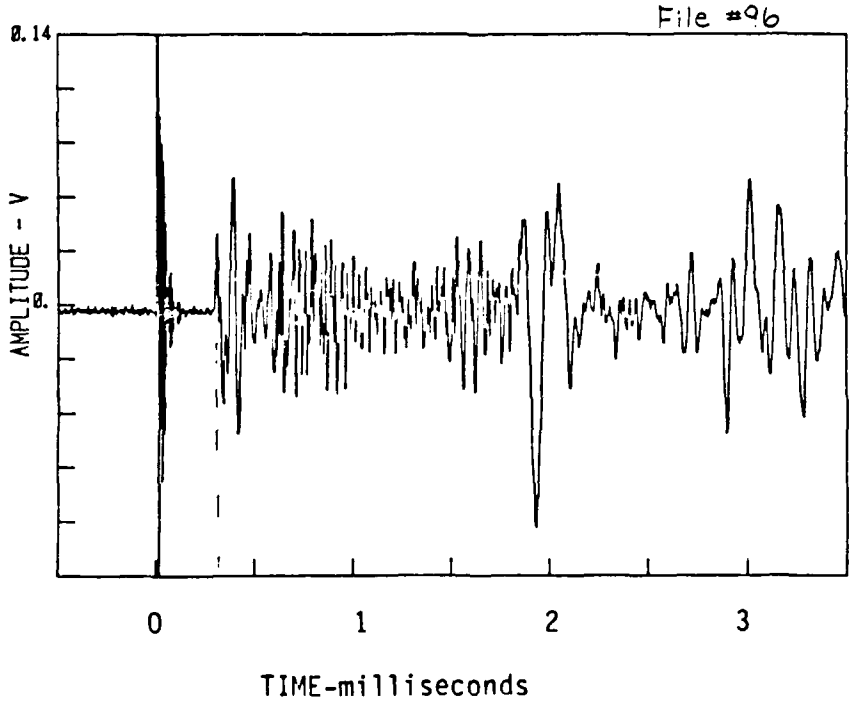
File #96
0.14
AMPLITUDE - V
0.
0
1
2
3
TIME-milliseconds

Figure B.4

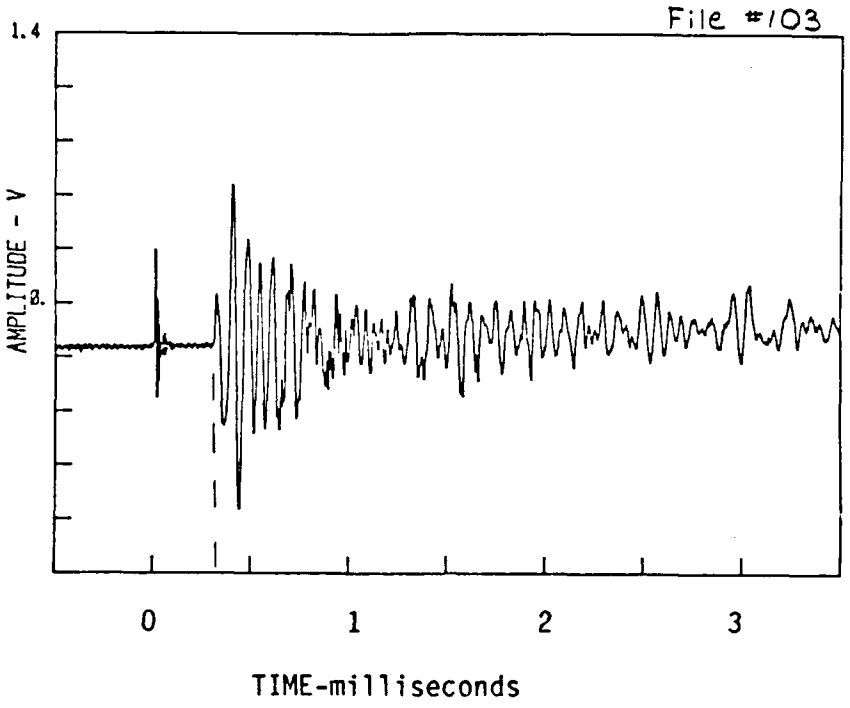

Figure B.5

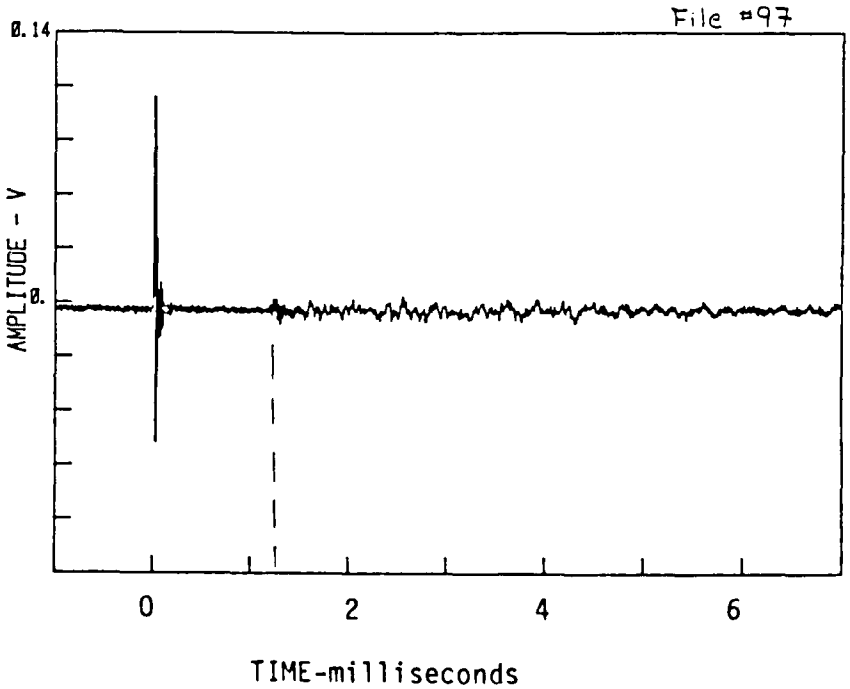

Figure B.6

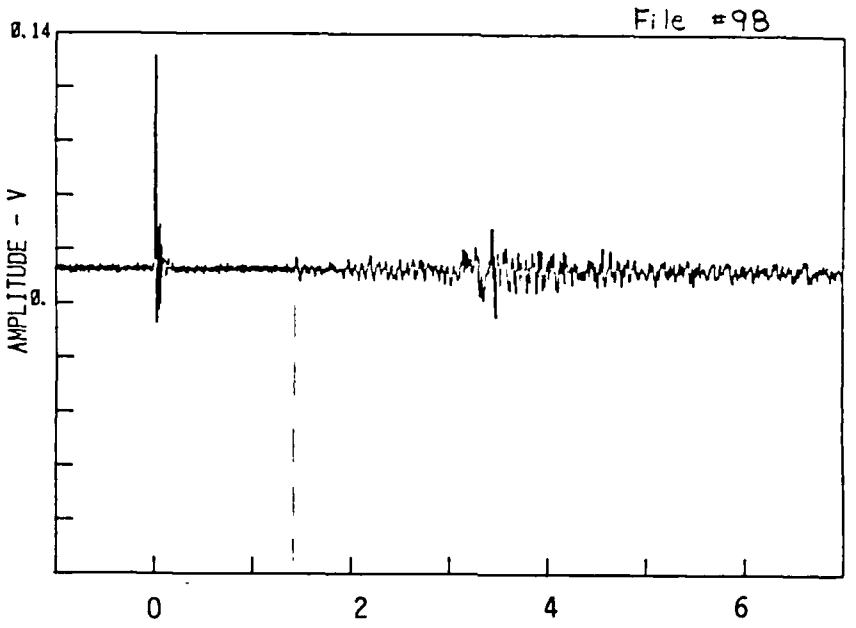

Figure B.7

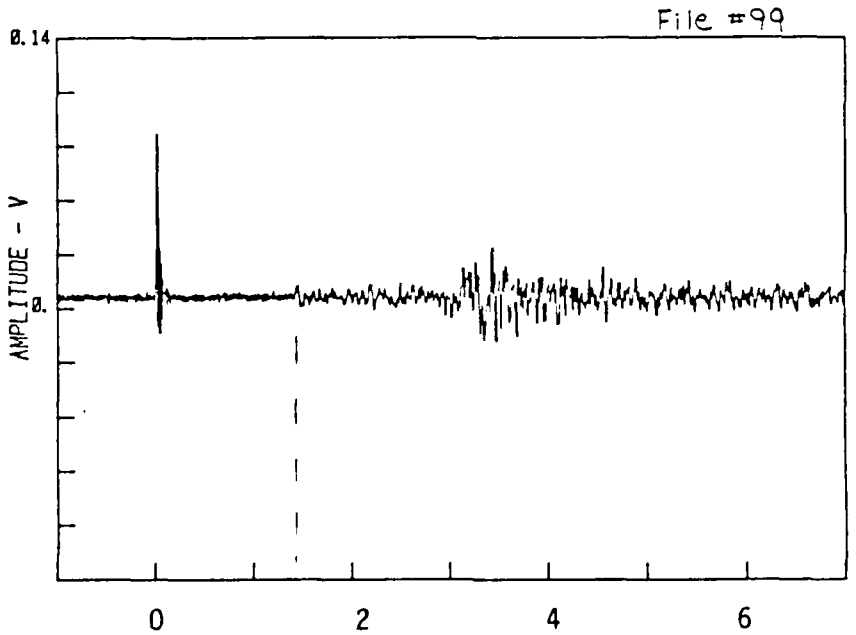

Figure B.8

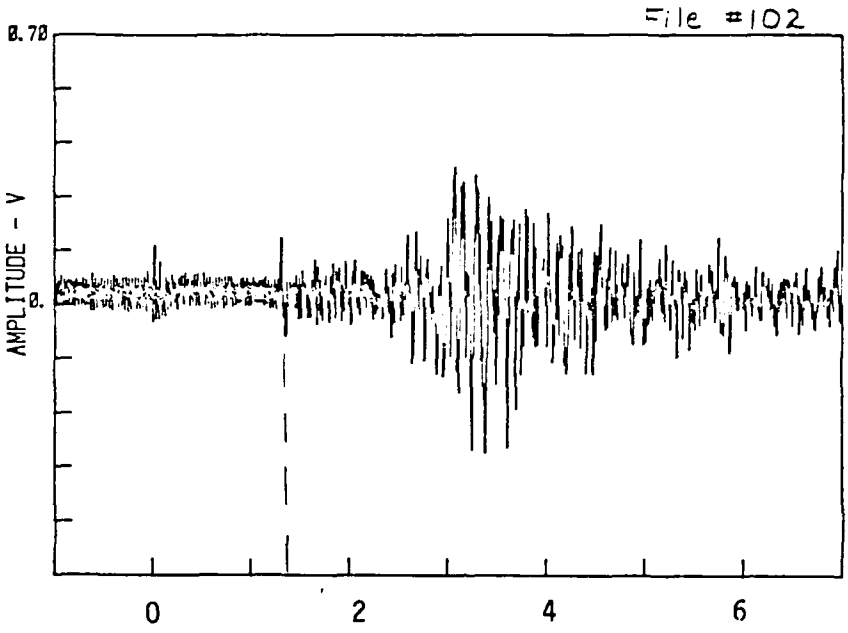

Figure B.9

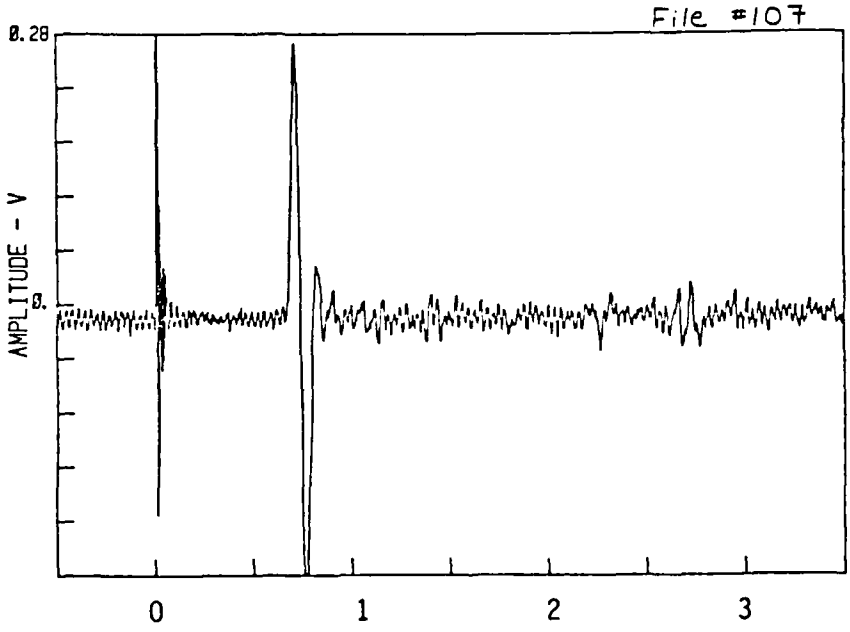

Figure B.10

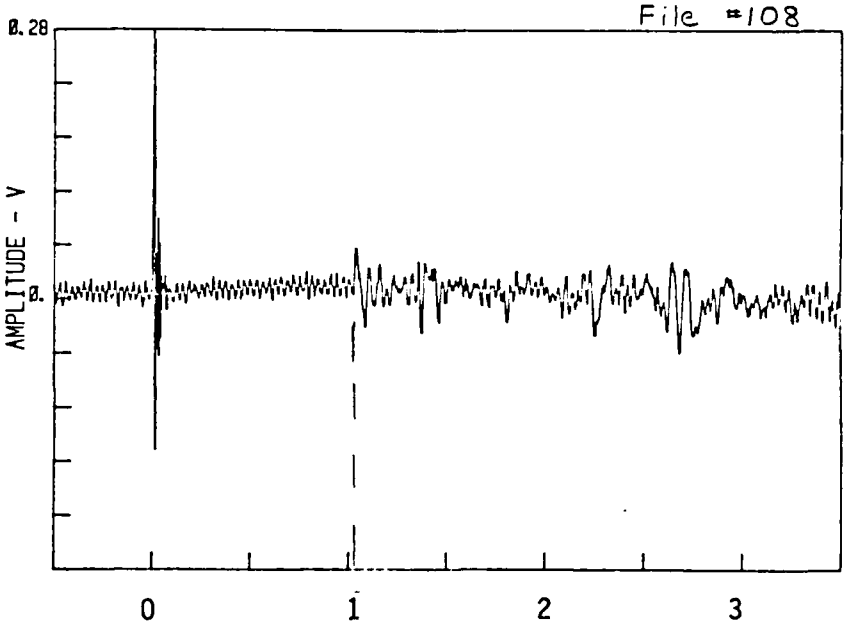

Figure B.11

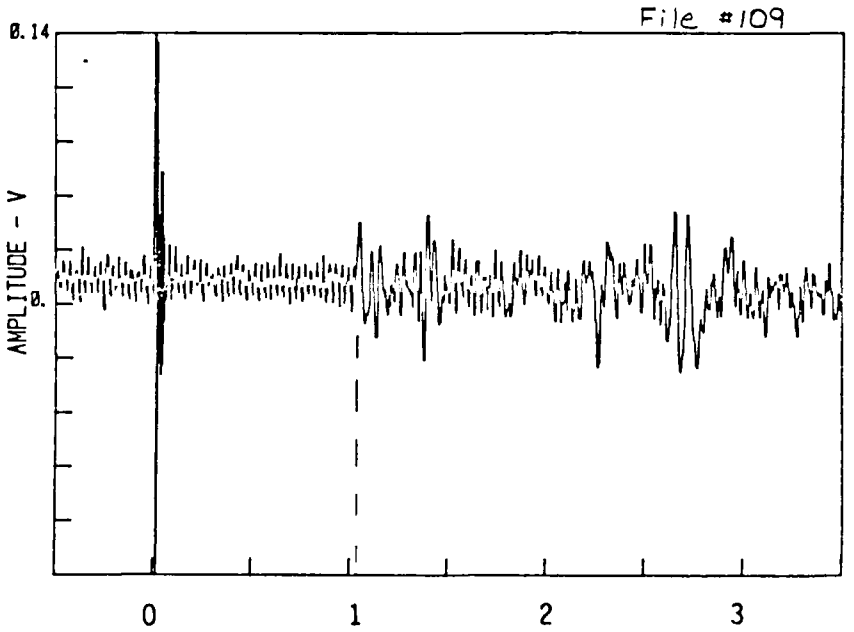

Figure B.12

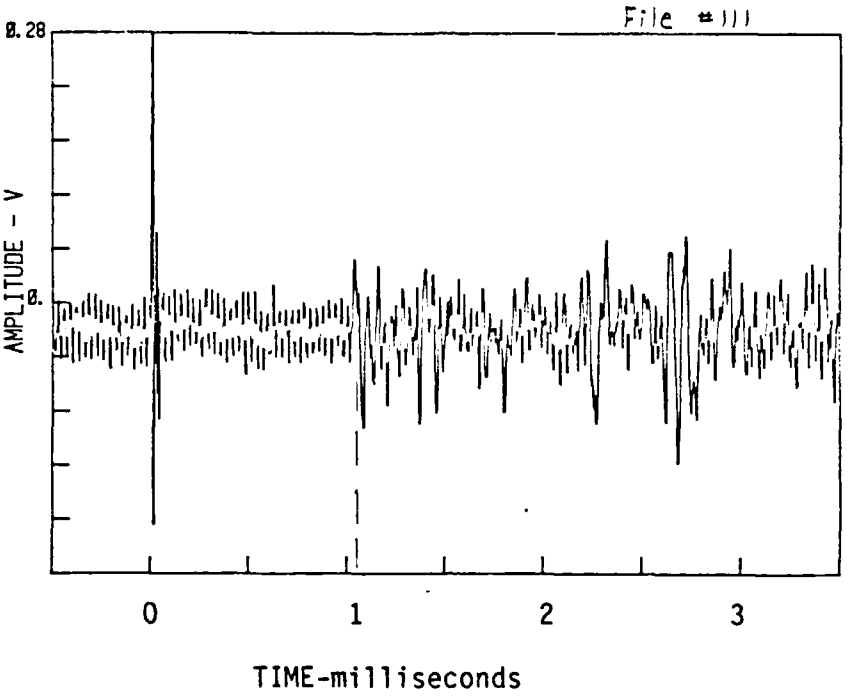

Figure B.13

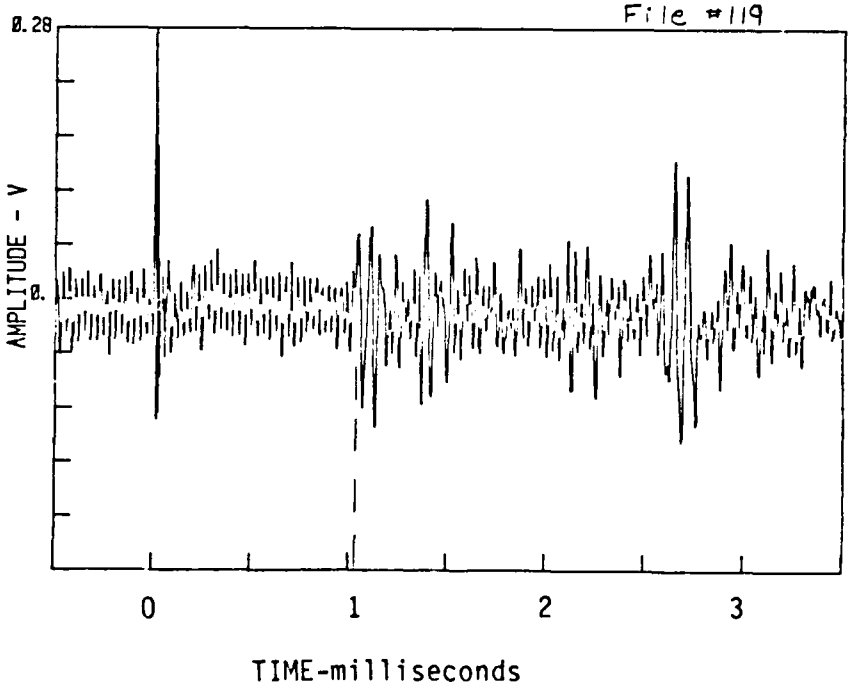

Figure B.14

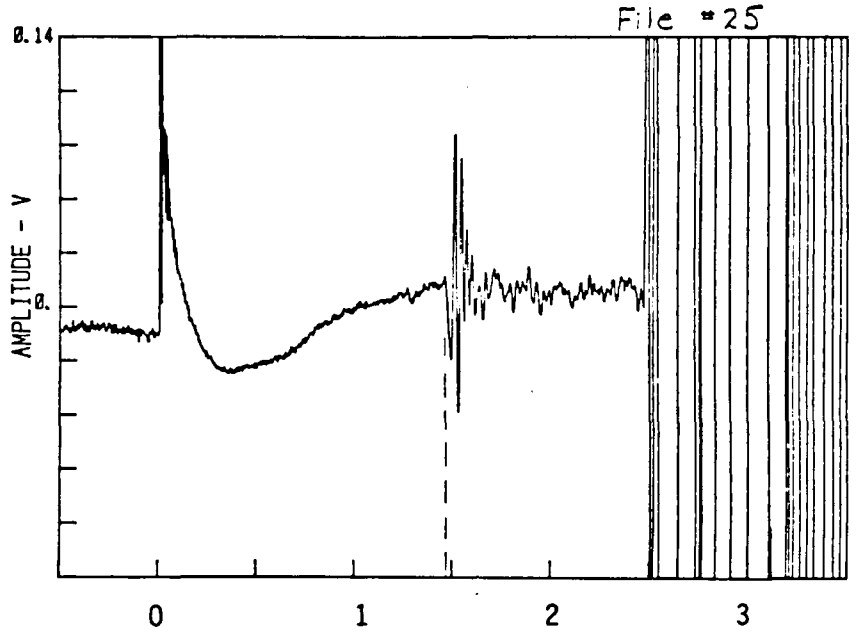

Figure B.15

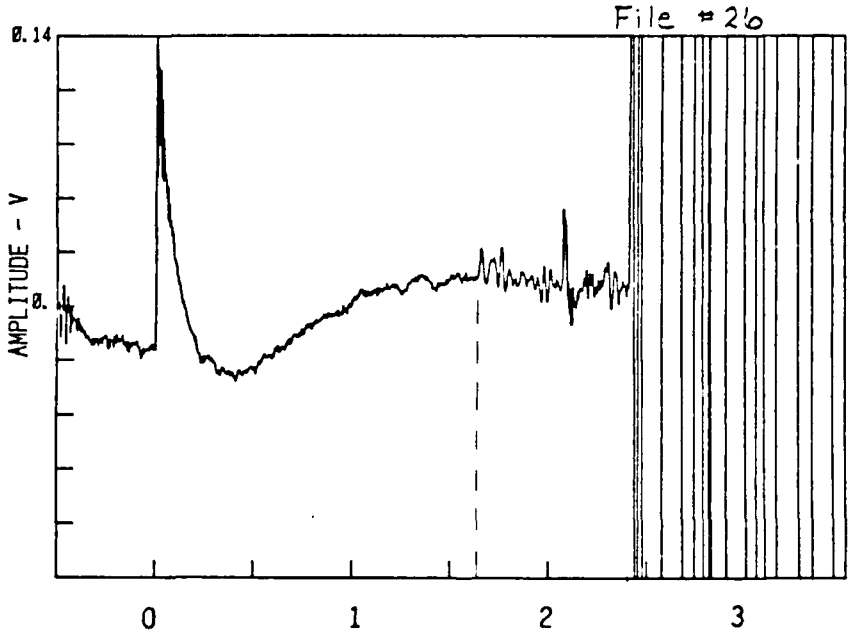

Figure B.16

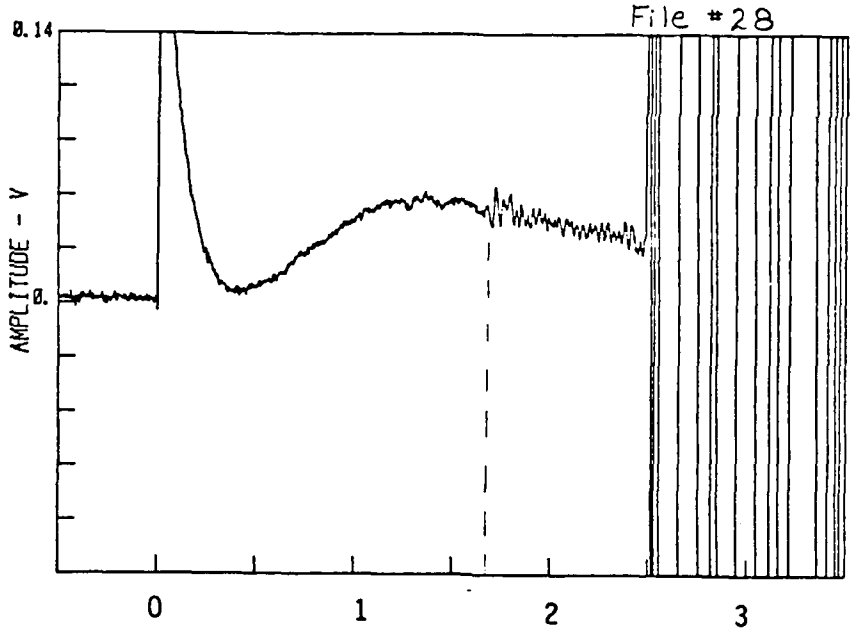

Figure B.17

Appendix C. Hydrophone Receiver Response

List of Figures

(March 1987)

Fig No.	L (m)	D (cm)	d (cm)	Equipment Settings: Spectrum Analyzer Sens(mV)	Analyzer Freq(kHz)	Filter (kHz)	Hydrophone Amp. (mV/div)	File No.	
1	4.6	91	0	200	50	7.5	10	98	
2	"	"	"	"	"	"	"	106	
3	"	"	"	"	100	"	"	100	
4	"	"	"	"	"	"	"	105	1
5	"	"	"	"	20	"	"	99	
6	"	305	"	100	100	"	"	113	
7	"	"	"	"	"	"	"	115	
8	"	"	91	"	"	"	"	129	
9	"	"	"	"	"	"	"	130	
10	"	"	183	"	"	"	"	132	
11	"	"	"	"	"	"	"	133	
12	"	"	"	"	"	"	"	134	2
13	"	"	"	"	50	"	"	135	
14	"	"	229	"	"	"	"	137	
15	"	"	"	"	100	"	"	139	
16	"	"	"	"	"	"	"	140	
17	"	610	38	"	"	"	"	150	1
18	"	"	"	"	"	"	"	151	
19	"	"	183	"	50	"	"	161	
20	"	"	229	"	100	"	"	154	
21	"	"	"	"	"	"	"	155	
22	"	"	"	"	50	"	"	159	2
23	"	"	"	"	"	"	"	165	
24	"	"	"	"	"	"	"	166	
25	"	914	"	"	"	"	"	148	

Note:

1) Hydrophone receiver in ice
2) Hydrophone receiver in H_2O

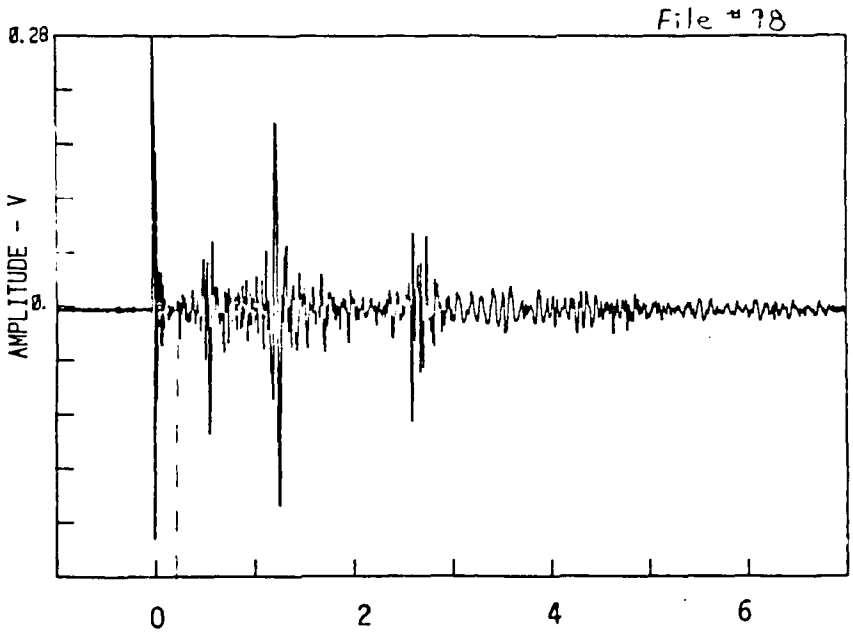

Figure C.1

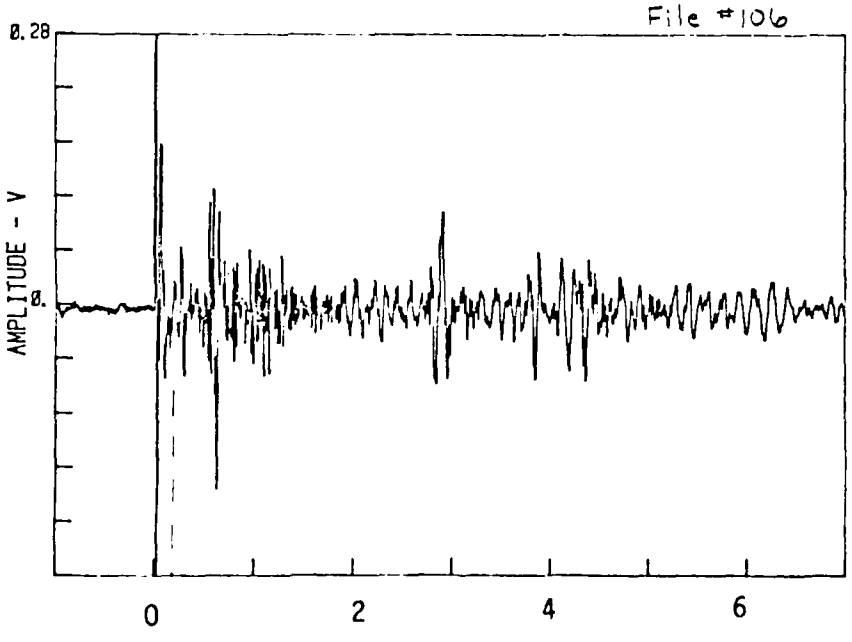

Figure C.2

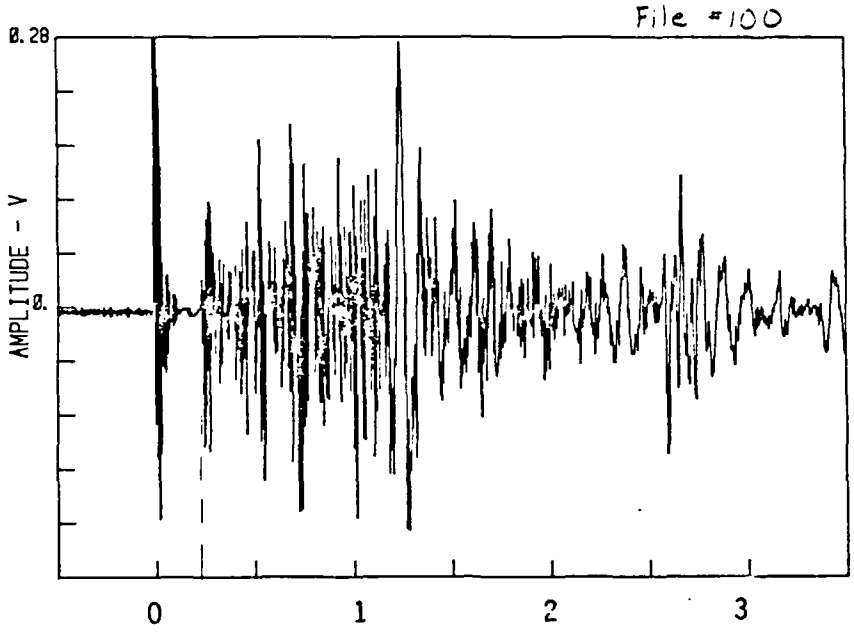

Figure C.3

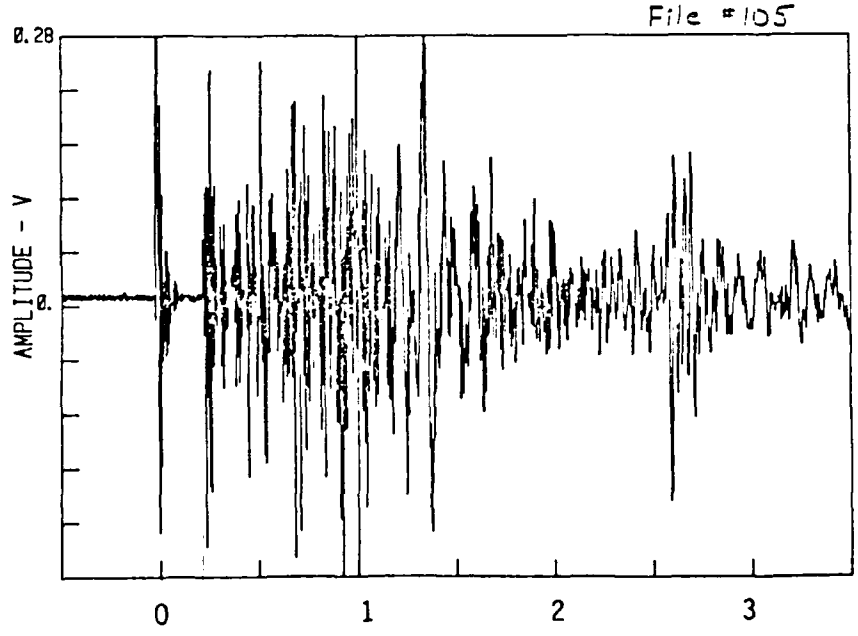

Figure C.4

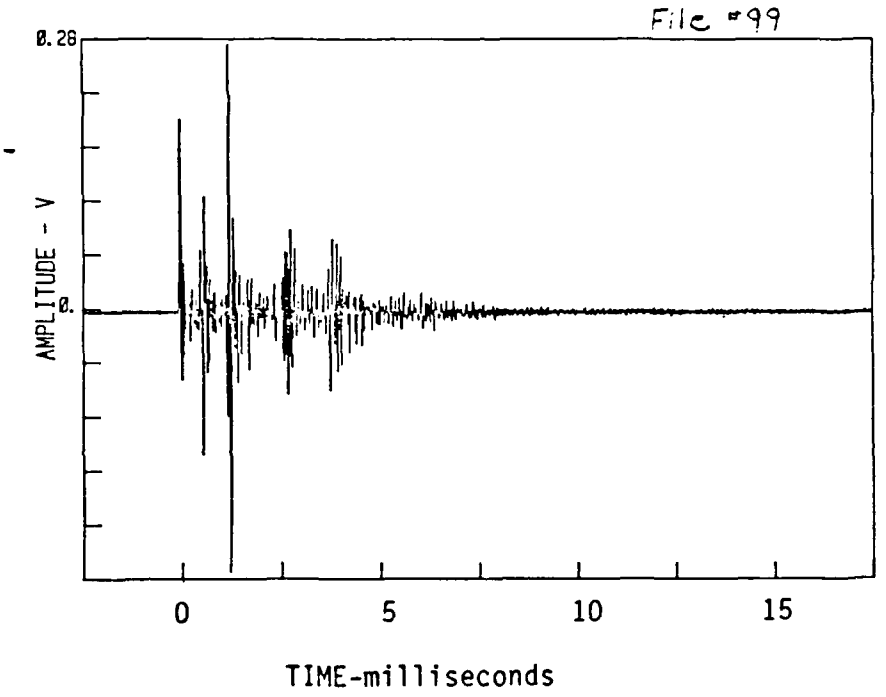

Figure C.5

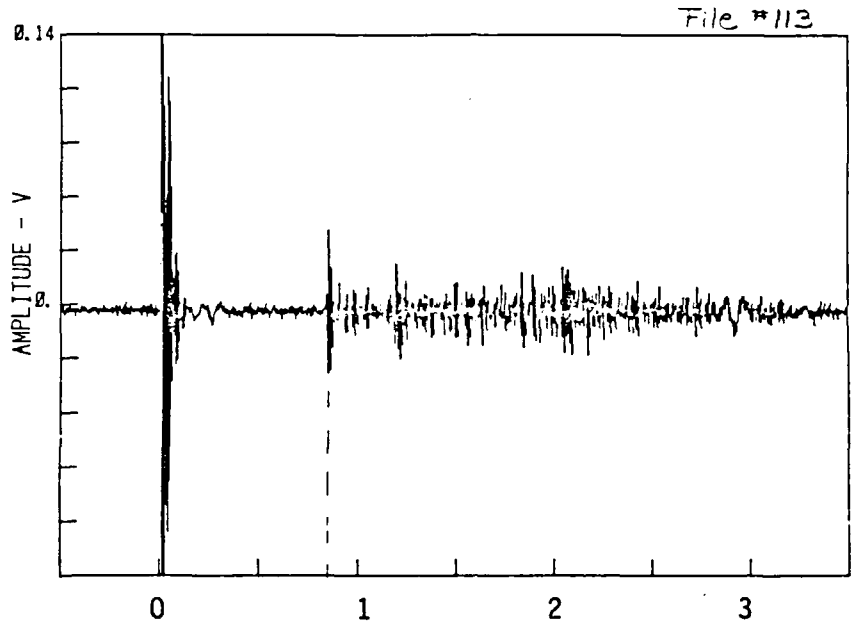

Figure C.6

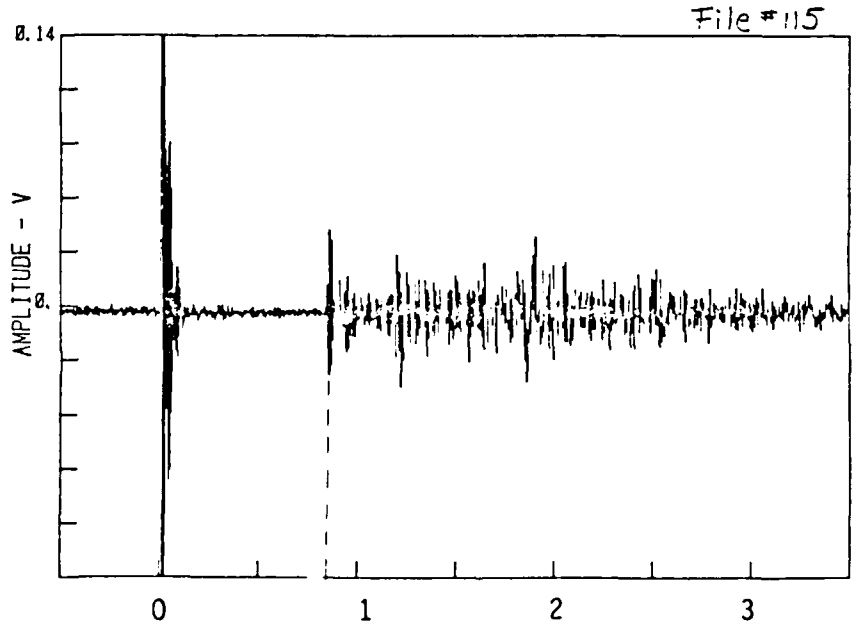

Figure C.7

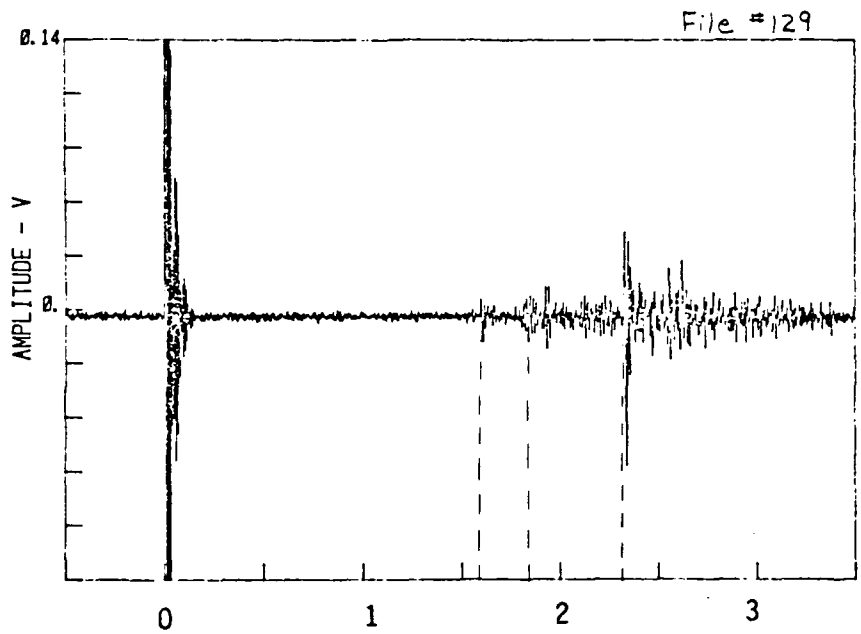

Figure C.8

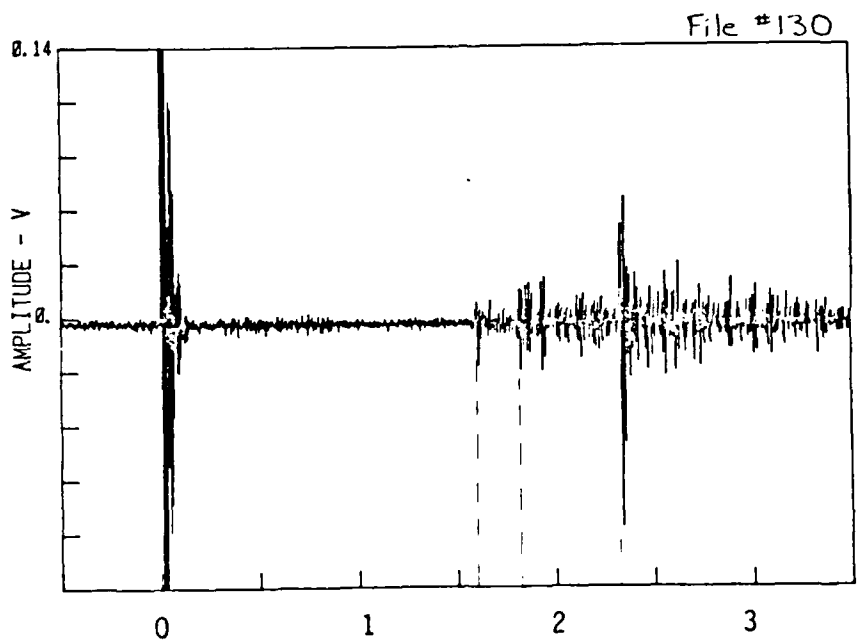

Figure C.9

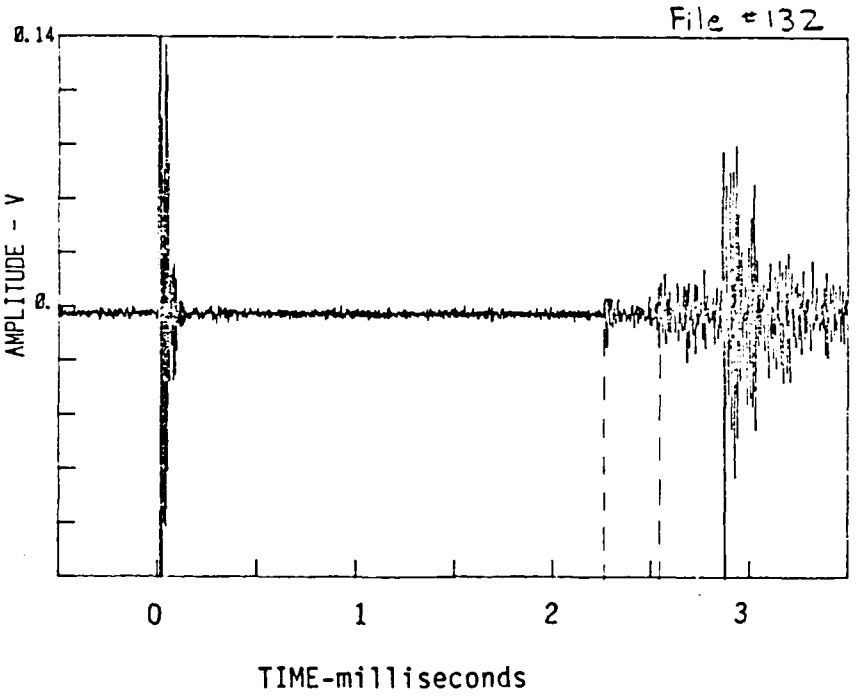

Figure C.10

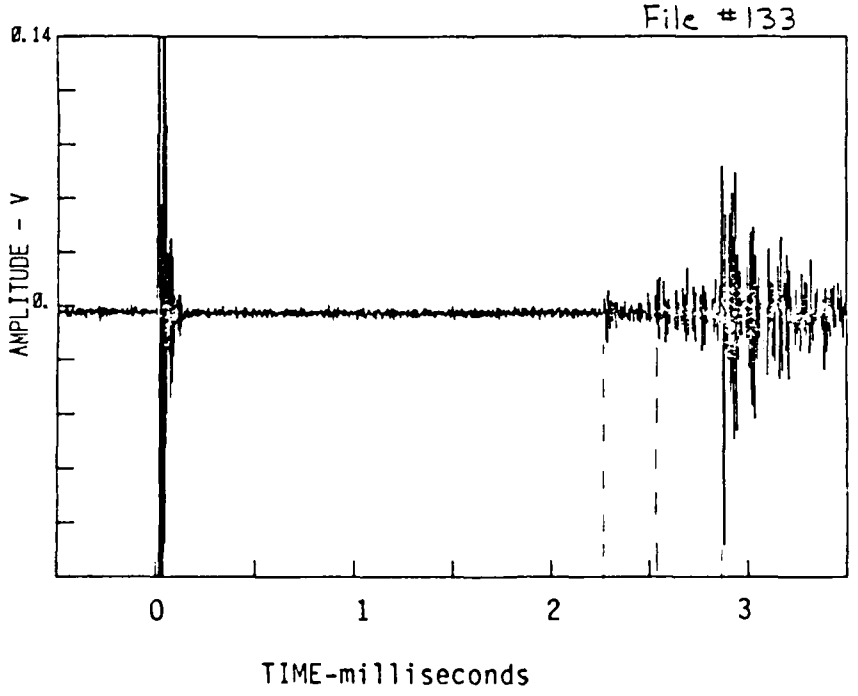

Figure C.11

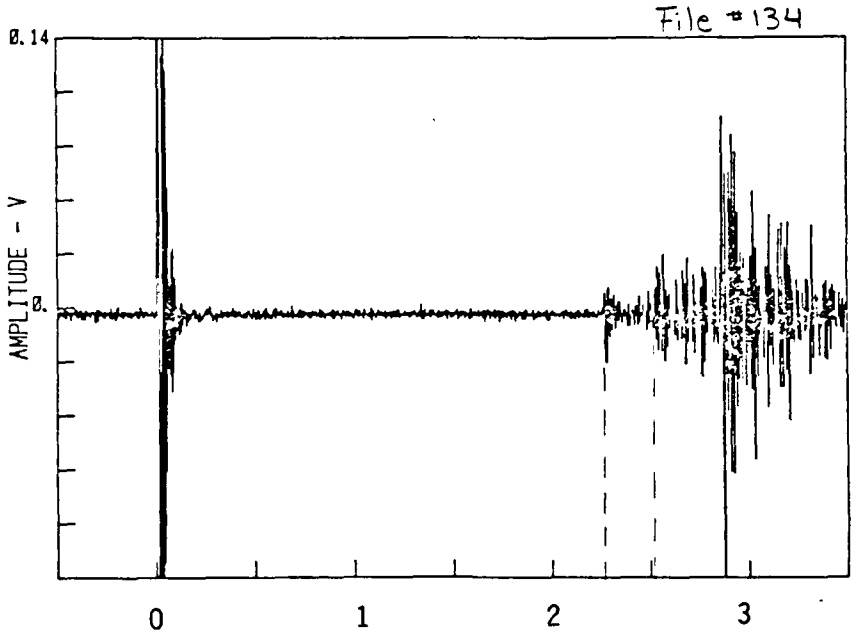

Figure C.12

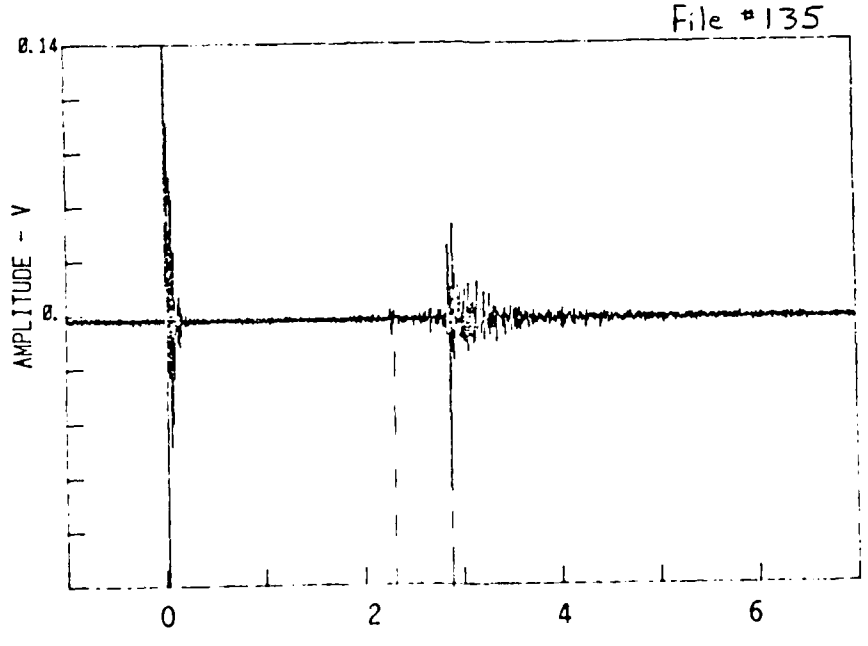

Figure C.13

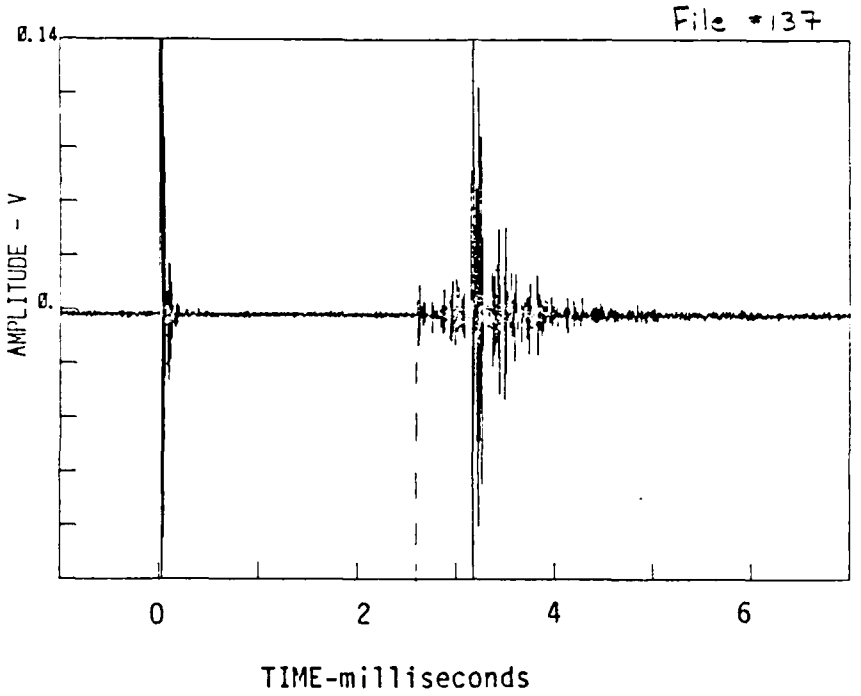

Figure C.14

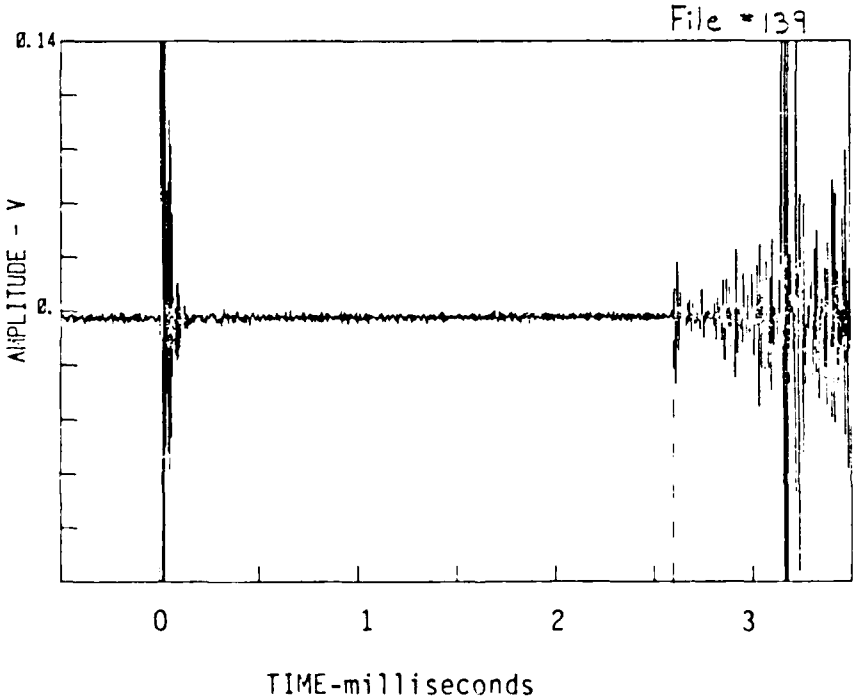

Figure C.15

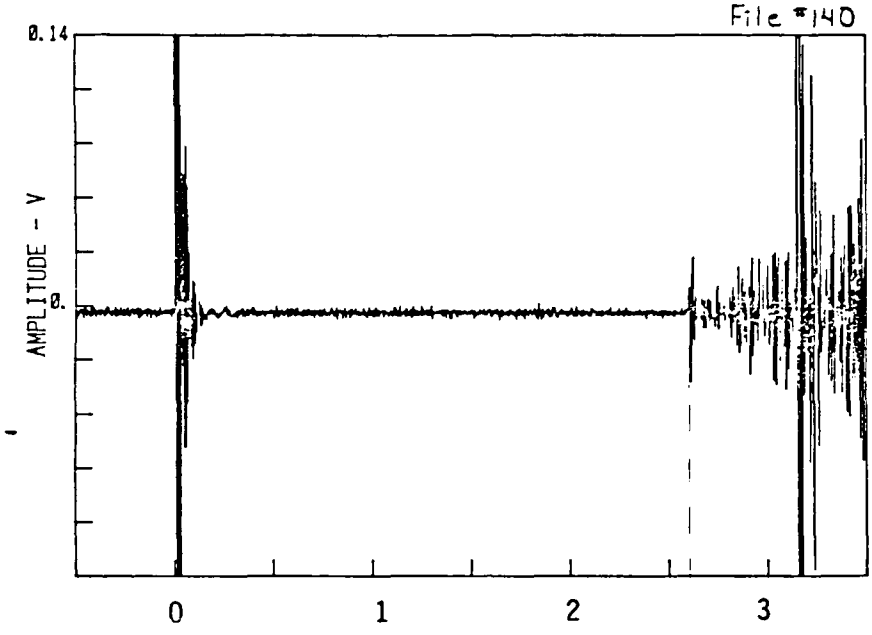

Figure C.16

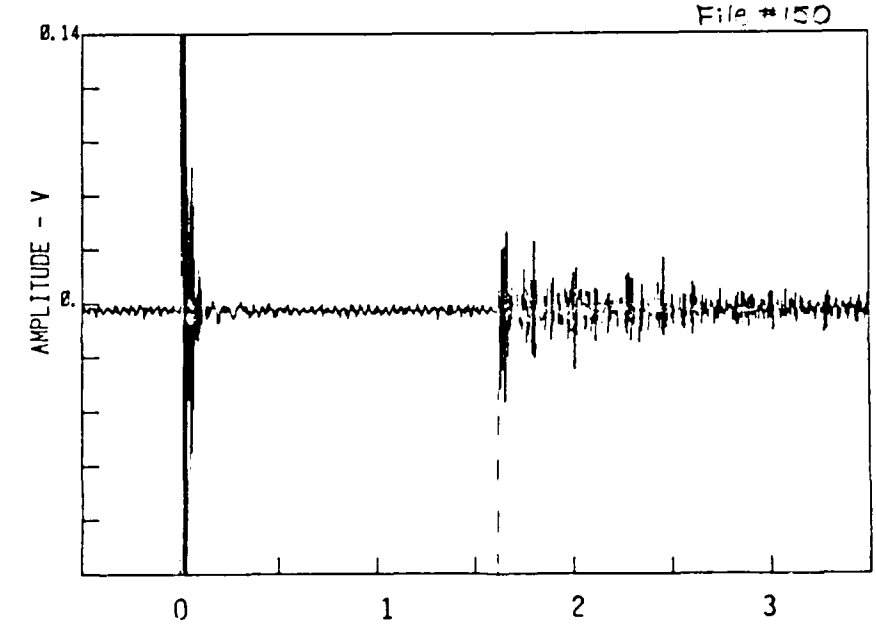

Figure C.17

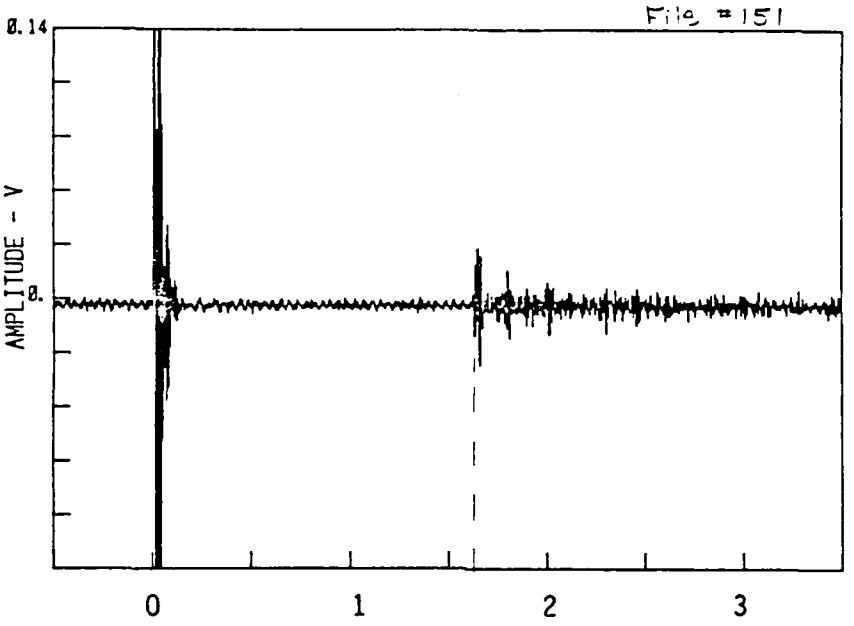

Figure C.18

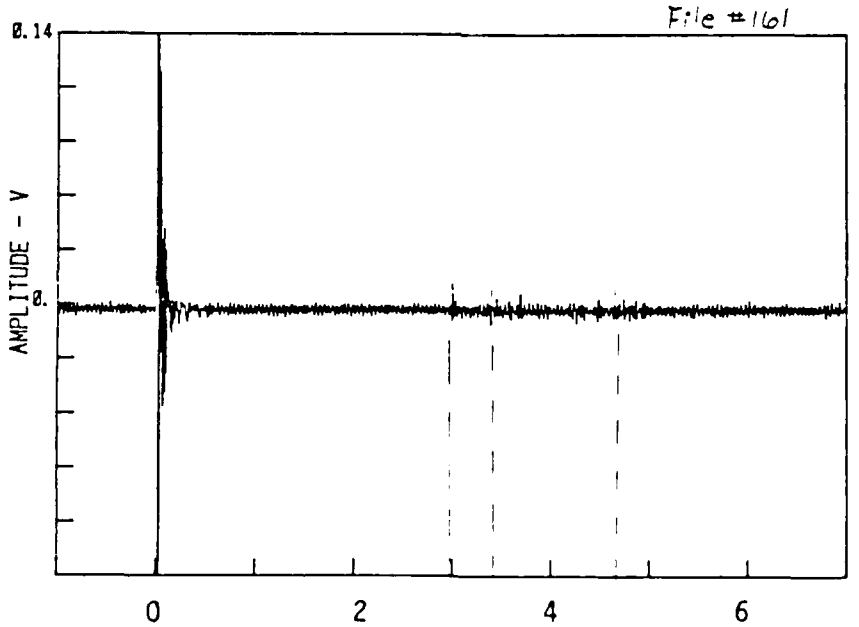

Figure C.19

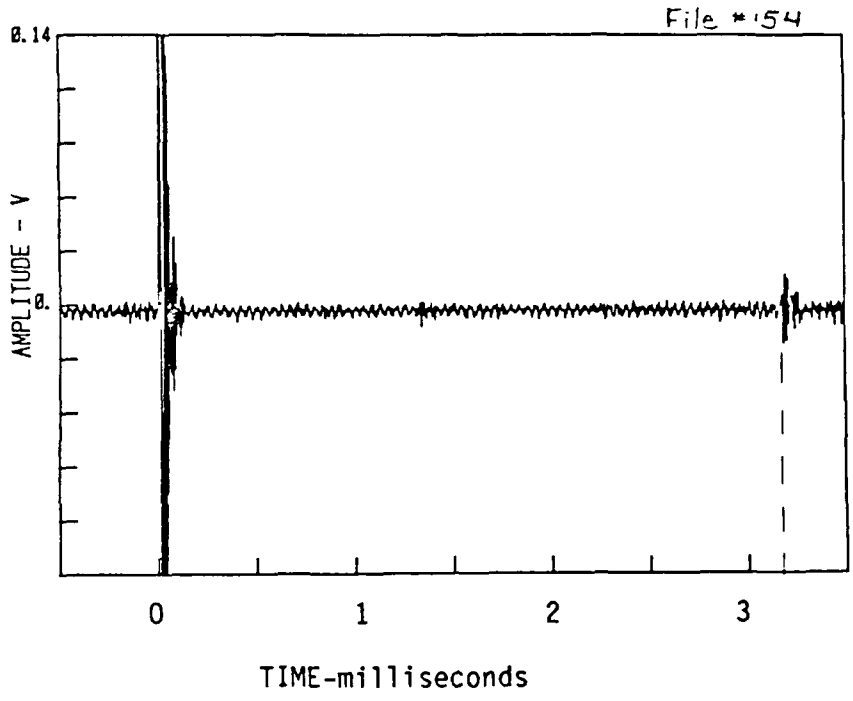

Figure C.20

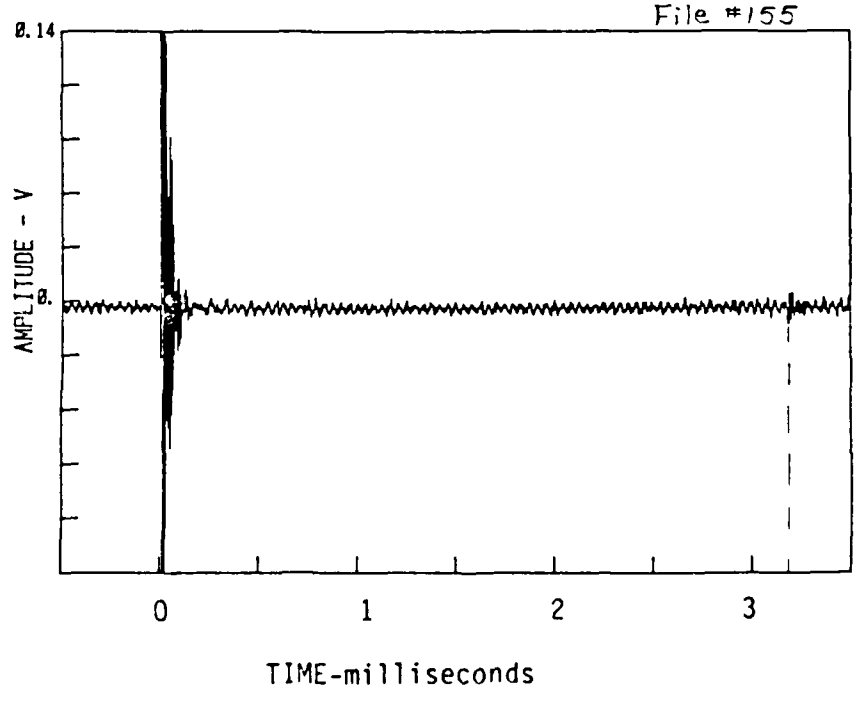

Figure C.21

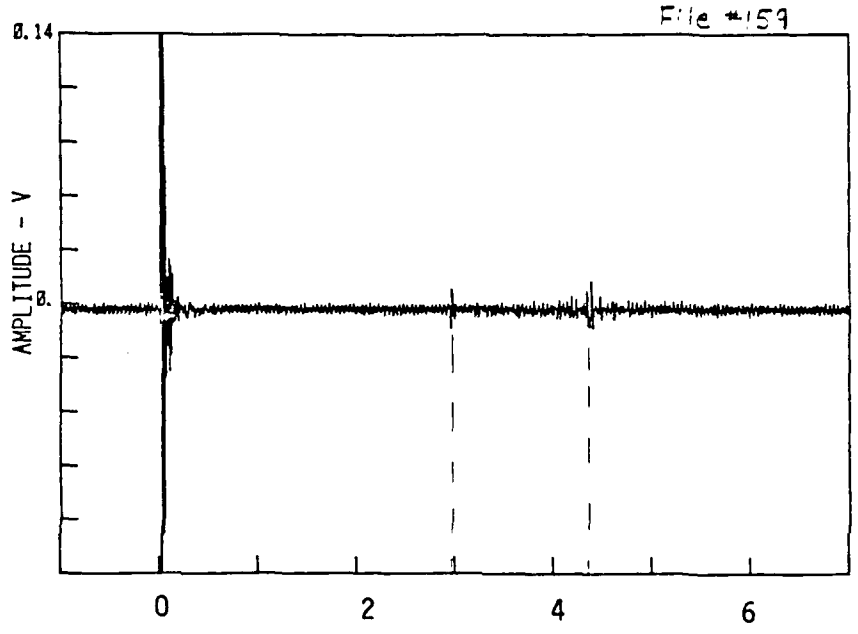

Figure C.22

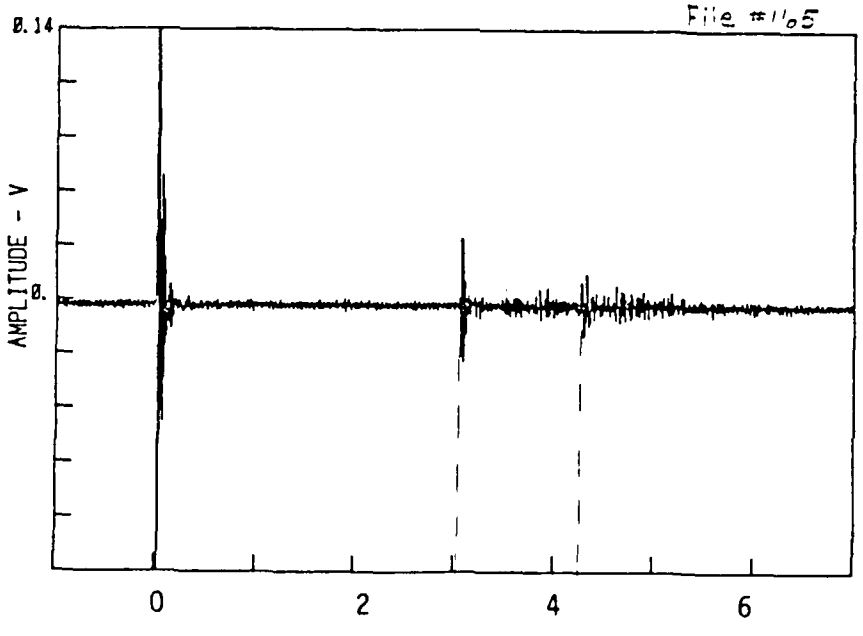

Figure C.23

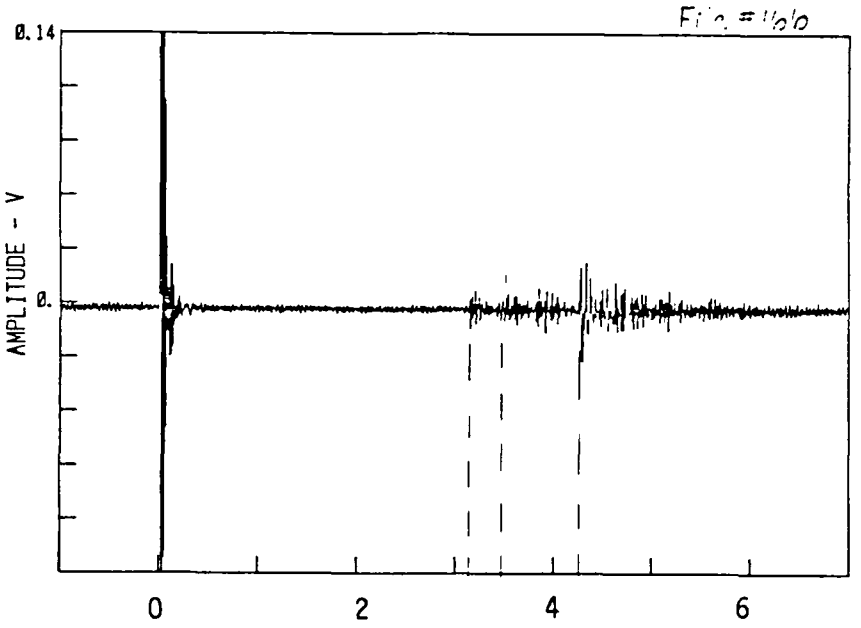

Figure C.24

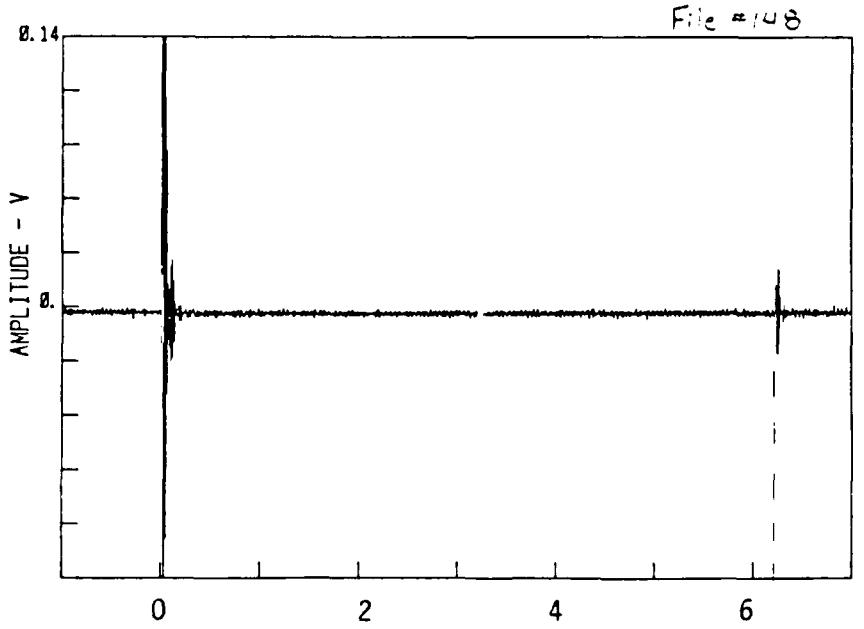

Figure C.25

Appendix D. Microphone Receiver Response

List of Figures

(March 1987)

Fig No.	L (m)	D (cm)	h (cm)	Equipment Settings				Snow Conditions		File No.
				Spectrum Analyzer Sens(mV)	Freq(kHz)	Filter (kHz)	Gain (dB)	10 cm at laser impact spot	10 cm between microphone & ice	
1	4.6	91	46	100	100	2	40			79
2	"	"	"	"	"	"	"			81
3	"	"	"	"	"	"	"			80
4	5.9	"	51	200	50	-	"			70
5	"	"	"	"	"	2	"			71
6	"	"	"	100	"	"	"			77
7	"	"	"	200	100	"	"			75
8	30.5	107	46	100	"	"	"			46
9	"	"	"	"	"	"	"			47
10	"	"	"	"	50	"	"		X	26
11	"	"	"	"	"	"	20		X	27
12	"	"	"	"	"	"	40		X	28
13	"	"	"	"	"	"	"		X	36
14	"	"	"	"	"	"	"		X	30
15	"	"	"	"	"	"	"		X	35
16	"	"	"	"	100	"	"		X	29
17	"	"	"	"	"	"	"		X	31
18	"	"	"	"	50	"	"	X		48
19	"	"	"	"	100	"	"	X		54
20	4.6	122	"	"	50	"	"			82
21	"	"	"	"	"	"	"			83
22	"	"	"	200	"	"	"			90
23	"	"	"	100	"	"	"			91
24	"	"	"	"	"	"	"	X		85
25	"	"	"	"	"	"	"	X		86
26	"	"	"	"	"	"	"	X	X	87
27	"	"	"	"	"	"	"	X	X	89
28	"	183	"	200	100	"	"			93
29	"	"	"	"	"	-	"			96

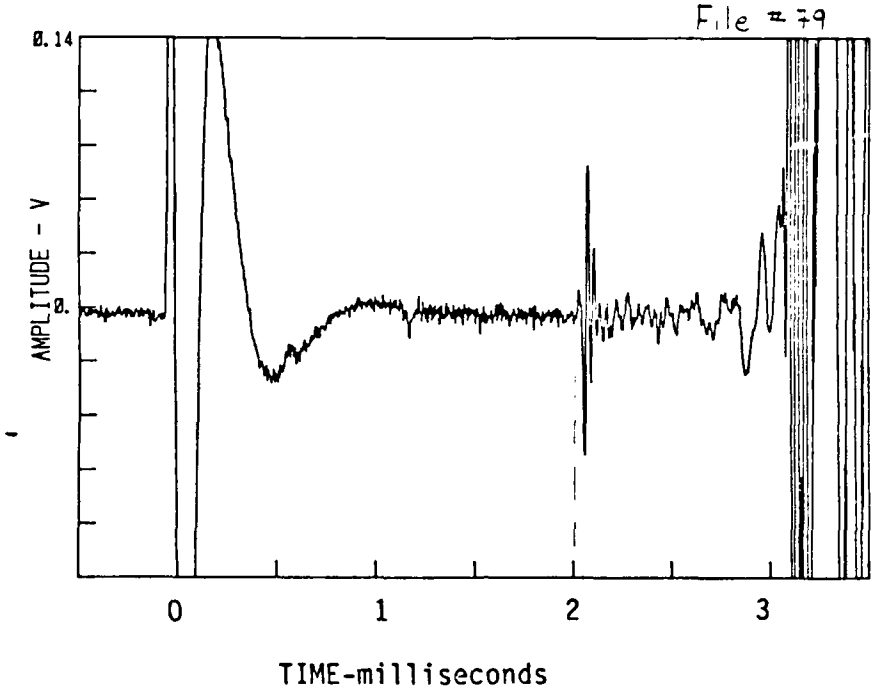

Figure D.1

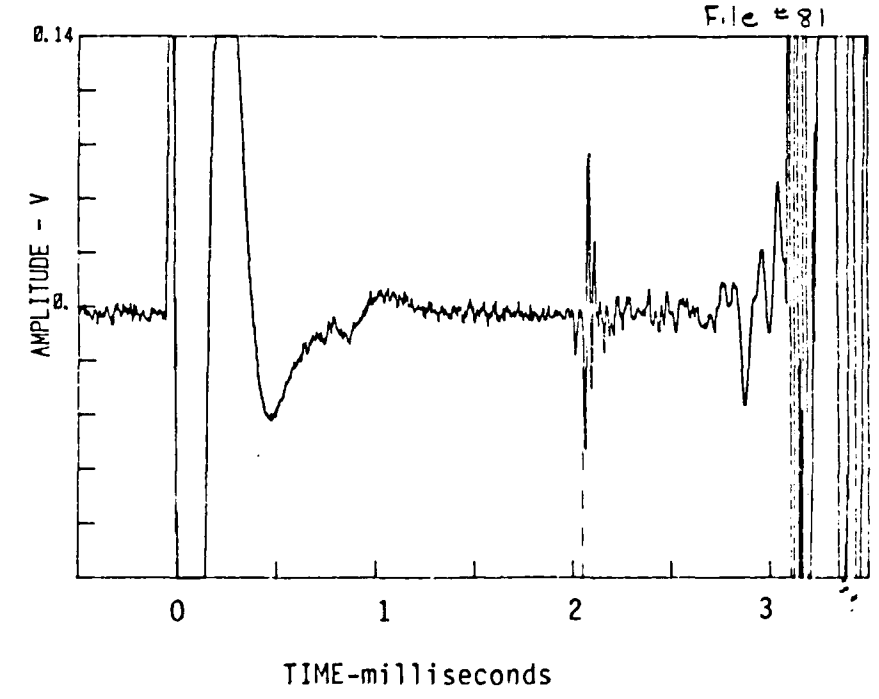

Figure D.2

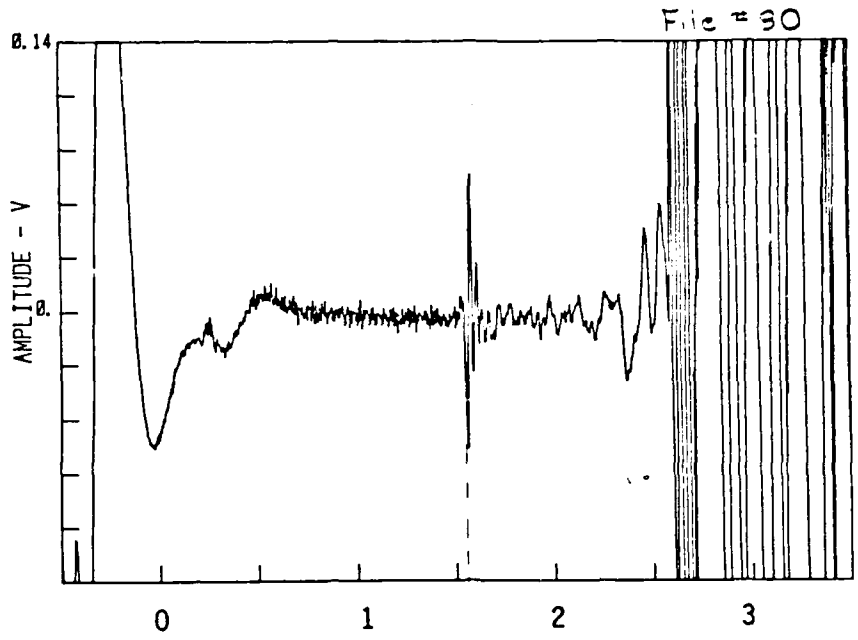

Figure D.3

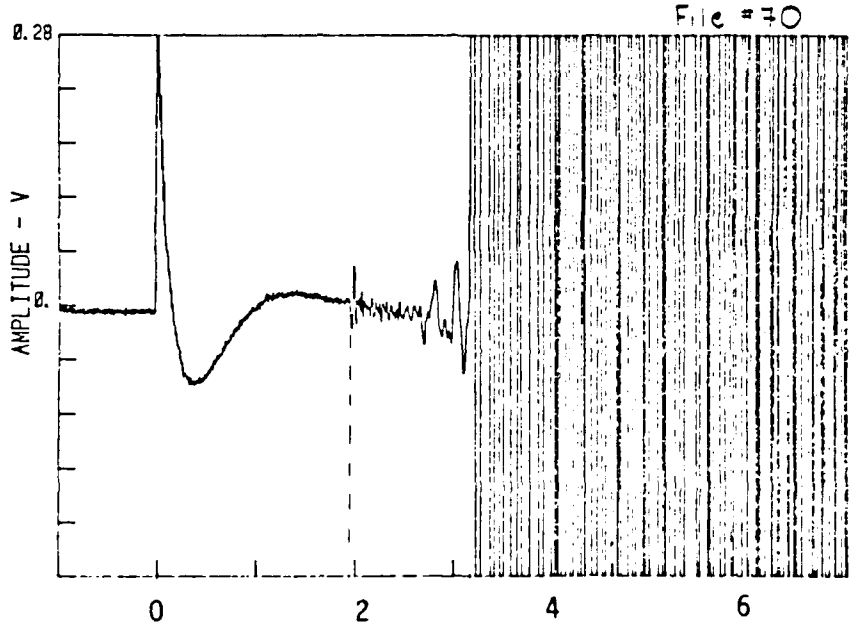

Figure D.4

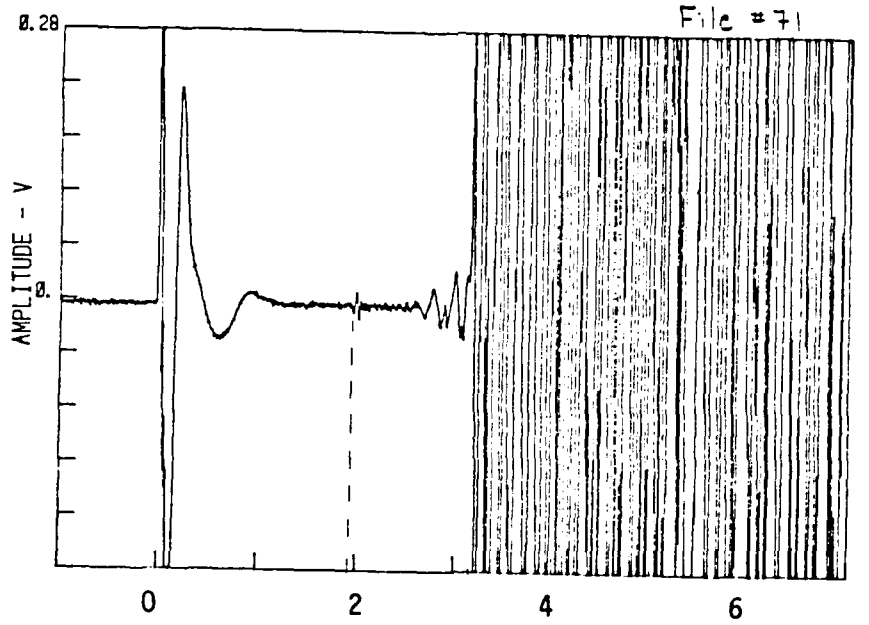

TIME-milliseconds

Figure D.5

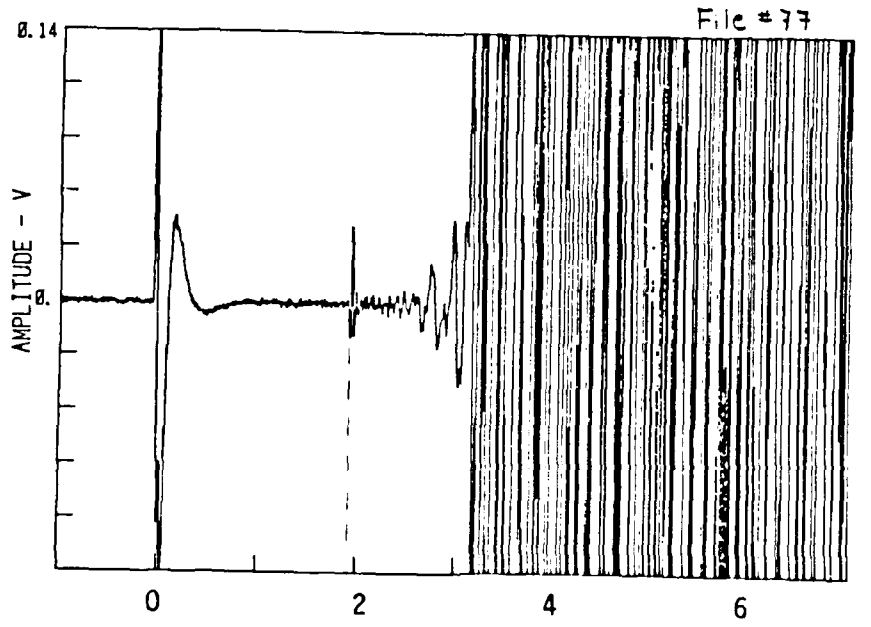

TIME-milliseconds

Figure D.6

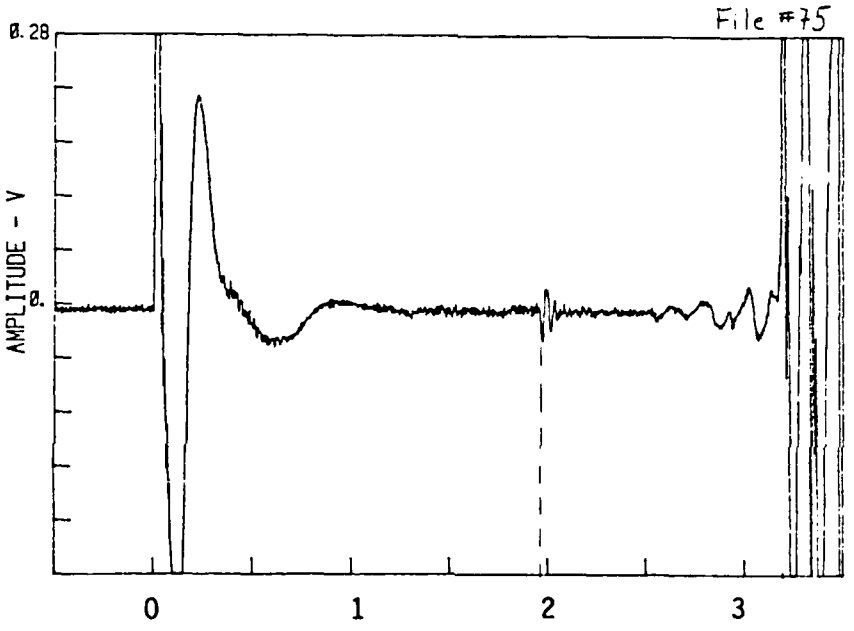

Figure D.7

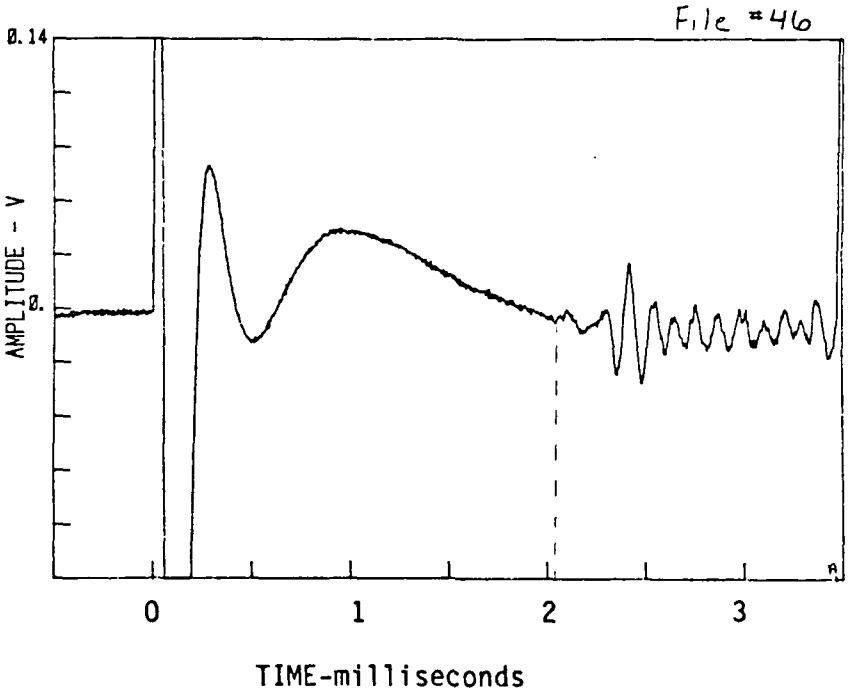

Figure D.8

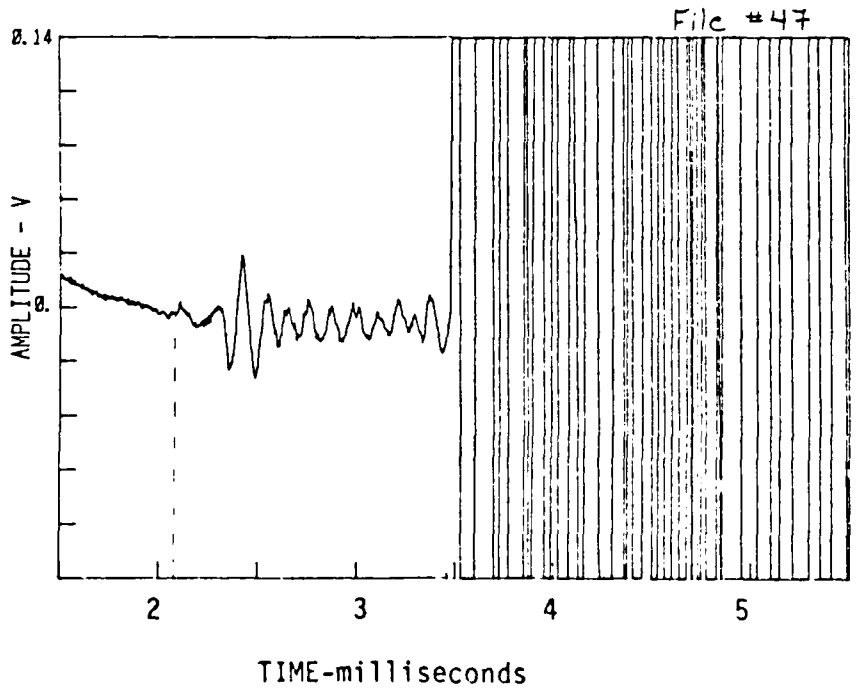

Figure D.9

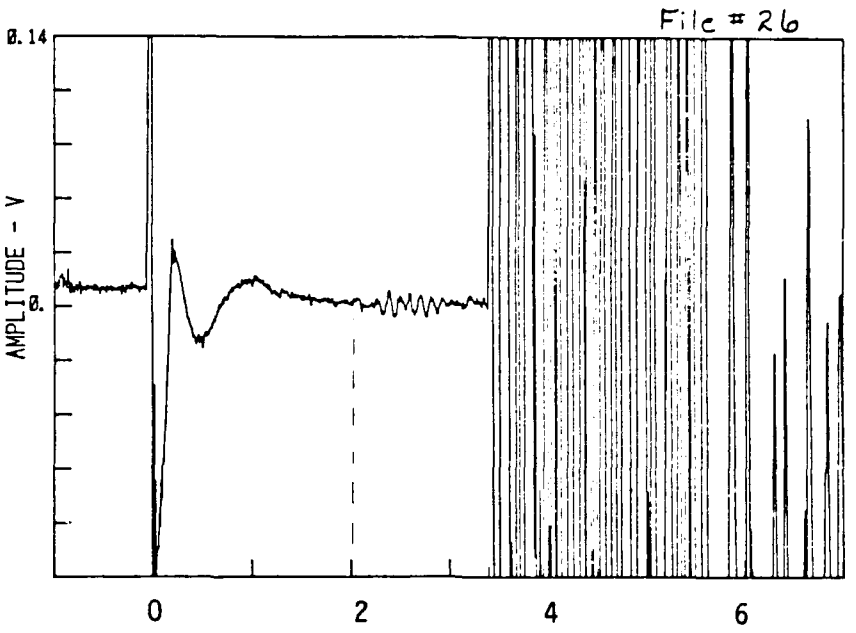

Figure D.10

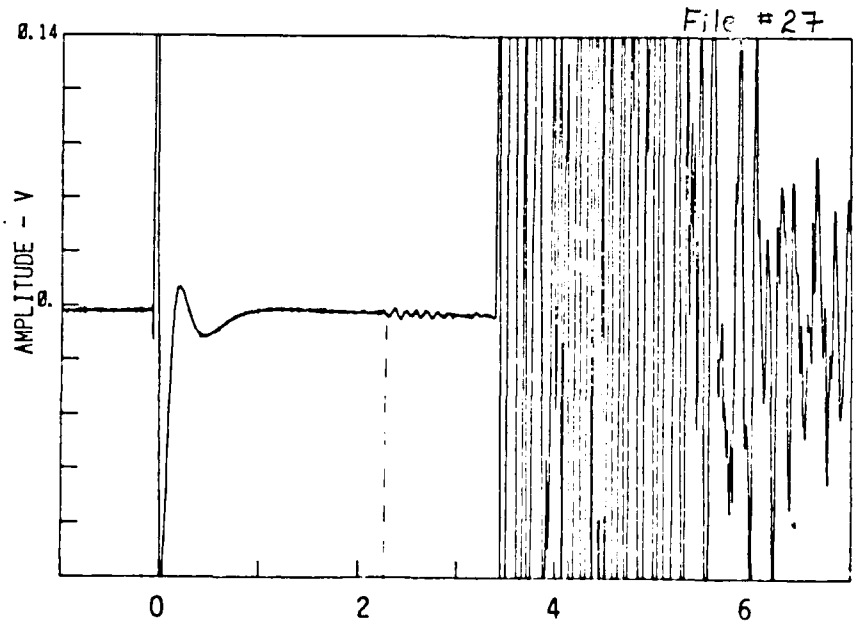

Figure D.11

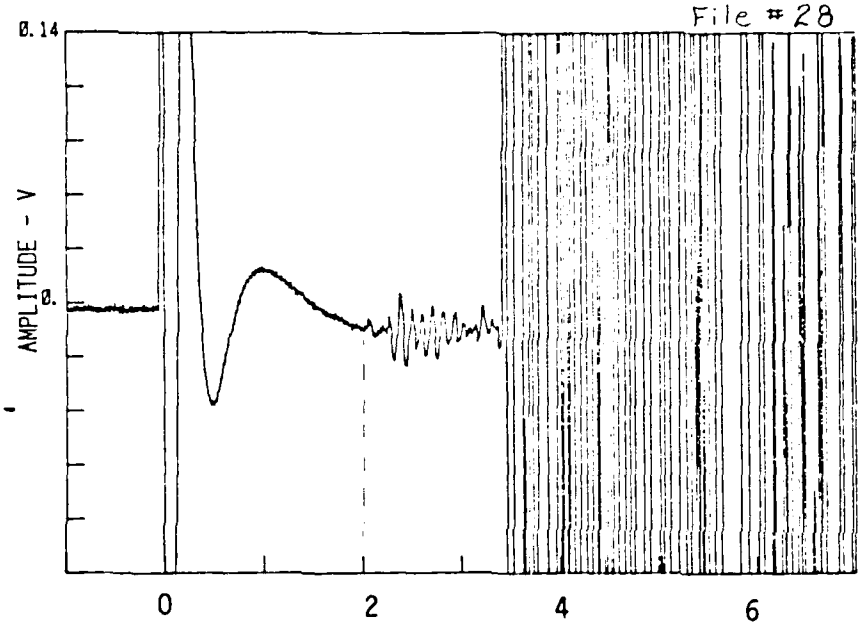

Figure D.12

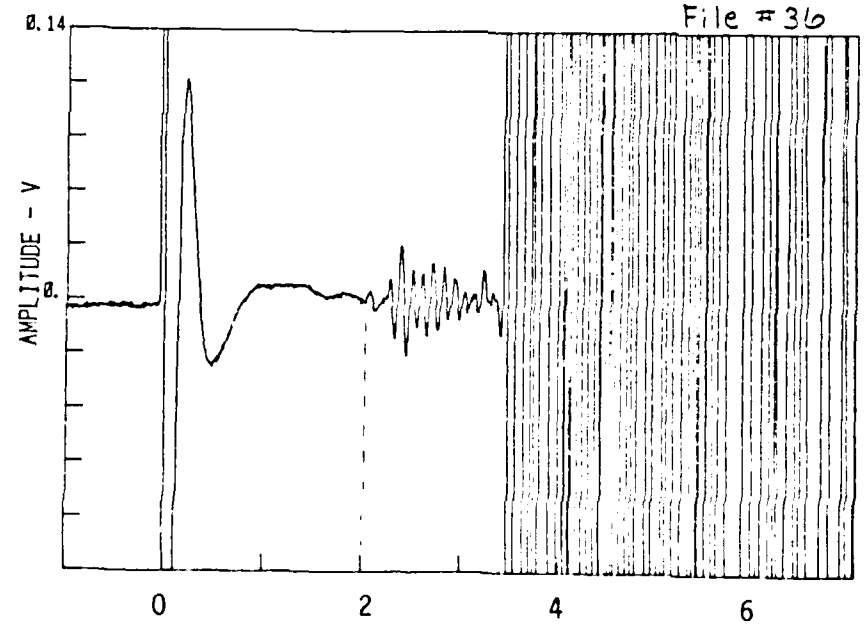

Figure D.13

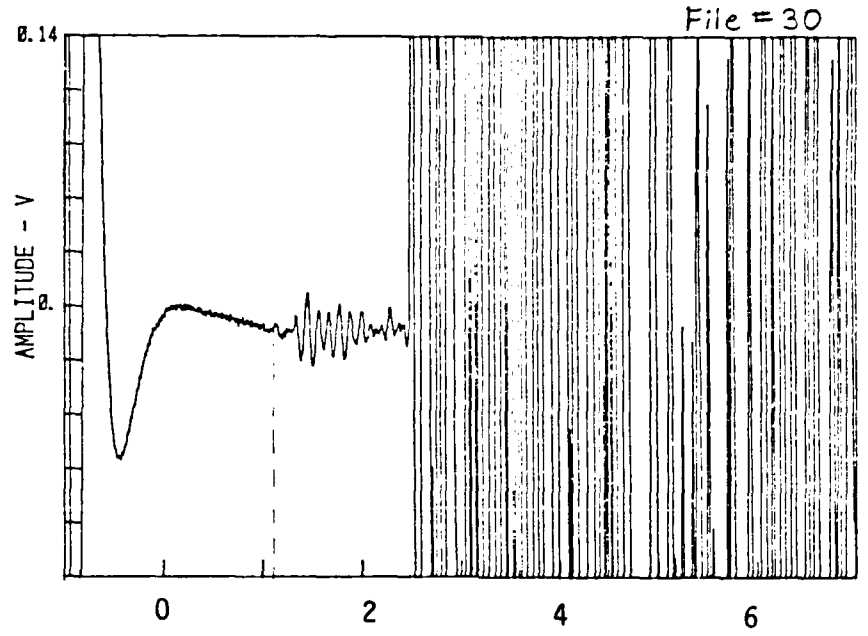

Figure D.14

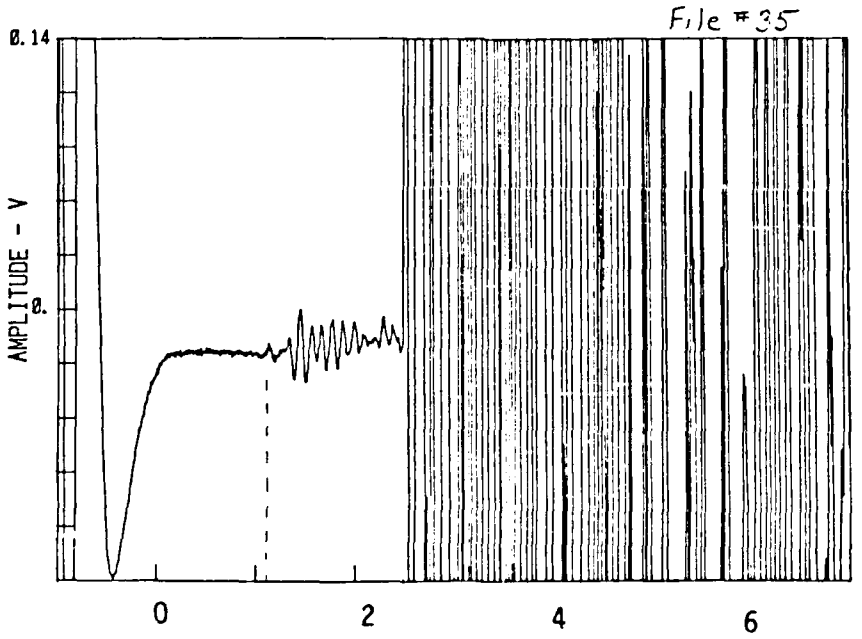

Figure D.15

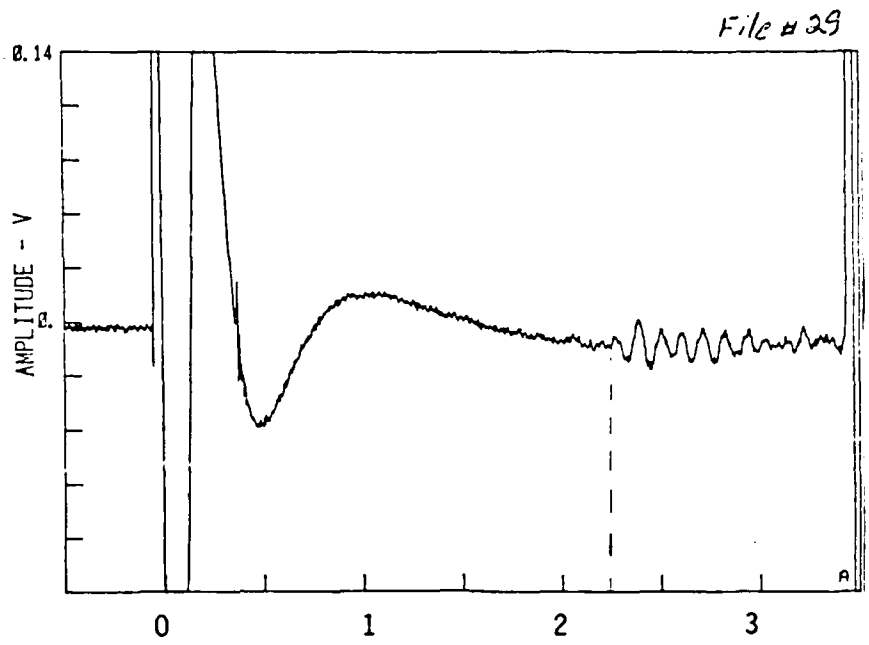

Figure D.16

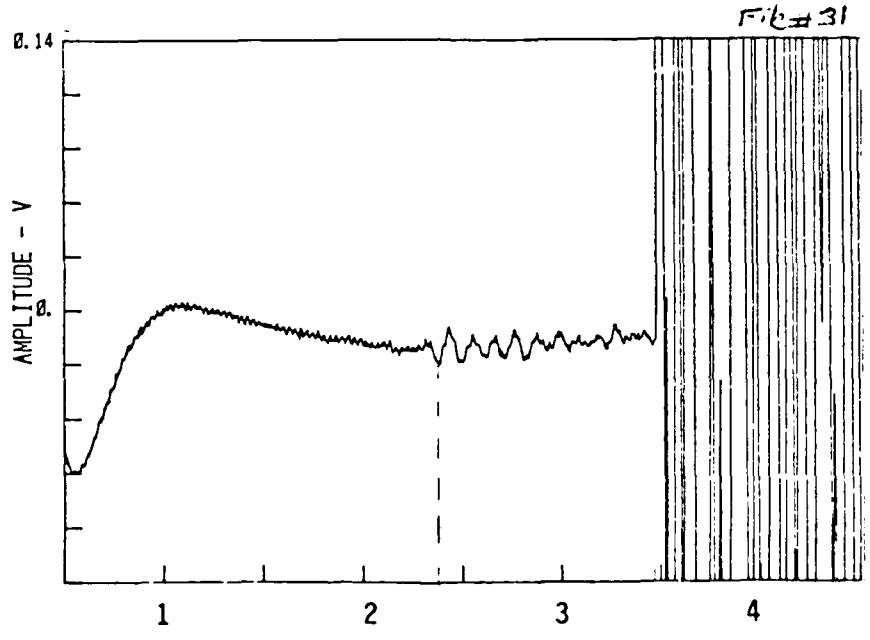

Figure D.17

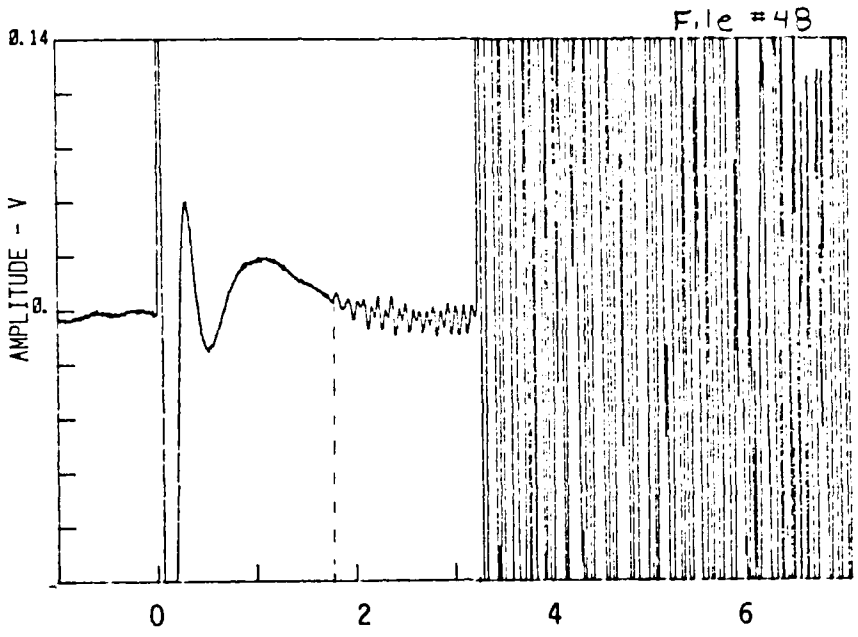

Figure D.18

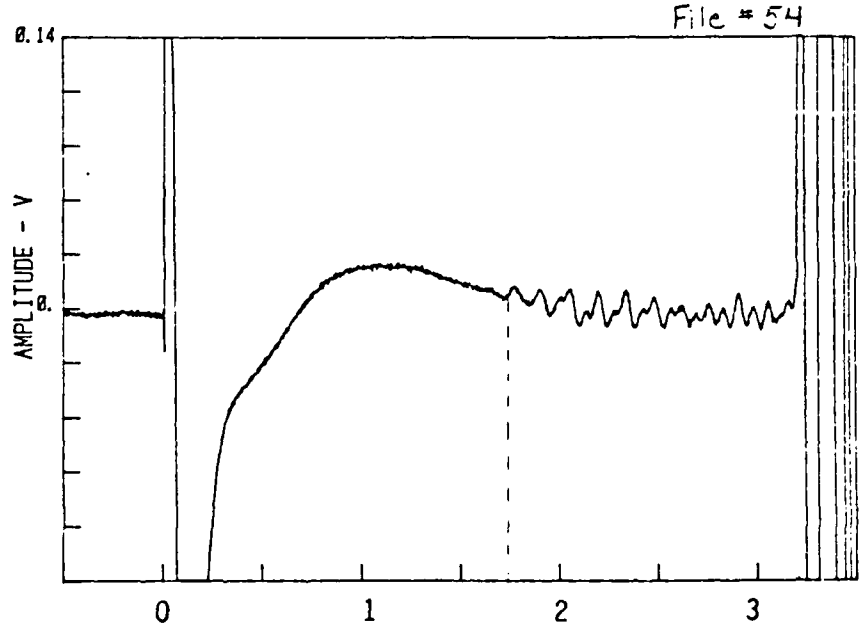

Figure D.19

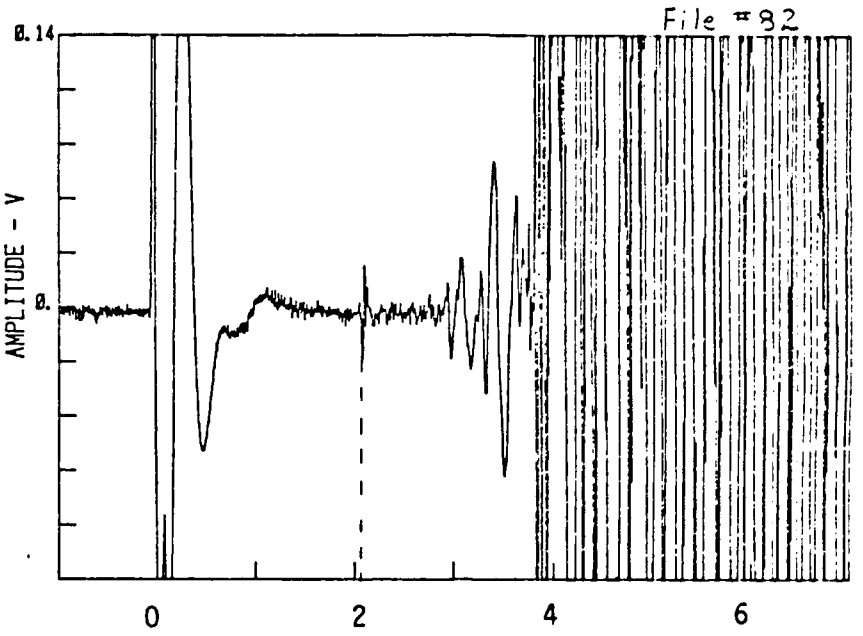

Figure D.20

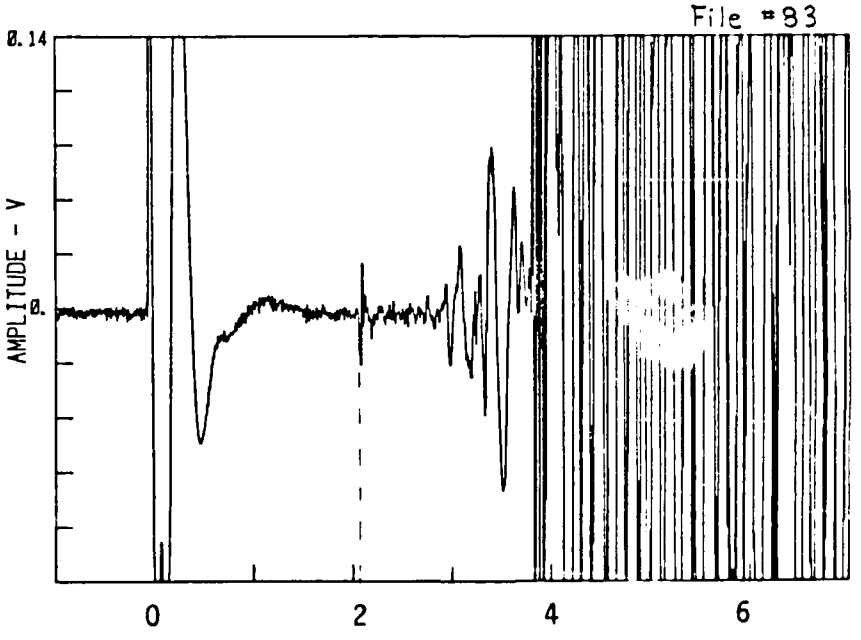

Figure D.21

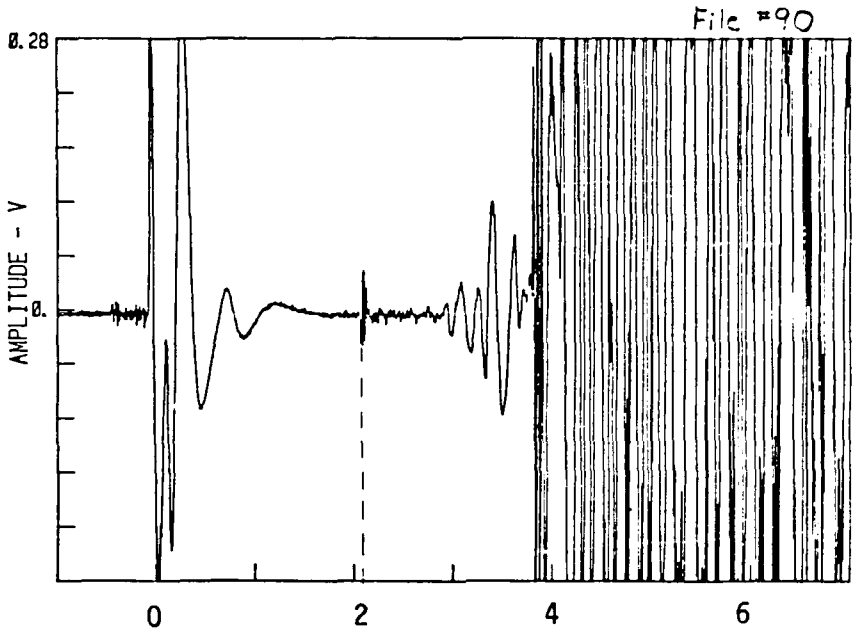

Figure D.22

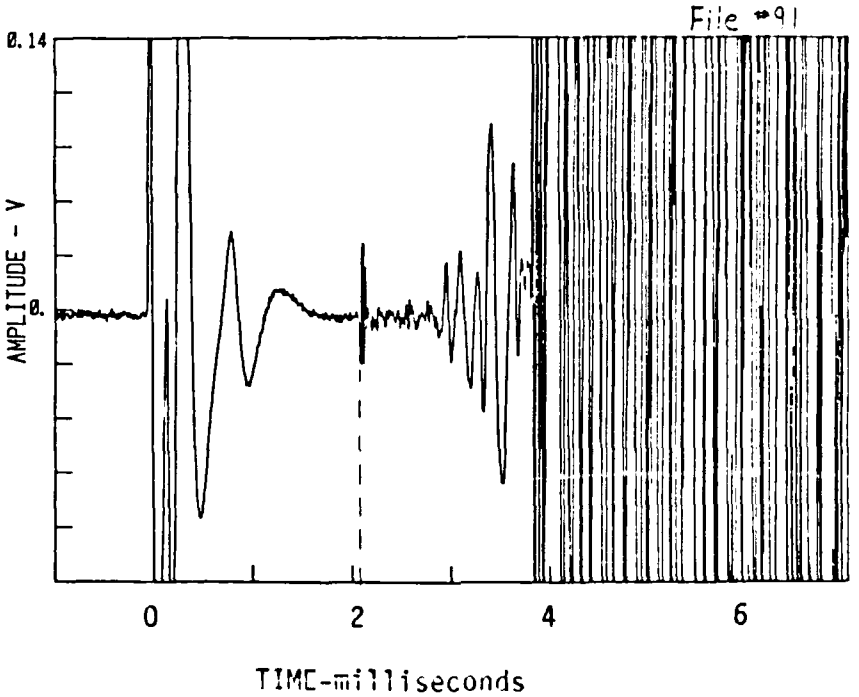

Figure D.23

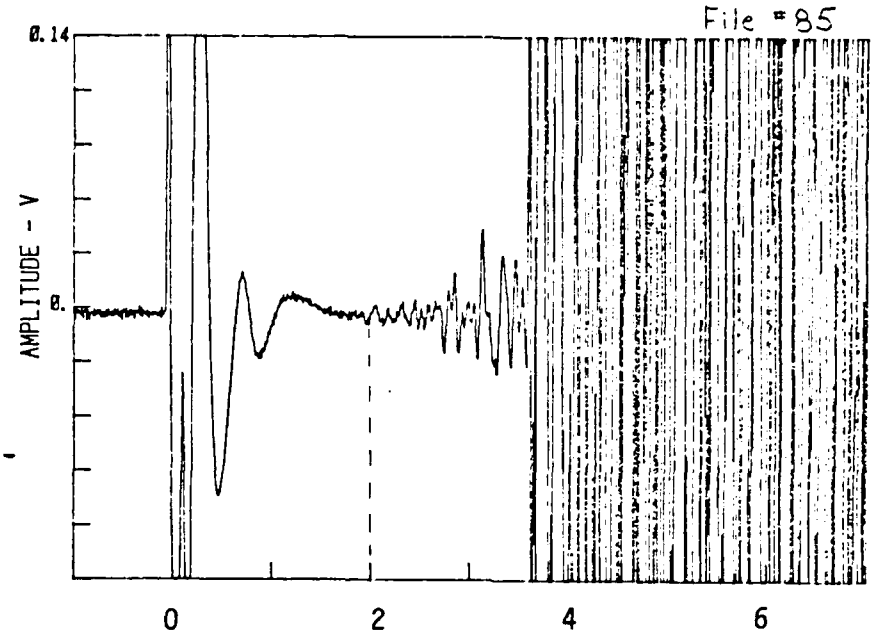

Figure D.24

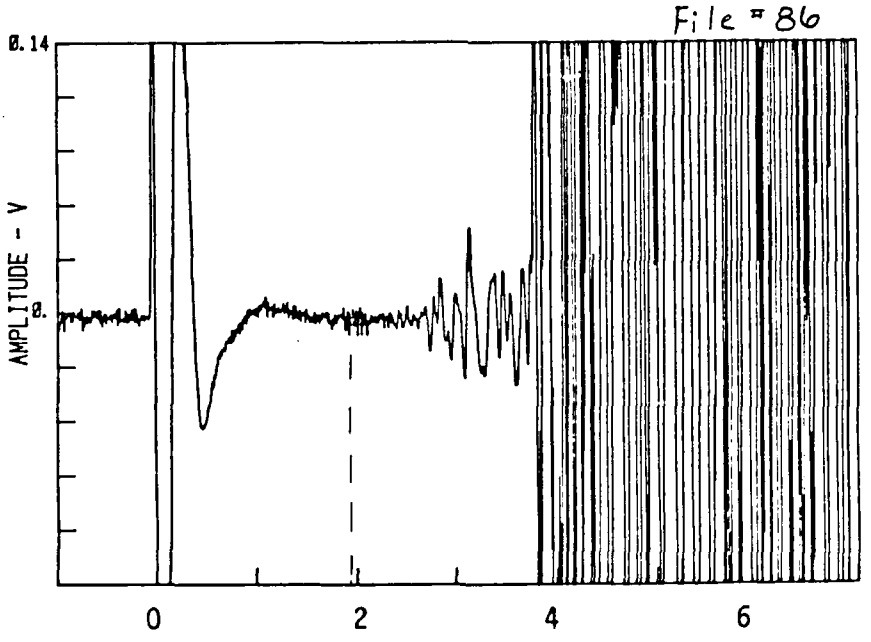

Figure D.25

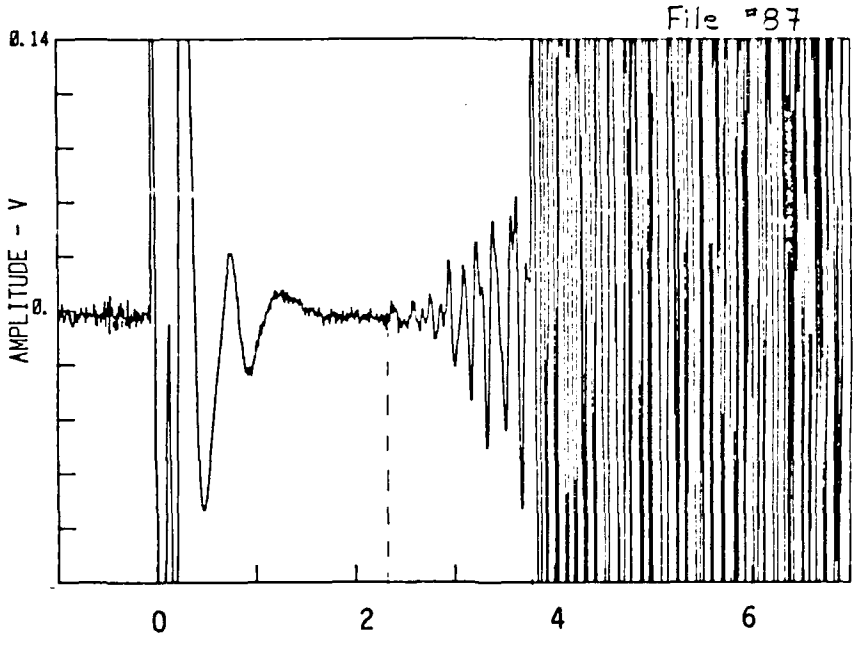

Figure D.26

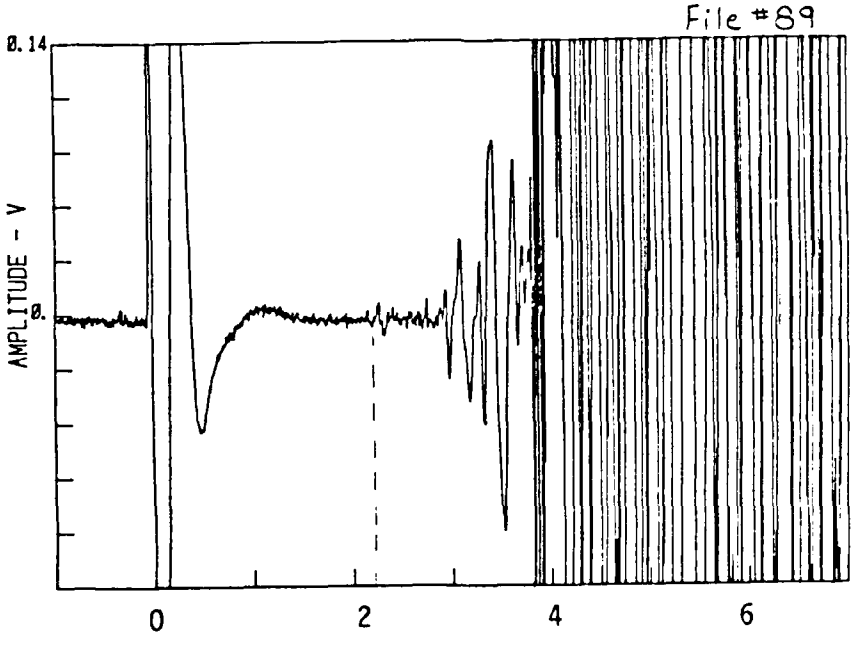

Figure D.27

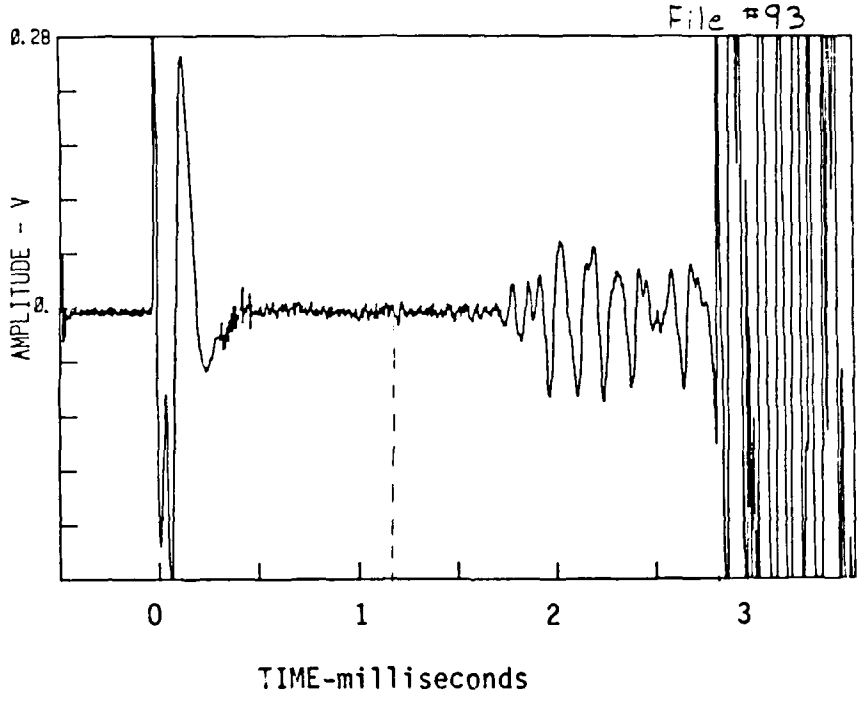

Figure D.28

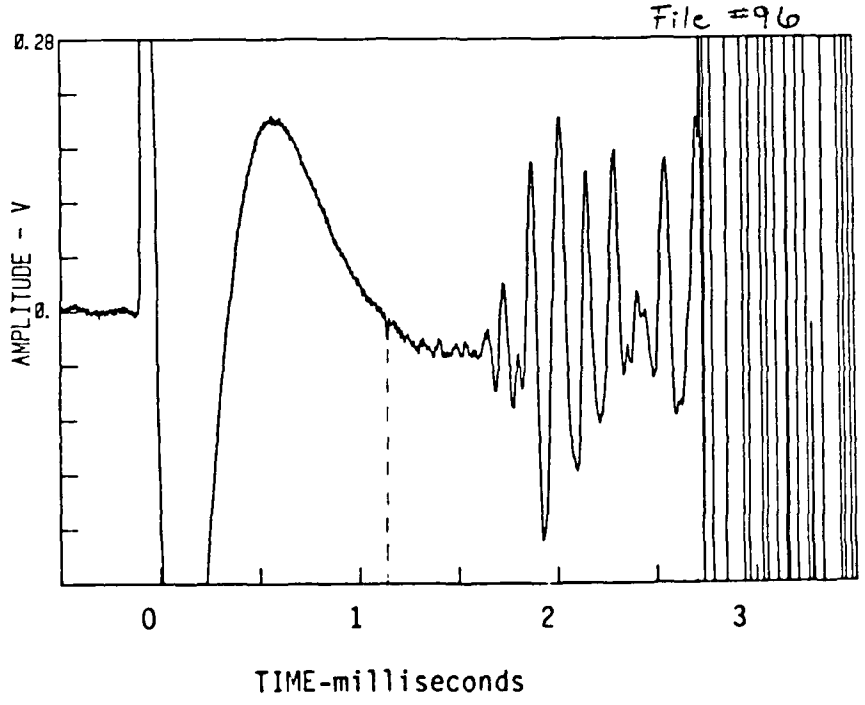

Figure D.29

Appendix E. References

Ackley, S.F., W.D. Hibler III, F.K. Kugzruk, A. Kovacs and W.F. Weeks, 1976. "Thickness and Roughness Variations of Arctic Multiyear Sea Ice," U.S. Army Corps of Engineers, Cold Regions Research and Engineering Laboratory, Report 76-18.

Assel, R.A., D.E. Boyce, B.H. DeWitt, J. Wartha and F.A. Keyes, 1979. "Summary of Great Lakes Weather and Ice Conditions Winter 1977-78," NOAA Technical Memorandum, ERL GLERL-26.

Bass, Bauer and Evans, 1972. J. Acoust. Soc. Am., 52: 821.

Bell, C.E. and J.A. Landt, 1967. Appl. Phys. Letters, 10: 46.

Bogorodskii, V.V. et al., 1976. "Sound Propagation in Ice Crystallized from Salt Water," Soviet Physics-Acoustics, 22: 158-159.

Brekhovskikh, L.M., 1960. Waves in Layered Media, Academic Press Inc., New York.

Brewer, R.G. and K.E. Rieckhoff, 1964. Phys. Rev. Letters, 13: 334.

Brown, David, 1972. "Baseline Noise Measurements of Army Helicopters," AD 887-625, USA AMRDL.

Bryan, M.L. and R.W. Larson, 1975. "The Study of Fresh-Water Lake Ice Using Multiplexing Imaging Radar," J. Glaciol., 14:445-457.

Bunkin, F.B., N.V. Karlov, V.M. Komissarov and G.P. Kuzmin, 1971. Sov. Phys. - JETP Letters, 13: 341.

Campbell, K.J. and A.S. Orange, 1974. "A Continuous Profile of Sea Ice and Fresh Water Ice thickness by Impulse Radar," Polar Record, 17: 31-41.

Carome, E.F., C.E. Moeller and N.A. Clark, 1966. JASA, 40: 1462.

Cawley, R.G. and C.E. Bell, "Propagation of CO_2 Laser (10.6 micrometers)Induced Pressure Transients in Water (U)," NOLTR-72-107, Confidential.

Copper, D.W. et al., 1976. "Measurement of Lake Ice Thickness with a Short-Pulse Radar System," NASA TN D-8189.

Foster, J.L., D. Schultz and W.C. Dallam, 1978. "Ice Conditions on the Chesapeake Bay as Observed from Landsat During the Winter of 1977," Proc. of the 1978 Eastern Snow Conf., Feb. 2-3, Hanover, NH, pp. 89-104.

Gavrilo, V.P. et al., 1980. "Seasonal Changes Affecting the Elastic Properties of Sea Ice Cover," Trans. AANII, 374: 73-74.

Hall, D.K. and J. Martinec, 1985. Remote Sensing of Ice and Snow, Chapman and Hall.

Hall, K.H. et al., 1981. "Freshwater Ice Thickness Observations Using Passive Microwave Sensors," IEEE Trans. Geoscience and Remote Sensing, GE-19(4).

Hengeveld, H.G., 1974. "Remote Sensing Applications in Canadian Ice Reconnaissance," Interdisciplinary Symposium on Advanced Concepts and Techniques in the Study of Snow and Ice, Monterey, California, 1973, compiled by National Academy of Sciences, Washington, D.C., pp. 504-512.

Hibler, W.D., III, 1975. "Characterization of Cold-Regions Terrain Using Airborne Laser Profilometry," J. Glaciology 15(73): 329-347.

Hickman, G.D. and J.A. Edmonds, 1981. "An Experimental Facility for Laser-Acoustic Applications," AST-R-1551181 (N00014-78-C-0764), AST, Inc., McLean, VA..

Hickman, G.D., J.A. Edmonds, B.S. Maccabee and C.E. Bell, 1982a. "Field Measurements of Laser-Acoustic Generated Signals in Water for Determination of Bathymetry", AST, Inc. Report No. AST-R-180382, Arlington, VA.

Hickman, G.D. and J.A. Edmonds, 1982b. "The Generation and Measurement of CO_2 Laser-Induced Acoustic Pulses in Sand," presented at the 104th Meeting of the Acoustical Society of America, Orlando, Florida, November 8-12.

Hickman, G.D. and J.A. Edmonds, 1983a. "Laser-Induced Acoustics in Ice," presented at the 17th International Symposium on Remote Sensing of the Environment, Ann Arbor, Michigan, May 9-13.

Hickman, G.D. and J.A. Edmonds, 1983b. "A Review of Technology for Sensing Ice Characteristics," AST-R-200183, AST, Inc., Arlington, VA.

Hickman, G.D. and J.A. Edmonds, 1983. "Laser-Acoustic Measurements for Remotely Determining Bathymetry in Shallow Turbid Waters," J. Acoust. Soc. Amer. 73(3): 840-843.

Kinsler, L.E., A.R. Frey et al., 1982. Fundamentals of Acoustics, John Wiley and Sons.

Koerneer, R.M., 1973. "The Mass Balance of the Sea Ice of the Arctic Ocean," J. Glac. 12(65): 173-185.

Kovacs, A., 1977. "Sea Ice Thickness Profiling and Under Ice Oil Entrapment," 9th Annual Offshore Tech. Conf., May 2-5.

Kovacs, A., 1978. "A Radar Profile of a Multi-Year Pressure Ridge Fragment," Arctic, 31(1).

Kovacs, A. and R.M. Morey, 1978. "Radar Anisotropy of Sea Ice Due to Preferred Azimuthal Orientation of the Horizontal C Axis of Ice Crystals," J. Geophys. Research 83(C12): 6037-6046.

Kovacs, A. and R.M. Morey, 1979. "Anisotropic Properties of Sea Ice in the 50- to 150- MHz Range," J. Geophys. Research, 84(C9): 5749-5759.

Kovacs, A. and R.M. Morey, 1980. "Investigations of Sea Ice Anisotropy, Electromagnetic Properties, Strength, and Under-Ice Current Orientation," U.S. Army Corps of Engineers Cold Regions Research and Engineering Laboratory Report 80-20.

Langleben, M.P., 1962. "Young's Modulus for Sea Ice," Can. J. Phys. 40(1): 1-8.

Langleben, M.P., 1969. "Attenuation of Sound in Sea Ice, 10-500 kHz," J. Glaciol., 8: 399-406.

Langleben, M.P., 1970. "Reflectior of Sound at the Water-Sea Ice Interface," J. Geophys. Res., 75(27).

Leshkevich, G.A., 1981. "Categorization of Northern Green Bay Ice Cover Using Landsat-1 Digital Data - A Case Study," NOAA Technical Memorandum, ERLGLERL-33.

Lo, R.C. and J.P. Hollinger, 1984. "The Mission Sensor Microwave Imager, its Applications and Validation," Conf. Record: Oceans, Sept 10-12, 162-166, Wash., D.C.

Lowney, J.R. and J.B. Sullivan, 1970. "Interaction of CO_2 Laser Radiation and Water," NOLTR 69-166 (Naval Ordnance Laboratory).

Maccabee, B., 1975. "An Experimental Study of Sound Transmission From Air Into Bubbly Water," NSWC/WOL/TR 75-69.

Maccabee, B.S. and C.E. Bell, 1977. "Properties of Laser Induced Sound in the Ocean (U)," Naval Surface Weapons Center, NSWC/WOL/TR, White Oaks, Md.

Meier, M.F., 1979. "Remote Sensing of Snow and Ice," Hydrological Sciences Bulletin, 25(3): 307-330.

Mellor, J.C., 1982. "Bathymetry of Alaskan Arctic Lakes: A Key to Resource Inventory with Remote-Sensing Methods," PhD Dissertation, Univ. of Alaska, Fairbanks, Ak.

Newman, J.S. et al., 1986. "Analysis of Helicopter Noise Using International Helicopter Noise Ce.," Federal Aviation Administration Washington DC Office of Envir., AD-A167 446.

Page, D.F. and R.O. Ramseier, 1975. "Application of Radar Techniques to Ice and Snow Studies," J. Glaciology 15(73): 171-191.

Reeves, R.G., A. Anson and D. Landen, 1975. Manual of Remote Sensing, American Society of Photogrammetry.

Rosner, H., 1985. "The Joint Ice Center Capabilities and Limitations in Sea Ice Analysis and Forecasting," Arctic Oceanography Conf. and Workshop.

Schmitz, F.H. and D.A. Boxwell, 1976. "In-Flight Far-Field Measurement of Helicopter Impulsive Noise," J. of the Amer. Helicopter Soc., October.

Schmitz, F.H. and Y.H. Yu, 1983. "Helicopter Impulsive Noise: Theoretical and Experimental Status," NASA TM-84390.

Sellman, P.V., J. Brown, R.I. Lewellen et al., 1975. "The Classification and Geomorphic Implications of Thaw Lakes on the Arctic Coastal Plain, Alaska," US Army Cold Regions Research and Engineering Laboratory, Hanover, NH, RR344.

Swift, C.T., L.S. Fedor and R.O. Ramseier, 1985. "An Algorithm to Measure Sea Ice Concentration With Microwave Radiometers," J. Geophysical Research, 90(C1): 1087-1099.

Swift, C.T., R.F. Harrington and H.F. Thornton, 1980. "Airborne Microwave Radiometer Remote Sensing of Lake Ice," EASCON 180 Record, Proc. of the IEEE Electronics and Aerospace Systems Convention, Sept 29-30 and Oct 1, pp. 369-73.

Thomas, R.H., R.A. Bindschadler et al., 1985. "Satellite Remote Sensing For Ice Sheet Research," NASA TM-86233.

Thorndike, A.S. and G.A. Maykut, 1973. "On the Thickness Distribution of Sea Ice," Division of Marine Resources, University of Washington, AIDJEX, Bull. No. 21, pp. 31-48.

Urick, R.J., 1975. Principles of Underwater Sound, McGraw-Hill, Inc.

Wartha, J.H., 1977. "Lake Erie Ice: Winter 1975-76," NOAA Technical Memorandum, NESS 90.

Watts, R.D. and D.L. Wright, 1981. "Systems For Measuring Thickness of Temperate and Polar Ice From the Ground or From the Air," J. Glaciology, 27(97): 459-469.

Weeks, W.F., A.G. Fountain, M.L. Bryan and C. Elachi, 1978. "Differences in Radar Return From Ice-Covered North Slope Lakes," J. Geophys. Res. 83:4069-73.

Weeks, W.F., A.J. Gow and R.J. Schertler, 1981. "Ground-Truth Observations of Ice-Covered North Slope Lakes Imaged by Radar," US Army Cold Regions Research and Engineering Laboratory, Hanover, NH, Report 81-19.

Wiesnet, D.R., 1979. "Satellite Studies of Fresh-water Ice Movement on Lake Erie," J. Glaciol., 24: 415-26.

Won, I.J. and K. Smits, 1985. "Frequency-Domain Electromagnetic Ice-Sounding," Proc. of the Arctic Oceanography Conf. and Workshop, NORDA, June 11-14.

Yang, T.C. and C.W. Votaw, 1981. "Under Ice Reflectivities At Frequencies Below 1 kHz," J. Acoust. Soc. Am. 70(3).

Zwally, H.J. and P. Gloersen, 1977. "Passive Microwave Images of the Polar Regions and Research Application," Polar Record, 18(116): 341-450.